Doctoral Dissertation

MULTIMEDIA MONITORING OF POLYCYCLIC AROMATIC HYDROCARBONS (PAHs) IN A LARGE INDUSTRIAL CITY: PHASE DISTRIBUTION AND EMISSION SOURCE IDENTIFICATION

Tuyet Nam Thi Nguyen

Department of Urban and Environmental Engineering
(Environmental Science and Engineering)

Graduate School of UNIST

2020

MULTIMEDIA MONITORING OF POLYCYCLIC AROMATIC HYDRCARBONS (PAHs) IN A LARGE INDUSTRIAL CITY: PHASE DISTRIBUTION AND EMISSION SOURCE IDENTIFICATION

Tuyet Nam Thi Nguyen

Department of Urban and Environmental Engineering
(Environmental Science and Engineering)

Graduate School of UNIST

Multimedia monitoring of polycyclic aromatic hydrocarbons (PAHs) in a large industrial city: Phase distribution and emission source identification

A dissertation
submitted to the Graduate School of UNIST
in partial fulfillment of the
requirements for the degree of
Doctor of Philosophy

Tuyet Nam Thi Nguyen

01/06/2020 Month/Day/Year of submission
Approved by

_____

Advisor
Sung-Deuk Choi

Multimedia monitoring of polycyclic aromatic hydrocarbons (PAHs) in a large industrial city: Phase distribution and source identification

Tuyet Nam Thi Nguyen

This certifies that the dissertation of Tuyet Nam Thi Nguyen is approved

01/06/2020 Month/Day/Year of submission

signature

_____

Advisor: Sung-Deuk Choi

signature

_____

Yongwon Seo: Thesis Committee Member #1

signature

_____

Chang Keun Song: Thesis Committee Member #2

signature

_____

Jaesung Jang: Thesis Committee Member #3

signature

_____

Young-Kyo Seo: Thesis Committee Member #4

Abstract

Ulsan is one of the largest industrial cities of South Korea and has several main industrial areas, including petrochemical, non-ferrous, shipbuilding, and automobile complexes. These industrial activities contribute to the need for monitoring of pollutants, especially the polycyclic aromatic hydrocarbons (PAHs), in Ulsan since the petrochemical and non-ferrous industrial activities are believed to be one of the important emission sources of PAHs. This dissertation aims to investigate PAHs (i.e., concentrations, profiles, phase distribution, and exchange) in the multimedia environment of Ulsan, including the air, soils, overland runoff, and surface water. Moreover, types (e.g., coal combustion and biomass burning) and areas (i.e., local and regional areas) of the PAH emission sources were also identified.

The diagnostic ratios, principal component analysis (PCA), and positive matrix factorization (PMF) were used to identify the emission source types. The emission source areas of PAHs were identified using hybrid receptor models and conditional bivariate probability function. Moreover, the fugacity approach and Whitman's two-film model were applied to investigate the multimedia exchange of PAHs between the air-water and air-soil. Regarding the atmospheric PAHs, winter and spring had the highest and lowest PAH concentrations, respectively. Fractions of the gaseous or 3- and 4-ring PAHs were high in summer, and those of the particulate or 5- and 6-ring PAHs increased in winter. For the seasonal emission sources of PAHs, pyrogenic (e.g., coal combustion) source was dominant in winter. Other types of the pyrogenic (e.g., industrial fuel combustion) and petrogenic sources were the main PAH sources in summer and fall. In spring, two types of the pyrogenic sources, diesel and coal combustion, were identified as the main PAH sources in this season.

Regarding the areas of emission sources, the particulate PAHs in Ulsan could be more affected by distant sources in the spring and winter, such as long-range transport from northeastern China (e.g., Beijing, Tianjin, and Hebei), northern China (e.g., Jilin and Liaoning), and North Korea. In contrast, the gaseous PAHs were affected by local emissions (i.e., industrial and vehicle emissions) mostly throughout the year. Particularly, in summer and fall, the local emission sources could more affect the gaseous and particulate PAHs compared to the outside sources (i.e., trans-boundary transport from China). However, the opposite trend was observed in spring and winter, that is, PAHs originated from northeastern China, northern China, and

North Korea could contribute to those in Ulsan.

The PAHs in other environmental media (i.e., overland runoff, surface water, and soils) of Ulsan were also studied to understand the interaction of PAHs in the air to those in the other media. For PAHs in the runoff and surface water, the runoff PAHs reached their highest concentrations in April (middle spring), which could be strongly affected by meteorological conditions before the sampling events (i.e., the long dry period and the lower rainfall amount). Moreover, the contributions of the dissolved PAHs were mostly higher than those of particulate ones, especially in July (summer) when the higher water temperature could lead to the desorption of PAHs from the particulate to the dissolved phase. Regarding the source identification, PAHs in the runoff and surface water could share similar emission sources, which were mixed sources from both petrogenic and pyrolysis sources. Additionally, the PAHs in the runoff of July could be also originated from coal/coke/heavy oil combustion as a result of industrial emissions and local advection.

Regarding the multimedia exchange, the surface water could be a source for most of the atmospheric PAHs in Ulsan. However, the contribution of the water to the atmospheric PAHs (i.e., volatilization from the water to the air) could be not important. The soil could be a source or a sink of the atmospheric PAHs, mostly depending on the molecular weights of the compounds (i.e., a source for 3-ring PAHs and a sink for 4-ring species). Additionally, the PAHs in Ulsan mostly distributed in the soil, followed by the air, and the surface water. The highest distributions of PAHs in the soil could be because of their strong affinity to the soil organic matter, leading to their accumulation in the soil. The PAHs secondly distributed in the air, however, the atmospheric PAHs in Ulsan should be concerned due to the effect of trans-boundary transport and local advection from the industrial complexes.

Overall, this dissertation can contribute to the understanding of PAHs in the multimedia environment, including the air, overland runoff, surface water, and soils, and can support the decision-making related to the environmental issues in Ulsan. Based on this dissertation, further studies should more focus on other PAH compounds, such as oxygenated and halogenated PAHs, in the air and soil of Ulsan. Moreover, trans-boundary transport of PAHs and other organic compounds should be further studied to more understand the effect of long-range transport on air pollution in Ulsan.

Contents

List of figures

List of tables

Chapter 1: Introduction

1.1. Overview of the polycyclic aromatic hydrocarbons

Polycyclic aromatic hydrocarbons (PAHs) are compounds having at least two aromatic rings in their chemical structures. The PAHs can be classified into two main sub-groups, namely low-molecular-weight (LMW) and high-molecular-weight (HMW) PAHs. The LMW PAHs consist of two or three aromatic rings, whereas the HMW PAHs contain five or six rings. Moreover, the 4-ring PAHs tend to be regarded as medium-molecular-weight (MMW) species. The number of 16 specific PAH species was selected as priority PAHs by the United States Environmental Protection Agency (US-EPA) based on their representative harmful effects, available information, and higher levels compared to other PAHs (Ravindra et al., 2008). The names and chemical structures of the priority PAHs are shown in Figure 1-1.

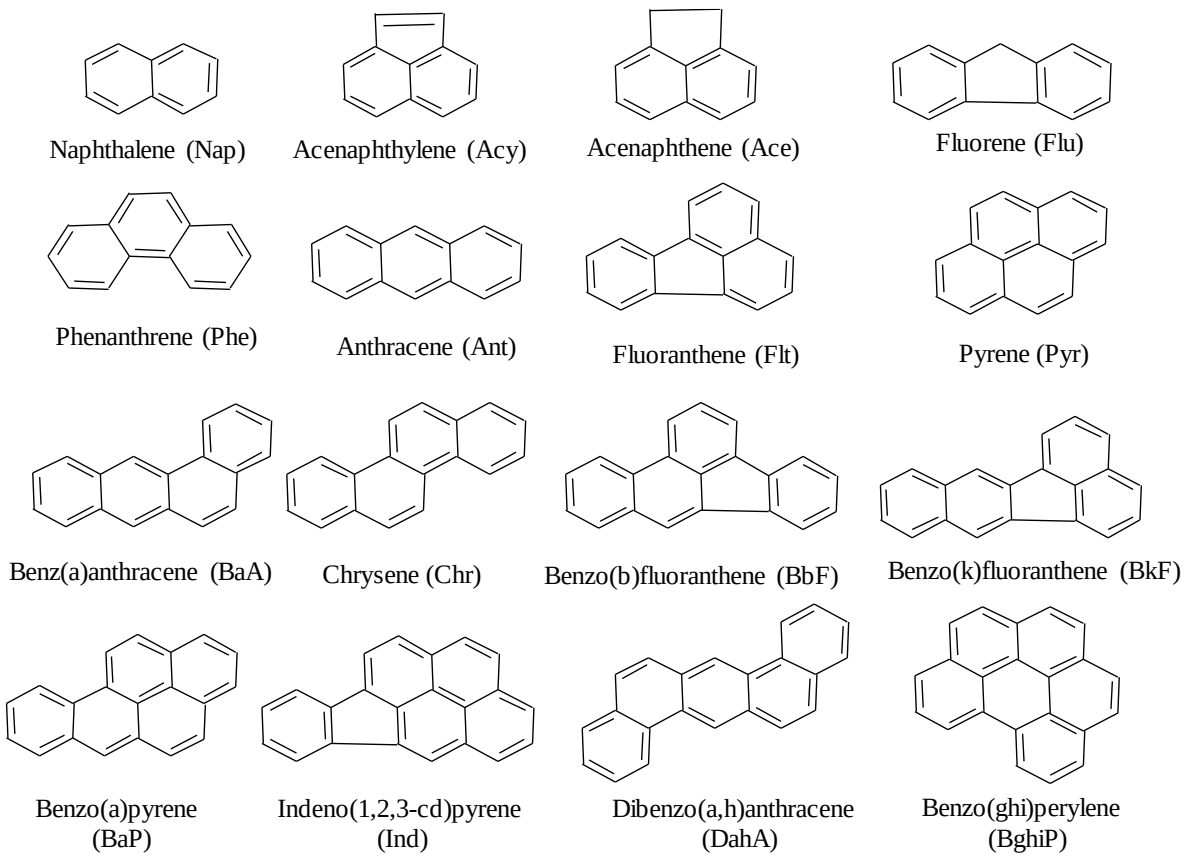

Figure 1-1. Chemical structures of the priority US EPA PAHs. Their abbreviation names are shown in the parentheses.

The PAHs are emitted from natural sources such as forest fires and volcanic eruptions (Ravindra et al., 2008). However, the most noticeable sources are related to human activities, such as combustion processes and petroleum spillage or leakage (Choi et al., 2012b). Some PAHs, especially the HMW species, negatively affect human health and are probably or possibly carcinogenic to humans. Several initial studies on PAHs provided some evidence that PAHs could cause lung cancer for workers in coal carbonization and gasification processes (Zedeck, 1980). For years, the effect of PAHs on human health has been continuously reported in many studies. For instance, lung cancer incidence correlated with the working time of workers in a coke oven plant (Moolgavkar et al., 1998). In addition, exposure to anthracene and benzo(a)pyrene is believed to induce skin irritation and inflammation (Unwin et al., 2006), bladder, and lung cancers (IARC, 2014). Therefore, it is essential to study and monitoring PAHs in the environment. The physiochemical properties of the priority PAHs, including molecular weight, water solubility, vapor pressure, octanol/water partition coefficient (K_{OW}), and octanol/carbon partition coefficient (K_{OC}), are shown in Table 1-1.

Table 1-1. Physiochemical properties of the target PAHs at 25 ºC (Mackay et al., 2006a).

PAHs	Formula	Molecular weight	Water solubility	Vapor pressure	Log Kow	Log Koc
Nap	$C_{10}H_8$	128.17	31.5	7.1×10^{-2}	3.37	3.11
Acy	$C_{12}H_8$	152.19	3.93	6.7×10^{-3}	4.07	3.75
Ace	$C_{12}H_{10}$	154.20	3.59	2.2×10^{-3}	3.92	3.79
Flu	$C_{13}H_{10}$	166.21	1.90	6.0×10^{-4}	4.18	3.95
Phe	$C_{14}H_{10}$	178.22	1.65	1.2×10^{-4}	4.46	4.36
Ant	$C_{14}H_{10}$	178.22	0.075	6.0×10^{-6}	4.63	4.42
Flt	$C_{16}H_{10}$	202.25	0.240	9.2×10^{-6}	4.85	4.81
Pyr	$C_{16}H_{10}$	202.25	0.165	4.5×10^{-6}	4.90	4.92
BaA	$C_{18}H_{12}$	228.28	0.011	2.1×10^{-7}	5.61	5.62
Chr	$C_{18}H_{12}$	228.28	0.0015	6.4×10^{-9}	5.73	5.74
BbF	$C_{20}H_{12}$	252.30	0.0015	5.0×10^{-7}	5.78	5.91
BkF	$C_{20}H_{12}$	252.30	0.0008	9.6×10^{-11}	5.94	5.99
BaP	$C_{20}H_{12}$	252.30	0.004	5.6×10^{-9}	6.31	6.04
DahA	$C_{22}H_{14}$	278.34	0.00056	9.6×10^{-10}	6.88	6.76
Ind	$C_{22}H_{12}$	276.33	0.00019	5.4×10^{-10}	6.72	6.80
BghiP	$C_{22}H_{12}$	276.33	0.00026	1.0×10^{-10}	7.04	6.93

Molecular weight: g/mol, water solubility: mg/L, vapor pressure: mmHg

The different physicochemical properties of the PAH species result in their different behaviors

in the environment. For instance, in the atmosphere, the LMW PAHs (e.g., Nap, Acy, Ace, Flu, and Phe) having higher vapor pressure tend to distribute in the gaseous phase. On the other hand, the HMW PAHs (e.g., BbF, BkF, BaP, Ind, and BghiP) tend to bind to atmospheric particles to form the particulate phase. Moreover, in the water, the LMW PAHs mostly distribute in dissolved phase since they have high water solubility, whereas the HMW PAHs prefer to bind to suspended solids and deposit onto bottom sediments of water bodies. In the soils, the HMW PAHs can be more dominant due to their stronger affinity to sorb to organic matter of the soils.

1.2. Study area

The study area of this dissertation is Ulsan, one of the largest industrial cities locating at the southeast of South Korea. The predominant industrial activities in Ulsan include petrochemical, chemical, non-ferrous, automobile, and shipbuilding production (Figure 1-2). Among them, the petrochemical and non-ferrous industrial activities, are believed to be the noticeable sources of PAHs because of the operational combustion processes used in their production (Kwon and Choi, 2014a). Previous studies reported that oil, diesel, and gasoline combustion (Kwon and Choi, 2014a; Van-Tuan et al., 2010), coal/biomass burning, and coke ovens (Kwon and Choi, 2014a) were the main sources of PAHs into the atmosphere of Ulsan. Moreover, it is known that prevailing seasonal winds play an important role in the contamination characteristics of PAHs in Ulsan (Choi et al., 2012b; Lee and Lee, 2004). Particularly, in summer and fall, winds blow from the East Sea to the inner city and pass through the industrial areas (Clarke et al., 2014), causing the urban and residential areas to become receptors for PAHs originated from the industrial activities. In reverse, in winter and spring, winds blow toward the East Sea and therefore can bring PAHs emitted in the city to the sea. Moreover, the monsoon system in winter and spring can also cause Ulsan to become downwind of other areas, such as western areas of South Korea and other regions in Northeast Asia (i.e., China and North Korea) (Inomata et al., 2017). As the PAHs can be detected in several environmental media, including the atmosphere, soils, and surface water, a study on PAHs in the multimedia environment of Ulsan is essential.

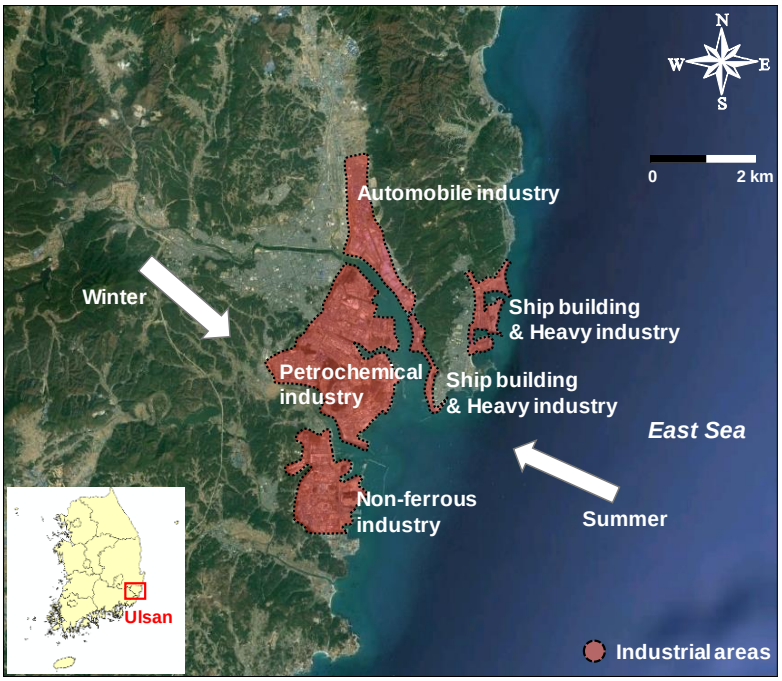

Figure 1-2. Industrial areas in Ulsan, South Korea. The arrows illustrate the prevailing wind direction in summer and winter.

For Ulsan, PAHs in the atmosphere, soils, sediments, and water were investigated (Choi et al., 2012b; Khim et al., 2001a; Kwon and Choi, 2014a). However, seasonal variations, regarding concentrations, profiles, and emission sources of PAHs in several environmental media (i.e., atmosphere, runoff, soils, and water) of Ulsan have not been studied yet. Moreover, as mentioned previously the downwind location of Ulsan, especially in winter and spring, induce an essential to identify areas and contributions of regional and local emission sources to PAHs in this city. Nevertheless, to the best of my knowledge, this issue has not been dealt with depth.

1.3. Literature review on PAHs in Ulsan

Previous studies on PAHs in Ulsan mostly focused on the atmosphere, followed by the soil and water. According to the searching results obtained from the Scopus and the Korean Research Information Searching Service (https://www.scopus.com/search and http://www.riss.kr/search, respectively), studies on PAHs in the air, soil, and water of Ulsan accounted for 40%, 35%, and 25%, respectively.

Regarding the atmosphere, the concentrations and profiles of PAHs bound to total suspended particles (Choi et al., 2013; Nguyen et al., 2018), PM_{10} (Van-Tuan et al., 2010), $PM_{2.5}$, and PM_1 (Lee et al., 2018) were investigated at the semi-rural, residential, urban, and industrial

areas of Ulsan. In addition, passive air sampling coupled with polyurethane (PUF-PAS) was also applied to simultaneously monitor the PAHs at several sites in semi-rural, urban, and industrial areas of Ulsan (Choi et al., 2012b; Nguyen et al., 2020; Vuong et al., 2020). In short, the PAH concentrations tended to be highest in the industrial, followed by the urban/residential, and semi-rural areas due to local advection. Additionally, results from human health risks of total (gas and particle) PAHs (Nguyen et al., 2020), PM_{10} -bound PAHs (Vu et al., 2011), and $PM_{2.5}$-bound PAHs (Lee et al., 2018) pointed out a safe level ($< 10^{-6}$) for residents in Ulsan regarding inhalation intake and dermal absorption of PAHs. The dry and wet deposition of atmospheric PAHs were also investigated (Lee and Lee, 2004) and the results showed that the low and intermedia PAHs (2- to 4-ring PAHs) were mostly dominant.

For the water, PAH concentrations in the Taehwa river and Ulsan bay had a tendency to be higher in the downstream surrounded by several industrial complexes, such as shipbuilding, petrochemical, and automobile industrial areas (Hyeon-Seo et al., 2012; Khim et al., 2001a; Ligaray et al., 2016). Moreover, the 2- to 4-ring PAHs were more dominant in the dissolved and particulate phases (Hyeon-Seo et al., 2012; Khim et al., 2001a; Khim et al., 2001b; Park et al., 2012) because these species are more mobile and have higher water solubility (Mackay et al., 2006a). In addition, the dissolved phase tended to more contribute to the total (dissolved and particulate) phase, especially at upstream of the Taehwa river. The PAHs in surface water of Ulsan were also mentioned to be affected by nonpoint sources, such as overland runoff, and this effect could be more strong in the semi-rural area (Park et al., 2012).

The PAH concentrations and profiles in road dust (Dong and Lee, 2009; Kim et al., 2019b; Lee and Dong, 2010) and soils (Jeon and Oh, 2019; Kim et al., 2019a; Kwon and Choi, 2014a) at several land-use types in Ulsan were also investigated. The results also revealed the concentration gradients from the industrial to the urban and semi-rural areas. The important emission sources of PAHs in Ulsan could be the industrial complexes (Kwon and Choi, 2014a; Nguyen et al., 2018) located at the southeast of the city, therefore, PAHs in several environmental media, including the air, water, and soil, in the industrial area have higher concentrations than those in the others. Additionally, the emission source types of PAHs in Ulsan were also identified using the diagnostic ratio, principal component analysis (PCA), and positive matrix factorization (PMF). The main emission sources of PAHs could be vehicle exhaust (i.e., gasoline and diesel emissions), coal/biomass burning, and coke oven (Choi et al., 2012b; Kwon and Choi, 2014b). Additionally, the industrial complexes in Ulsan, especially the

petrochemical and non-ferrous industrial areas were believed to emit a large amount of PAHs (Kwon and Choi, 2014a; Vuong et al., 2020) due to the heavy oil/coke usage in their productions.

1.4. Objectives

In order to address limitations on the understanding of PAHs in Ulsan, this dissertation aims to investigate the concentrations, profiles, and phase distributions of PAHs in the multimedia environment (i.e., atmosphere, surface water, runoff, and soils) of Ulsan. Moreover, the types of PAH emission sources (i.e., petrogenic or pyrolysis) and areas of these sources were also identified. In addition, the magnitude and direction exchange of PAHs between the environmental media (i.e., air-soil and air-water) were also determined. This dissertation can help to improve the understanding of PAHs in the multimedia environment of Ulsan and can support the decision-making related to environmental issues in this city.

1.5. Dissertation structure

To achieve the objectives mentioned previously, this dissertation has several chapters. Chapter 1 provides general information. Chapter 2 focuses on the investigation of seasonal variations and source identification of PAHs in the atmosphere of Ulsan. On the basis of chapter 2, chapter 3 aims to identify areas of the PAH emission sources regarding local and regional scales.

From chapter 4, PAHs in the other environmental media (e.g., surface water, runoff, and soil) of Ulsan are investigated to understand the interaction of PAHs in the multimedia environment. In particular, chapter 4 investigates the seasonal and temporal variations and identifies emission sources of PAHs in the overland runoff and surface water of Ulsan. Based on the results of the previous chapters, chapter 5 reveals the magnitude and direction exchange of PAHs between the air-soil and air-water systems. Finally, a summary and suggestions for further studies on PAHs in Ulsan are provided in the conclusion.

Chapter 2: Seasonal variation, phase distribution, and source identification of atmospheric polycyclic aromatic hydrocarbons at a semi-rural site in Ulsan, South Korea

Abstract

Polycyclic aromatic hydrocarbons (PAHs) in gaseous and particulate phases (n = 188) were collected in Ulsan, South Korea, over a period of one year (June 2013–May 2014) to understand the seasonal variation and phase distribution of PAHs as well as to identify the seasonal PAH emission sources. The target compounds were the 16 US-EPA priority PAHs, with the exception of naphthalene, acenaphthylene, and acenaphthene. Winter and spring had the highest and lowest PAH concentrations, respectively. The mean of the Σ_{13} PAHs in the gaseous phase (4.11 ng/m^3) was higher than that in the particulate phase (2.55 ng/m^3). Fractions of the gaseous or 3- and 4-ring PAHs (i.e., Flu, Phe, and Ant) were high in summer, and those of the particulate or 5- and 6-ring PAHs (i.e., BkF, BaP, Ind, DahA, and BghiP) increased in winter. Gas/particle partitioning models also demonstrated the increased contributions of the particulate PAHs in spring and winter. Source identification of PAHs was undertaken using diagnostic ratios, principal component analysis, and positive matrix factorization. The results indicated that pyrogenic sources (e.g., coal combustion) were dominant in winter. Other types of pyrogenic (e.g., industrial fuel combustion) and petrogenic sources were the main PAH sources in summer and autumn. The influence of both sources, especially in summer, might be due to seasonal winds transporting PAHs from the industrial areas. Two types of pyrogenic sources, diesel and coal combustion, were identified as the main PAH sources in spring. This study clearly demonstrates a source–receptor relation of PAHs at a semi-rural site in a heavily industrialized city.

2.1. Introduction

In the atmosphere, the LMW PAHs (i.e., 2- and 3-ring PAHs) exists predominantly in the vapor phase, whereas the MMW and HMW PAHs (i.e., 4- to 6-ring PAHs) tend to bind to airborne particles (Baek et al., 1991b). Levels and the phase distribution of PAHs have been reported to differ seasonally (Albuquerque et al., 2016). In particular, winter tends to show the highest PAH concentration among the four seasons due to a decline in atmospheric vertical dispersion and an increase in domestic burning for heating. Fractions of the gaseous PAHs are higher in summer, while the particulate PAHs contribute more in winter since lower temperatures can generate condensation of PAHs on atmospheric suspended particles (Gustafson and Dickhut, 1997).

PAHs are emitted from natural sources such as forest fires and volcanic eruptions (Ravindra et al., 2008). However, the most noticeable sources are related to human activities such as combustion processes and vehicle exhaust (Choi et al., 2012b). The emission sources of PAHs can be identified through several methods, including diagnostic ratios (DRs), principal component analysis (PCA), chemical mass balance (CMB), and positive matrix factorization (PMF). The DR method determines the possible sources of PAHs by comparing the observed ratios to those from previous studies. This method assumes that the PAH isomers are regarded to have the same physicochemical properties and that they are transformed or decomposed at the same rate (Biache et al., 2014). Hence, it is inferred that DR values are preserved when PAHs are transported from emission sources to receptors. However, the fact is that isomeric PAHs have different chemical properties, leading to a change in the ratios when PAHs are transported in the atmosphere. As a result, the emission sources of PAHs can be misinterpreted, and the applicability of DRs should be considered carefully.

Statistical tools such as PCA are also applied for PAH source identification. PCA converts a data set into a few important explanatory factors, or principal components (PCs), accounting for most of the variance and highlighting the most important information of the original data set. Emission sources of PAHs can, therefore, be interpreted based on the PC values. However, a drawback of PCA is that it might not entirely separate the emission sources (Cesari et al., 2016; Jain et al., 2017). In other words, more than two emission sources might overlap in one PC, resulting in a deficiency of emission sources when interpreting the PCA results. Apart from PCA, PMF, a model developed by the US-EPA, can also be used to determine the PAH emission sources. In the PMF, the initial data sets are structured into two new data matrices or factors,

including factor contributions and factor profiles (US-EPA, 2014). The emission sources of PAHs can be determined by comparing PAH profiles from the PMF results with those from previous studies. The number of factors or sources can be set in the PMF, and the stability of a selected solution can be checked (Brown et al., 2015; US-EPA, 2014). Thus, an under- or overestimation of emission sources can be controlled.

In this study, both gaseous and particulate PAHs were collected from a semi-rural site in Ulsan over four seasons (June 2013–May 2014) to understand the seasonal variation and phase distribution of PAHs. In addition, the seasonal emission sources of PAHs were identified. Data on meteorological conditions and criteria air pollutants around the study area were also collected to examine their relations with atmospheric PAHs. This is the first study to observe the gas/particle partitioning of PAHs at a relatively high temporal resolution in Ulsan.

2.2. Materials and methods

2.2.1. High volume air sampling

Air samples were collected at 5 m above the ground level at the Ulsan National Institute of Science and Technology (UNIST), Ulsan, South Korea. UNIST (35° 34N, 129° 11E; 47 m above sea level) is at a semi-rural area, located west side of the urban and industrial areas of Ulsan (Figure 2-1). Two high volume air samplers (Sibata HV-700F, Japan) were used to collect duplicate PAH samples in the gaseous and particulate phases (n = 188) over four seasons (June 2013–May 2014). Samples from the November and December 2013 sampling efforts were lost [n = 16: 8 glass fiber filters (GFFs) and 8 polyurethane foam disks (PUFs)]. The air sampling was conducted once a week for 24 h (from 11:00 AM to 11:00 AM of the next day). The total air volume of each sample was 1,007.9 m^3, and the operational flow was set at 700 L/min. Samples in the particulate and gaseous phases were collected using a GFF (20.3 cm × 25.4 cm, Advantec, Japan) and a PUF disk (4.5 cm radius × 5.0 cm height, Ziemer Chromatographie, Germany), respectively.

Prior to sampling, the GFFs were pre-treated by baking at 400 °C for 4 h and the PUFs were cleaned by sonication respectively with acetone and n-hexane for 30 min. The GFFs and PUF disks were kept in aluminum foil and transported to the sampling site without exposure to ambient air. After sampling, they were put in aluminum foil and polyethylene double zippered bags and stored at −4 °C until analysis.

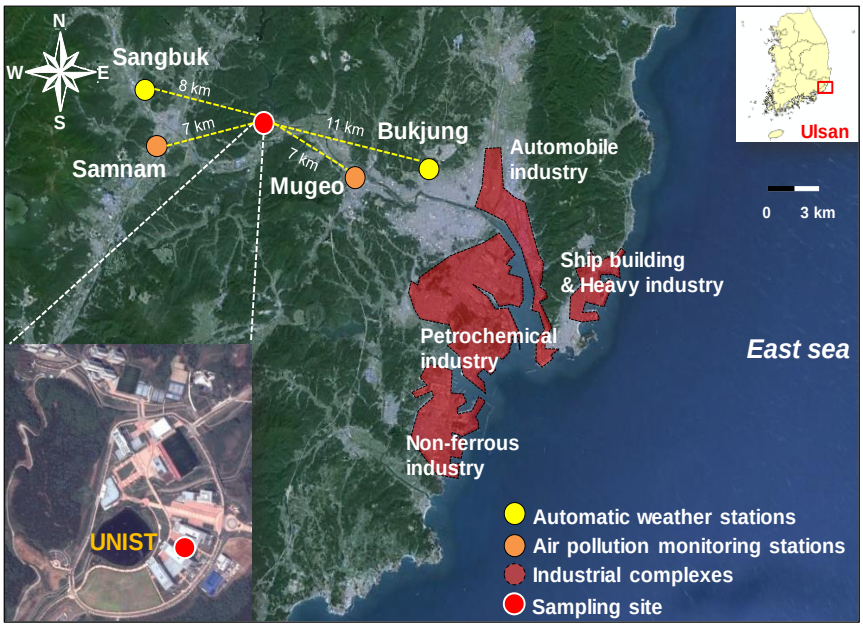

Figure 2-1. Sampling site location (UNIST). Industrial areas are shaded in red. Automatic weather stations and air pollution monitoring stations located near the sampling site are shaded in yellow and orange, respectively.

2.2.2. Meteorological conditions and criteria air pollutant data

Meteorological conditions are one of the most important factors governing the levels and behavior of atmospheric PAHs (Tham et al., 2008). Hence, meteorological data were collected from two of the Korean meteorological administration (http://kma.go.kr) automatic weather stations located near the sampling site, namely Sangbuk (35º 34N, 129º 05E) and Bukjung (35° 33N, 129° 19E). In addition, the Hysplit model (http://ready.arl.noaa.gov/HYSPLIT_traj.php) was used to evaluate the possibility of long-range transport of PAHs to the sampling site.

Criteria air pollutant data (SO_2, CO, O_3, NO_2, and PM_{10}), measured at air pollution monitoring stations in Ulsan, were also obtained via the website of the Ulsan Institute of Health and Environment (http://air.ulsan.go.kr). The Samnam (35º 29N, 129º 18E) and Mugeo (35° 33N, 129° 15E) stations were selected for data collection because they are in the vicinity of the sampling site.

2.2.3. Chemical analysis and QA/QC

PAHs were separately extracted from the GFFs and PUFs using Soxhlet extractors with 350 mL of n-hexane/acetone (9:1) (Choi et al., 2012b). Prior to the extraction, the samples were spiked with surrogate standards (naphthalene-d_8, acenaphthene-d_{10}, phenanthrene-d_{10}, chrysene-d_{12}, and perylene-d_{12}). The extracted samples were then concentrated to 10 mL using a Turbo Vap (Caliper, USA). Subsequently, 1 mL of the extract underwent silica gel cleanup on a column comprising 2 g of sodium sulfate, 5 g of silica gel (activated at 130 °C for 4 h), and 2 g of anhydrous sodium sulfate. An elution solvent composed of 70 mL of n-hexane/dichloromethane (9:1) was used. The sample was then concentrated to 0.5 mL using a nitrogen evaporator (Eyela, Japan), transferred to gas chromatography (GC) vials, and finally spiked with an internal standard (p-terphenyl-d_{14}).

The final samples were analyzed using gas chromatography coupled to a mass spectrometer (GC-MS, 5975C, Agilent, USA). The analyte separation process was performed on a DB-5MS column (30 m × 0.25 mm × 0.25 μm). An amount of 1 μL of the final sample was injected into the GC at 300 °C under splitless mode. The initial temperature of the GC was 70 °C and was increased to 240 °C at 10 °C/min increments; finally, it was increased to a final temperature of 300 °C at 5 °C/min increments. Helium was used as the carrier gas in the GC/MS and was set at a flow rate of 1 mL/min.

Among the 16 US-EPA priority PAHs, naphthalene, acenaphthylene, and acenaphthene were not considered in this study due to their low recoveries, blank contamination, and potential sampling artifacts. Field blanks were also collected (n = 15). The pre-treatment and analytical methods used for the blanks were the same as those used for the real samples. The concentrations of PAHs in this study were field-blank corrected to eliminate errors stemming from contamination during the sampling events. Average recoveries of the GFF samples were 54%, 78%, and 73% for phenanthrene-d_{10}, chrysene-d_{12}, and perylene-d_{12}, respectively. Regarding the PUF samples, average recoveries were 68% for phenanthrene-d_{10}, 84% for chrysene-d_{12}, and 78% for perylene-d_{12}. Method detection limits (MDL) of the gaseous and particulate PAHs were individually determined based on the following equation:

$$MDL = SD \times 3.14 \quad (2\text{-}1)$$

where SD denotes the standard deviation of 7 replicate spiked samples, and 3.14 is the Student's t value for a 99% confidence interval. Method detection limit (MDL) values were 0.04–0.19

ng/m^3 for the GFF samples and 0.04–0.25 ng/m^3 for the PUF samples. Data below the MDLs were designated as non-detects (ND). For data sets with ND, mean values were estimated using the ProUCL 5.0 software (https://www.epa.gov/land-research/proucl-software).

2.2.4. Gas/particle partitioning calculation

The gas/particle partitioning of PAHs was investigated by fitting the original Junge-Pankow equation to the particulate fractions of the measured individual PAHs. This approach was reported to provide better results for PAHs than the log-linear regression using partition coefficients (Su et al., 2006). Equations for the gas/particle partitioning calculation are as follows:

Fraction in the particulate phase: $$\Phi = \frac{C_p}{C_p + C_g} \quad (2\text{-}2)$$

One-parameter model: $$\Phi = \frac{A}{A + P_L} \quad (2\text{-}3)$$

Two-parameter model: $$\Phi = \frac{1}{1 + 10^{-m \log (P_L/\mathrm{Pa}) - b'}} \quad (2\text{-}4)$$

where Φ is the fraction in the particulate phase. C_p and C_g (ng/m^3) are the concentrations in the particulate and gaseous phases, respectively. P_L (Pa) is the sub-cooled liquid vapor pressure of PAHs. The P_L values were adjusted corresponding to the sampling temperature by using the P_L and enthalpies of vaporization ($\Delta_{vap}H$) data at 25 °C from Lei et al. (2002). A, m, and b' are fitting parameters, determined by fitting values of Φ and temperature-adjusted P_L into the non-linear regressions. OriginPro 9.2 (OriginLab, USA) was used for parameter fitting.

2.2.5. Methods for source identification

Three methods (i.e., DRs, PCA, and PMF) were simultaneously used to elucidate potential sources of PAHs in the sampling area. The comparison of results from these methods enabled a more precise interpretation of the emission sources of PAHs.

2.2.5.1. Diagnostic ratios (DRs)

Two PAH ratios, Ind/(Ind + BghiP) and Flt/(Flt + Pyr), were applied in this study since they classified the samples into two clear sets and explained the data well. The DR method is straightforward; however, a change in DR values during the atmospheric transport of PAHs (Biache et al., 2014) can result in an ambiguous interpretation of PAH sources.

2.2.5.2. Principal component analysis (PCA)

The total (gas + particle) concentrations of PAHs were used as input data for the PCA and were normalized by dividing them by the total concentration of each sample. To avoid detection limit issues (Meglen, 1992), only PAHs having high detected frequencies were chosen for the PCA. In this study, the PCA was conducted using SPSS 22.0 software (Spss Inc, USA). The rotation method was varimax, and eigenvalues higher than one were used for the PC extraction criterion.

2.2.5.3. Positive matrix factorization (PMF)

Total (gas + particle) concentrations of PAHs were used as input data for PMF. The input data for calculating uncertainty were based on the MDLs. Details on the calculation method for data uncertainty can be found elsewhere (US-EPA, 2014). For the PMF application, the accuracy of the results is affected by the identification of the number of factors or sources. In this study, a change in the Q value based on several solutions was noted to determine the number of factors. Specifically, a smaller variation in $Q_{robust}/_{expected}$ when moving from lower to higher factor numbers, suggests a potential overestimation of the factor numbers (Brown et al., 2015). Moreover, the effect of each species on the source results can be controlled in the PMF approach, based on a signal/noise value. For this study, four PAHs, including Flu, Phe, Flt, and Pyr, were set as strong species. Weak species comprised Ant, Chr, BaA, BbF, BkF, BaP, Ind, and BghiP. Only DahA was set as bad and excluded from the PMF (US-EPA, 2014).

2.3. Results and discussion

2.3.1. Concentrations of PAHs

Table 2-1 shows the PAH concentrations observed over the sampling period. Mean concentrations of the Σ_{13} PAHs in the gaseous, particulate, and total phases were 4.11 ng/m^3, 2.55 ng/m^3, and 6.67 ng/m^3, respectively. The mean concentration of the gaseous phase was 1.6 times higher than that of the particulate phase (Mann-Whitney rank-sum test, $p < 0.01$). This is consistent with results from previous studies (Jamhari et al., 2014; Tomaz et al., 2016; Wang et al., 2011b; Wei et al., 2015). The gaseous PAHs can be decomposed easier than the particulate ones because of their high mobility (Ravindra et al., 2008). Additionally, the PAHs in the gaseous phase tend to have lower levels at the receptors in case of long-range transport (Choi et al., 2012a) because they can undergo degradation during transportation from the emission sources to the receptors. Hence, higher fractions of the gaseous PAHs during all the sampling period might reflect stronger effects of local emission sources. Note that a mean G/P

partitioning ratio of Phe (17.8), a dominant compound among the target PAHs, is 10.4 and 1.7 times higher than those at a background site in Jeju and an urban site in Seoul, Korea (Kim et al., 2012). This result suggests that a G/P partitioning ratio of total PAHs or individual PAHs can be used for an indicator of local pollution or long-range transport in Northeast Asia.

Table 2-1. Range and mean of PAH concentrations (ng/m^3) for the entire sampling period in Ulsan, South Korea. Mean values for each compound with non-detected values below 50% and values in the range of 50%–80% were estimated using the Kaplan-Meier method and the regression on order statistics method, respectively.

Compounds	Gas			Particle			Total		
	Range	Mean	ND (%)	Range	Mean	ND (%)	Range	Mean	ND (%)
Fluorene (Flu)	ND–3.09	0.53	2	ND–0.12	0.07	53	ND–3.13	0.59	2
Phenanthrene (Phe)	0.47–5.96	2.14	0	ND–0.44	0.12	23	0.53–6.03	2.26	0
Anthracene (Ant)	ND–0.52	0.11	28	ND–0.10	0.08	53	ND–0.59	0.18	28
Fluoranthene (Flt)	0.11–1.48	0.64	0	ND–1.36	0.29	17	0.22–2.41	0.94	0
Pyrene (Pyr)	0.08–1.48	0.50	0	ND–0.91	0.24	32	0.18–2.16	0.76	0
Benzo(a)anthracene (BaA)	ND–0.13	0.05	55	ND–0.77	0.14	30	ND–0.84	0.20	30
Chrysene (Chr)	ND–0.26	0.09	19	ND–1.30	0.30	9	ND–1.42	0.38	4
Benzo(b)fluoranthene (BbF)	ND–0.13	0.02	83	0.10–2.38	0.51	0	0.10–2.47	0.57	0
Benzo(k)fluoranthene (BkF)	ND	ND	100	ND–0.74	0.22	4	ND–0.88	0.29	4
Benzo(a)pyrene (BaP)	ND	ND	100	ND–0.83	0.16	15	ND–0.91	0.19	15
Indeno(123-cd)pyrene (Ind)	ND	ND	100	ND–1.13	0.23	2	ND–1.38	0.32	4
Dibenzo(ah)anthracene (DahA)	ND	ND	100	ND–0.17	0.07	51	ND–0.28	0.08	51
Benzo(ghi)perylene (BghiP)	ND–0.07	0.01	91	0.05–0.90	0.23	0	0.06–0.97	0.27	0
Σ_{13} PAHs	1.04–10.9	4.11		0.84–10.3	2.55		2.02–21.3	6.67	

ND: Not detected

PAH concentrations in the four sampling seasons are illustrated in Figure 2-2. The total concentration in winter (11.07 ng/m^3) was approximately two times higher than those of the other seasons (Figure 2-2a) (summer: 5.12 ng/m^3, autumn: 6.10 ng/m^3, and spring: 5.01 ng/m^3). A statistically significant difference between winter and the other seasons was found (Mann-Whitney rank-sum test, $p < 0.05$). This result is in good agreement with those from previous studies (Baek et al., 1991b; Gustafson and Dickhut, 1997). The higher PAH concentrations in winter could be explained by an increase in condensation due to low temperatures, poor atmospheric dispersion, and elevated emissions from fossil fuel and wood burning for residential heating.

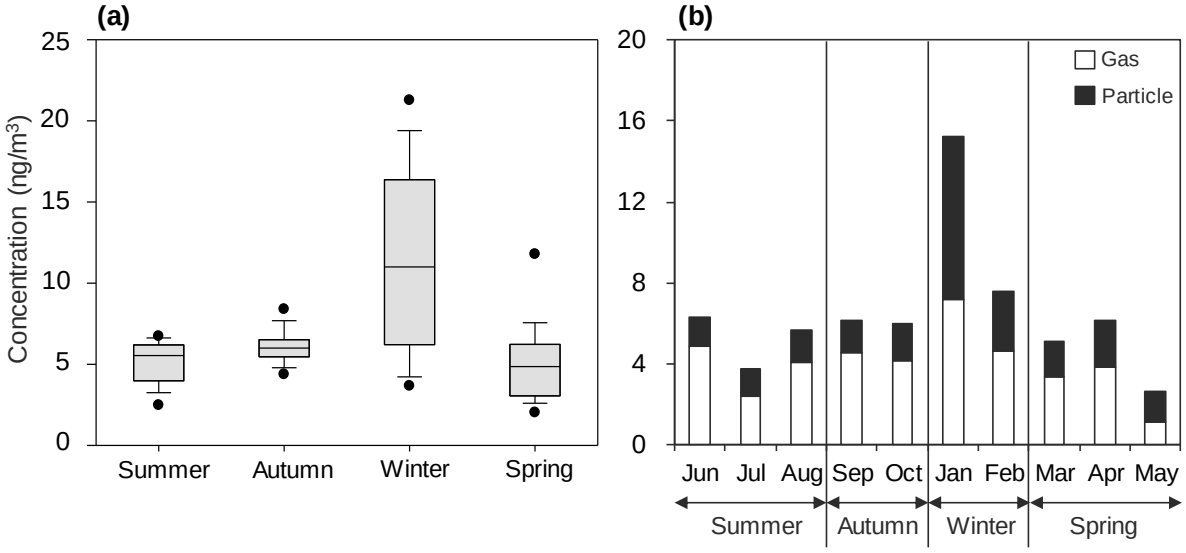

Figure 2-2. (a) Seasonal concentrations of the Σ_{13} PAHs and (b) monthly mean concentrations in the gaseous and particulate phases. The box plots denote the 25th and 75th percentiles and the total concentration. The solid dash is the median. The 90th and 10th percentiles are shown in the upper and lower whiskers, respectively. The outlying points denote the 5th and 95th percentiles.

The concentration of the Σ_{13} PAHs reached the lowest value in spring (May 26th: 2.02 ng/m^3) (Figure 2-2a). Generally, summer experiences the lowest PAH levels among the four seasons (Albuquerque et al., 2016; Lai et al., 2011) because the higher ambient temperatures and solar radiation are likely responsible for an increase in the decomposition reactions between PAHs and photochemical oxidants (i.e., OH radicals, O_3, and NO_3) (Baek et al., 1991a). Additionally, emission reduction (i.e., lack of coal combustion or biomass burning for warming) could be an explanation for the lower concentrations observed in summer. In Ulsan, the lowest Σ_{13} PAH concentration was found in spring. However, no significant difference was highlighted between the total concentration in the spring and those in summer or autumn (Mann-Whitney rank-sum test, $p > 0.05$). During the spring period, May showed the lowest and highest concentrations of PAHs and O_3, respectively (Figure 2-2b and 2-3f). This high O_3 level could activate more PAH degradation (Baek et al., 1991a) and result in the lower PAH concentrations observed in May. This interpretation is supported by a negative correlation between PAHs and O_3 in spring (Table 2-2). Moreover, May experienced the highest rainfall level over the sampling period (Figure 2-4), which could lead to higher wet deposition and the removal of PAHs from the atmosphere through deposition on the surface environment.

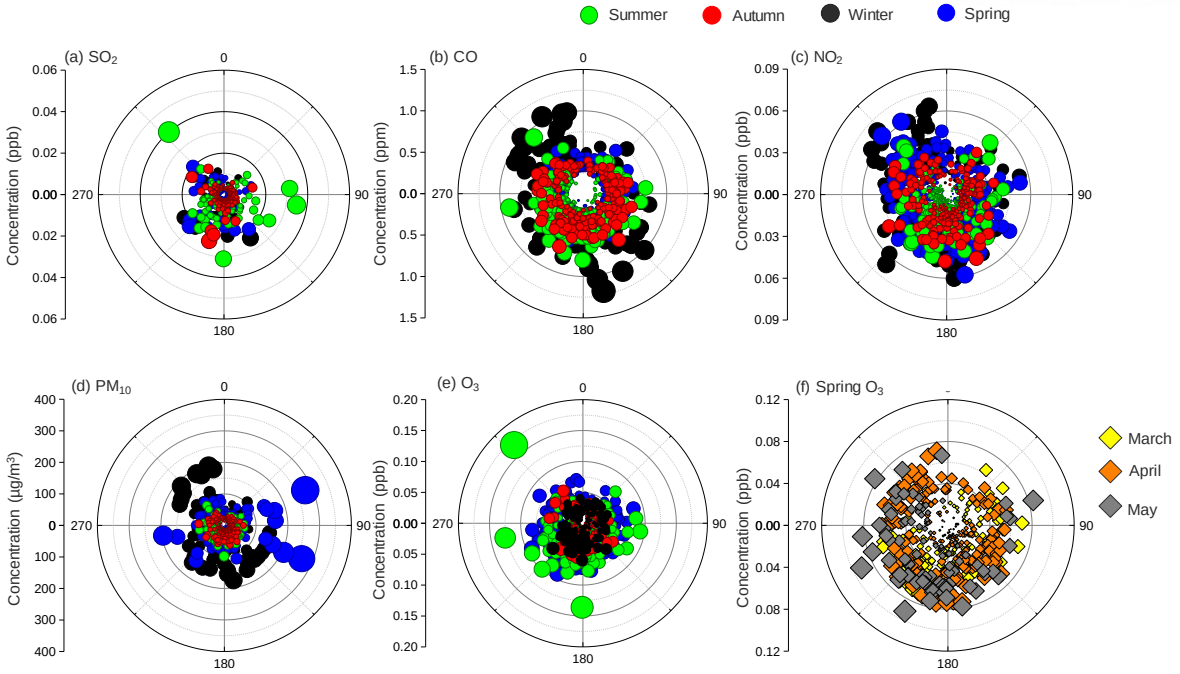

Figure 2-3. Pollutant-rose diagrams of criteria air pollutants in the four sampling seasons: (a) SO_2, (b) CO, (c) NO_2, (d) PM_{10}, (e) O_3, and (f) O_3 in spring. Concentration data were obtained from the air pollution monitoring stations located near the sampling site. Data on wind direction were gathered from automatic weather stations of the Korea Meteorological Administration, located near the selected air pollutant monitoring stations. The collected data have the same monitoring periods as the sampling events.

Table 2-2. Correlation of criteria air pollutants and PAHs in the gaseous, particulate, and total phases.

Season	Phase	SO_2	CO	O_3	NO_2	PM_{10}	Rainfall	Temp.	Wind speed
Summer	Gaseous	0.610*	0.292	0.395	0.686**	0.336	-0.367	-0.308	-0.662*
	Particulate	0.179	0.212	0.394	0.190	0.553*	0.409	-0.198	-0.500
	Total	0.669*	0.332	0.476	0.704**	0.460	-0.249	-0.374	-0.758**
Autumn	Gaseous	0.087	-0.362	-0.489	-0.254	0.140	-0.016	0.384	-0.174
	Particulate	0.130	0.240	0.105	0.288	0.374	0.455	-0.570	-0.311
	Total	0.234	-0.222	-0.411	0.119	0.056	0.216	0.076	-0.323
Winter	Gaseous	0.733*	0.509	-0.648*	0.567	0.364	-0.284	0.091	-0.464
	Particulate	0.696*	0.373	-0.697*	0.330	0.064	-0.541	-0.473	0.044
	Total	0.788**	0.480	-0.736**	0.485	0.264	-0.456	-0.200	-0.220
Spring	Gaseous	-0.016	0.398	-0.563*	0.312	0.345	-0.197	-0.749**	-0.484
	Particulate	0.329	0.147	-0.140	0.333	0.020	-0.200	-0.310	-0.189
	Total	0.357	0.465	-0.530	0.537*	0.085	-0.274	-0.670**	-0.569*

* Correlation is significant at the 0.05 level.
** Correlation is significant at the 0.01 level.

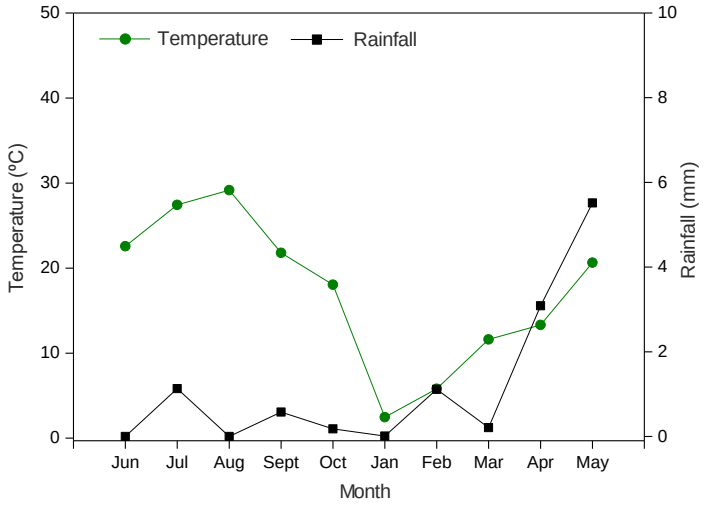

Figure 2-4. Average temperature and rainfall levels in each sampling month. Data were collected from automatic weather stations located near the sampling site (Sangbuk and Bukjung), operated by the Ulsan meteorological observatory.

In Ulsan, the industrial complexes are located in the eastern and southeastern areas of the city, and the sampling site is located west side of the industrial complexes (Figure 2-1). Several previous studies revealed that seasonal prevailing winds had an effect on the dispersion of air pollutants emitted from the industrial complexes into other areas of the city (Choi et al., 2012b; Clarke et al., 2014). In particular, southeasterly winds in summer (Figure 2-5a) could transfer PAHs from the industrial complexes to the sampling site. On the contrary, in winter and spring, large amounts of PAHs can be transported to the East Sea by northwesterly winds (Figures 2-

5c, d). Consequently, the influence of PAH emissions from industrial activities on the sampling site was expected to be higher and lower in summer and winter, respectively.

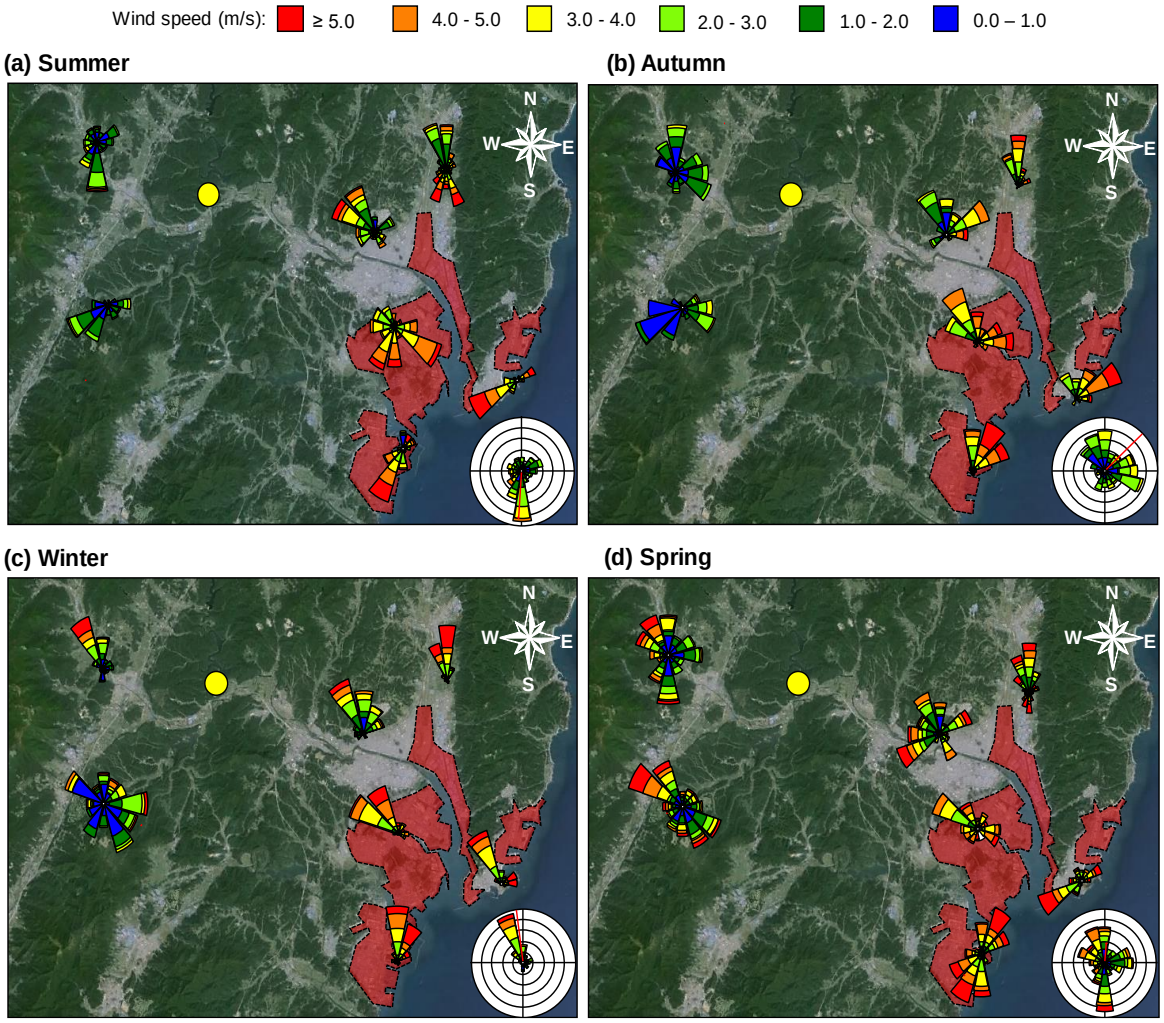

Figure 2-5. Wind-rose maps of the four sampling seasons: (a) summer, (b) autumn, (c) winter, and (d) spring. The yellow circle represents the sampling site. The industrial areas are shaded in red. The wind-rose plot at the right-bottom side represents the average values of two automatic weather stations located near the sampling site. The red line of this plot is a resultant vector. Only data during the sampling events were selected for wind roses. Data for wind roses have the same monitoring periods as the sampling events.

The gaseous, particulate, and total concentrations of the Σ_{13} PAHs in this study (gas: 4.11 ng/m^3, particle: 2.55 ng/m^3, total: 6.67 ng/m^3) were compared with former data from Korea and other Asian countries (Table 2-3). As the sampling and meteorological conditions were different, this is an approximate comparison to evaluate the PAH levels in Ulsan. Generally, the

concentrations of gaseous and particulate PAHs from this study were lower than those found in other countries, such as a suburban site of Guangzhou in China (gas: 103 ng/m^3, particle: 17.3 ng/m^3, total: 120 ng/m^3) (Yang et al., 2010). However, the concentrations of PAHs of this study were higher (gas: 4.11 ng/m^3, particle: 2.55 ng/m^3) than those at rural sites of the Hengchun Peninsula in Taiwan (total: 0.42–2.79 ng/m^3) (Cheng et al., 2016) or some background sites of Korea, such as Gosan (gas: 0.89 ng/m^3, particle: 1.74 ng/m^3) (Choi et al., 2012a) and Taean (particle: 0.37 ng/m^3) (Choi et al., 2013). Additionally, the level of particulate PAHs observed in this study (2.55 ng/m^3) was comparable to those from a suburban site of Bangi in Malaysia (2.54 ng/m^3) (Jamhari et al., 2014), which was reported to be affected by industrial activities, such as chemical and automobile production.

Table 2-3. Comparison of the PAH concentrations (ng/m^3) from selected Asian countries.

Country	Location	Type	Year	Gas	Particle	Total	Reference
China	Guangzhou [a,*]	Suburban	2005–2006	103	17.3	120	Yang et al. (2010)
China	Guangzhou [a,*]	Urban	2005–2006	110	19.5	130	Yang et al. (2010)
Japan	Yokohama[d,*]	Suburban	1999–2005	-	1.02	-	Salam et al. (2011)
Japan	Yokohama [d,*]	Urban	1999–2005	-	2.07	-	Salam et al. (2011)
Malaysia	Bangi [a,*]	Suburban	2010–2011	-	2.54	-	Jamhari et al. (2014)
Malaysia	Kuala Lumpur [a,*]	Urban	2010–2011	-	2.03	-	Jamhari et al. (2014)
Malaysia	Petaling Jaya [a,*]	Industrial	2010–2011	-	3.56	-	Jamhari et al. (2014)
Taiwan	Hengchun peninsula [a,*]	Rural	2010	0.39–2.31	0.01–1.36	0.42–2.79	Cheng et al. (2016)
Korea	Gosan [b,*]	Background	2002	0.89	1.74	2.63	Choi et al. (2012a)
Korea	Taean [c,**]	Background	2006–2009	-	0.37	-	Choi et al. (2013)
Korea	Seoul [c**]	Residential	2006–2009	-	3.70	-	Choi et al. (2013)
Korea	Gwangyang [c,**]	Iron & metal industrial	2006–2009	-	1.05	-	Choi et al. (2013)
Korea	Ulsan [b,*]	Semi-rural	2013–2014	4.11	2.55	6.67	This study

- No data
[*] High volume air sampler, [**] Medium volume air sampler
[a] 16 US-EPA PAHs
[b] 16 US-EPA PAHs except for Nap, Acy, and Ace
[c] 7 particulate PAHs (BaA, BaP, BbF, BkF, Chr, DahA, and Ind)
[d] 10 particulate PAHs (Flt, Pyr, BaA, Chr, BbF, BkF, BeP, BaP, Ind, and BghiP)
Nap: naphthalene, Acy: acenaphthylene, Ace: acenaphthene, BeP: benzo(e)pyrene

2.3.2. Phase distributions and profiles

Figure 2-6 presents the monthly gas/particle phase distributions of the Σ_{13} PAHs and profiles of ring-number groups. The dominant phases of PAHs varied seasonally. The contributions of the particulate (Figure 2-6a) and 5- and 6-ring (Figure 2-6b) PAHs in winter were apparently greater than those observed in the other seasons. This observation can be explained by the changes in emission profiles (i.e., combustion elevation for residential heating) and meteorological conditions (i.e., lower ambient temperature and lower mixing layer) that increase the adsorption of PAHs on particles. Fractions of the gaseous and 3- and 4-ring PAHs during summer and autumn (June to October) were higher than those in the other seasons. A higher temperature in this period (Figure 2-4) could result in an aerodynamic dilution effect, enhancing the desorption of particulate PAHs to the gas phase (Baek et al., 1991a). In addition, an influence of PAHs released from secondary sources (i.e., surface soils and surface water) (Keyte et al., 2013a; Wang et al., 2011b) could also contribute to the greater fractions of the gaseous PAHs during the high-temperature seasons.

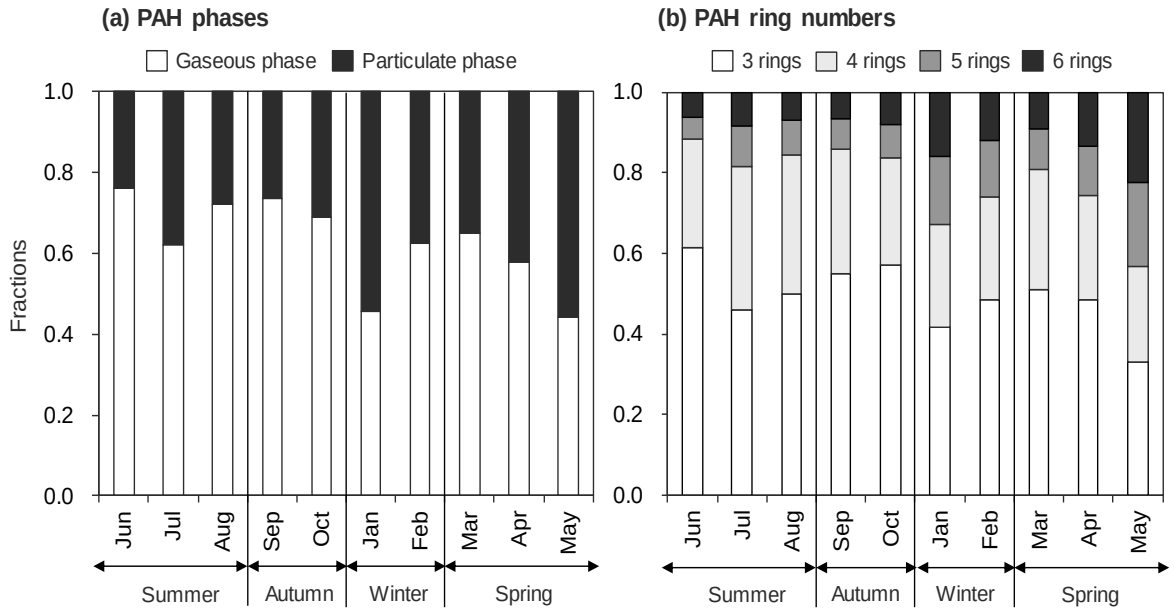

Figure 2-6. Temporal variations of (a) gas/particle phase distributions of the Σ_{13} PAHs and (b) ring-number fractions of individual PAHs.

Regarding the PAH species, 3- and 4-ring (i.e., Flu, Phe, and Flt) and 5- and 6-ring compounds (i.e., BkF, BaP, Ind, DahA, and BghiP) were dominant in the gaseous and particulate phases, respectively (Figure 2-7). This is because the vapor pressure of PAHs declines as the ring

numbers increase (Baek et al., 1991a), resulting in the LMW PAHs mainly existing in the gaseous phase, whereas most of the HMW PAHs occur in the particulate phase. These findings are in line with those from previous studies (Choi et al., 2012a; Yang et al., 2010).

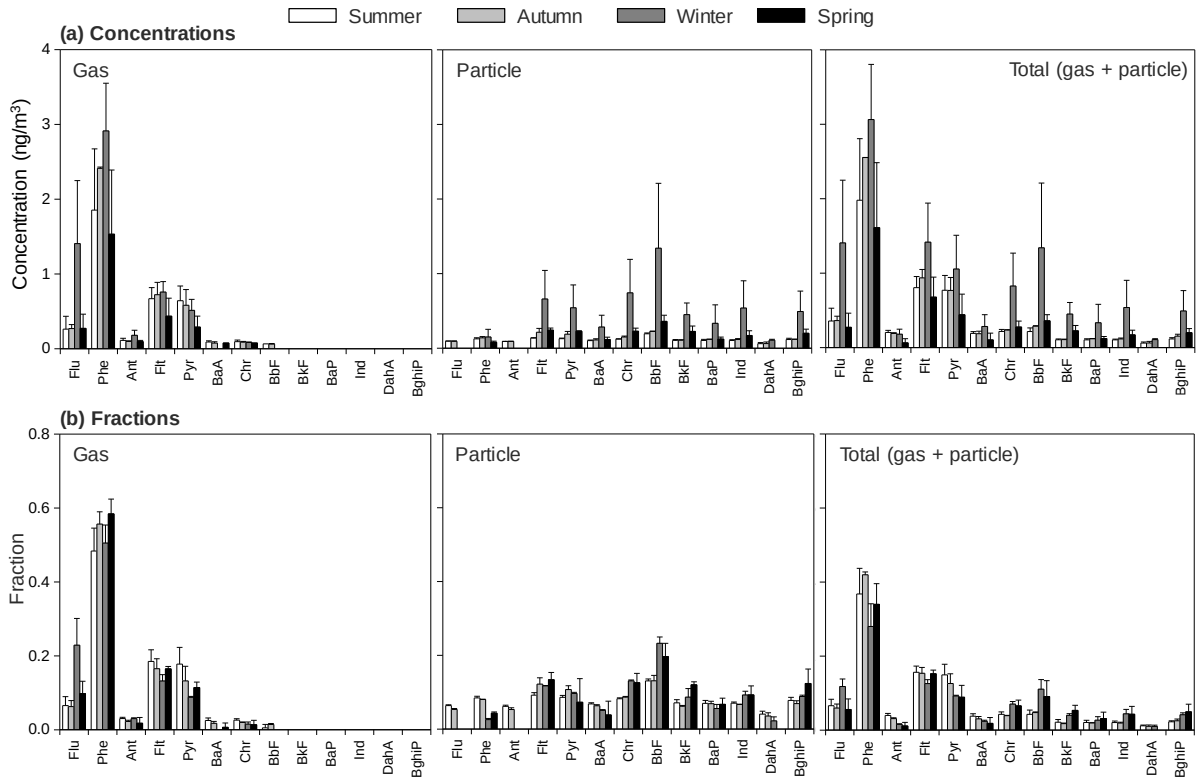

Figure 2-7. (a) Concentrations and (b) fractions of PAH species in the gaseous, particulate, and total phases during four sampling seasons.

Noticeably, the proportions of the particulate and 5- and 6-ring PAHs were elevated in April and May (Figure 2-6). Previous studies reported that the particle-bound PAHs with longer half-lives were more affected by long-range transport in South Korea (Choi et al., 2012a; Lee and Kim, 2007). According to air mass trajectories in these two months, the air masses that arrived at the sampling site were originated from the outside of South Korea, such as the Yellow Sea and northern regions of China (Figure 2-8). This might be attributed to the high fractions of the particulate PAHs in April and May.

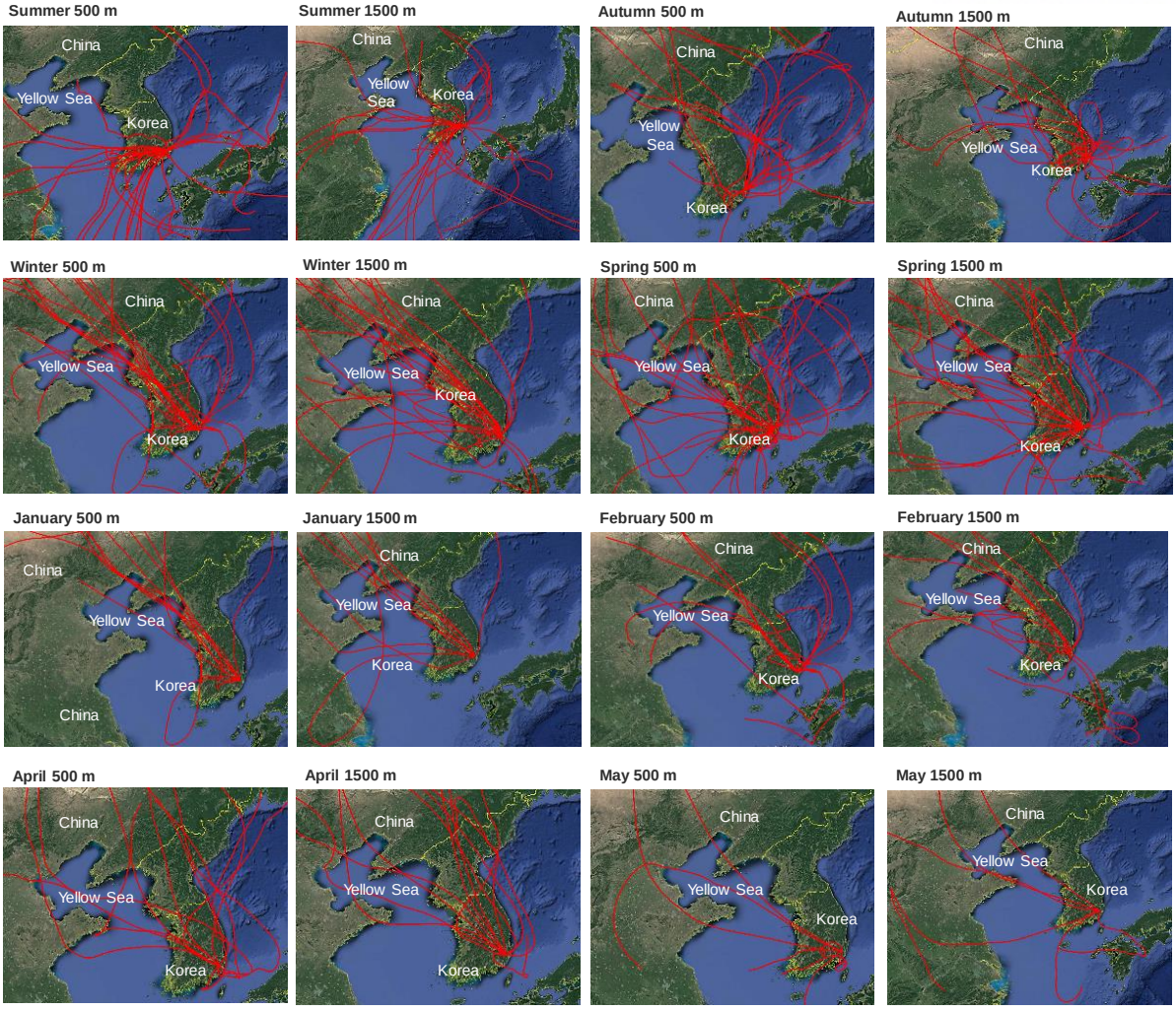

Figure 2-8. Backward air trajectories with starting heights of 500 m and 1,500 m arriving at UNIST, Ulsan, South Korea. The trajectories, shown in three-day intervals, were calculated twice a day at 00 and 12 UTC (coordinated universal time) for the entire sampling period.

2.3.3. Gas/particle partitioning of PAHs

Figure 2-9 illustrates the fitting curves and gas/particle partitioning behavior of PAHs for all the sampling seasons. The seasonal fitting curves for the one- and two-parameter models showed fairly similar orders: summer, autumn, spring, and winter from the left to the right of the figures. These results indicate that summer and winter exhibited the lowest and highest contribution of the particulate PAHs, respectively. The profiles of PAHs over the sampling period (Figure 2-6) also support this observation.

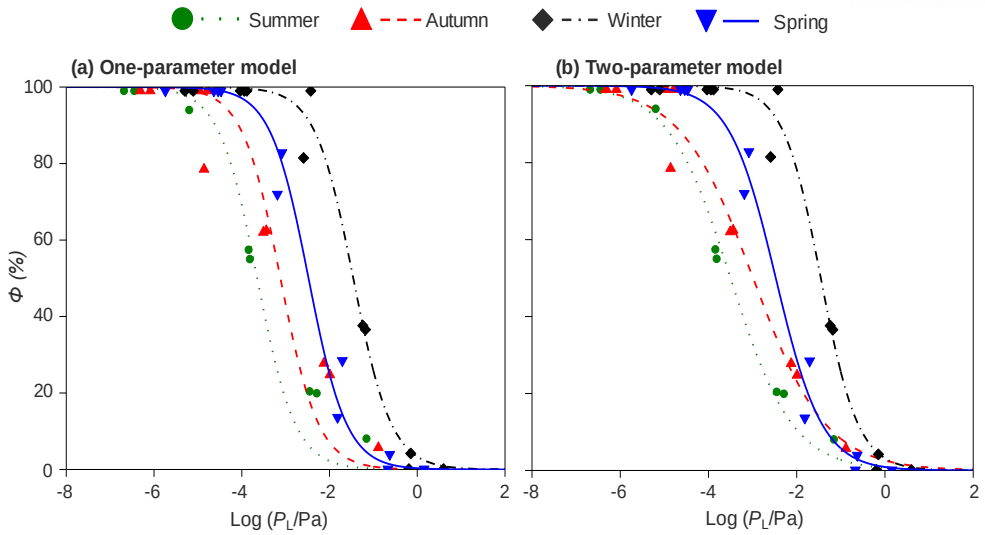

Figure 2-9. Seasonal mean gas/particle partitioning of PAHs and nonlinear fitting curves for (a) the one-parameter model and (b) the two-parameter model.

For the one-parameter model, A is relevant to the capacity of particles for PAHs (Su et al., 2006). The greater A values in winter and spring (Table 2-4) (Mann-Whitney rank-sum test, $p < 0.05$) reflected higher contributions of the particulate PAHs in these two seasons. As discussed in Sections 2.3.1 and 2.3.2, the seasonal changes in profiles of PAHs and meteorological conditions (e.g., lower mixing height) could be an explanation for this gas/particle partitioning behavior.

Table 2-4. Regression results of two different non-linear G/P partitioning models.

Period	One-parameter model		Two-parameter model		
	$A \times 10^5$	R^2	m	b'	R^2
Summer	21.9	0.9996	-0.63	-2.19	0.9998
Autumn	76.2	0.9991	-0.53	-1.57	0.9992
Winter	3,510	0.9997	-1.02	-1.48	0.9997
Spring	334	0.9997	-0.82	-2.04	0.9971
June	29.9	0.9996	-0.67	-2.31	0.9684
July	23.0	0.9995	-0.61	-2.11	0.9696
August	17.1	0.9996	-0.61	-2.22	0.9719
September	54.9	0.9995	-0.61	-1.92	0.9764
October	64.0	0.9967	-0.37	-0.93	0.8331
January	8,950	0.9999	-1.47	-1.53	0.9970
February	1,420	0.9995	-1.06	-1.93	0.9723
March	441	0.9907	-0.95	-2.21	0.5063
April	384	0.9914	-0.64	-1.55	0.4898
May	332	0.9958	-0.83	-2.88	0.7350

Regarding the two-parameter model, the mean values of *m* in summer, autumn, winter, and spring were -0.63, -0.53, -1.02, and -0.82, respectively. The values of *m* for winter and spring were statistically different from those of the other seasons (Mann-Whitney rank-sum test, $p < 0.05$). This result also indicates that winter and spring exhibited the different behavior of the gas/particle partitioning, i.e., increased contributions of particulate PAHs.

The slope *m* can be applied to interpret the contribution of particulate PAHs. In general, the lower *m* value implies a higher fraction of the particle-bound PAHs (Su et al., 2006). In this study, a smaller *m* value (mean: -0.83) in May compared to that in April (mean: -0.64) (Table 2-4) indicates the relatively higher fractions of particulate PAHs. As discussed in Section 2.3.2, the elevated contribution of particulate PAHs in May might be due to long-range transport. The influence of springtime long-range transport on gas/particle partitioning of PAHs in South Korea was also demonstrated in previous studies (Choi et al., 2012a; Kim et al., 2012; Lee and Kim, 2007).

2.3.4. Source identification

2.3.4.1. Diagnostic ratios (DRs)

Figure 2-10 illustrates a scatter plot of two selected DRs for samples from the four sampling seasons. These isomer ratios are considered as good PAH source markers because their photodegradation rates are comparable (Yunker et al., 2002). The total concentrations (gas + particle) of PAHs were used to avoid the effect of gas-particle partitioning (Tobiszewski and Namieśnik, 2012). The Ind/(Ind + BghiP) ratio was used to distinguish petroleum combustion from grass/wood/coal burning, and the Flt/(Flt + Pyr) ratio was used to discriminate between pyrogenic and petrogenic sources (Yunker et al., 2002).

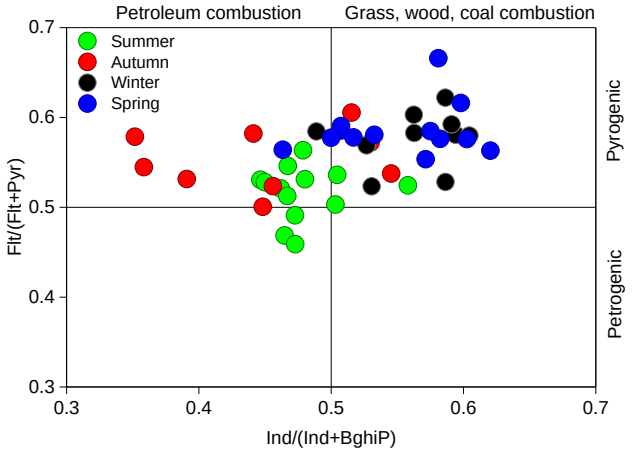

Figure 2-10. Scatter plot of Ind/(Ind + BghiP) versus Flt/(Flt + Pyr). The thresholds of PAH sources are illustrated as horizontal and vertical lines.

As shown in Figure 2-10, pyrogenic sources (i.e., grass/wood/coal combustion) were obviously dominant in winter and spring. Other pyrogenic sources (e.g., petroleum combustion) and petrogenic sources were identified in summer and autumn. The influence of pyrogenic and petrogenic sources, especially in summer, might stem from seasonal winds bringing PAHs from the petrochemical and the non-ferrous industrial complexes that use crude oil, coke, and coal (Kwon and Choi, 2014a). In particular, the predominant southeasterly winds in summer and autumn (Figure 2-5) could transport PAHs emitted from these areas toward the sampling site. The influence of the industrial activities on Ulsan's inner areas during summer has been previously reported (Clarke et al., 2014). Moreover, higher levels of SO_2, the main pollutant derived from fossil fuel burning, in summer and autumn (Figure 2-3) support the impact of industrial activities on the conditions observed at the sampling site.

2.3.4.2. Principal component analysis (PCA)

Figure 2-11 describes the PCA results for PAHs across the four sampling seasons. Three PCs having eigenvalues greater than one were extracted; overall, they span 83% of the total data variance (first PC: 35%, second PC: 24%, and third PC: 22%). The score and loading plots were used to elucidate relations between the samples and PAH species.

Generally, the samples from summer and autumn overlapped each other (Figure 2-11), reflecting the same major emission sources during these seasons. Their positions were primarily to the left (Figure 2-11a,b) and bottom side (Figure 2-11c) of the score plots,

characterized by Phe, Flu, Pyr, and Flt. These PAHs were reported to be dominant in sources such as exhaust from highway tunnels (Khalili et al., 1995) or diesel and gasoline engines (Cheruiyot et al., 2015). Hence, exhaust from transportation activities could be an important source of PAHs in summer and autumn. In addition, the combustion of fuel oil (i.e., kerosene, bunker A, bunker B, and bunker C) releases higher fractions of Phe, Flt, Pyr, and Flu (US-EPA, 1995). In 2014, bunker A (97 barrels) and a large amount of bunker C (1,566 barrels) in the industrial areas of Ulsan were used for energy production, especially the petrochemical industrial complex (KEEI, 2014). PAHs derived from these areas could be transported to the sampling site by the prevailing winds in summer and autumn (Figure 2-5). Therefore, fuel oil combustion could also be another important source of PAHs during the two seasons.

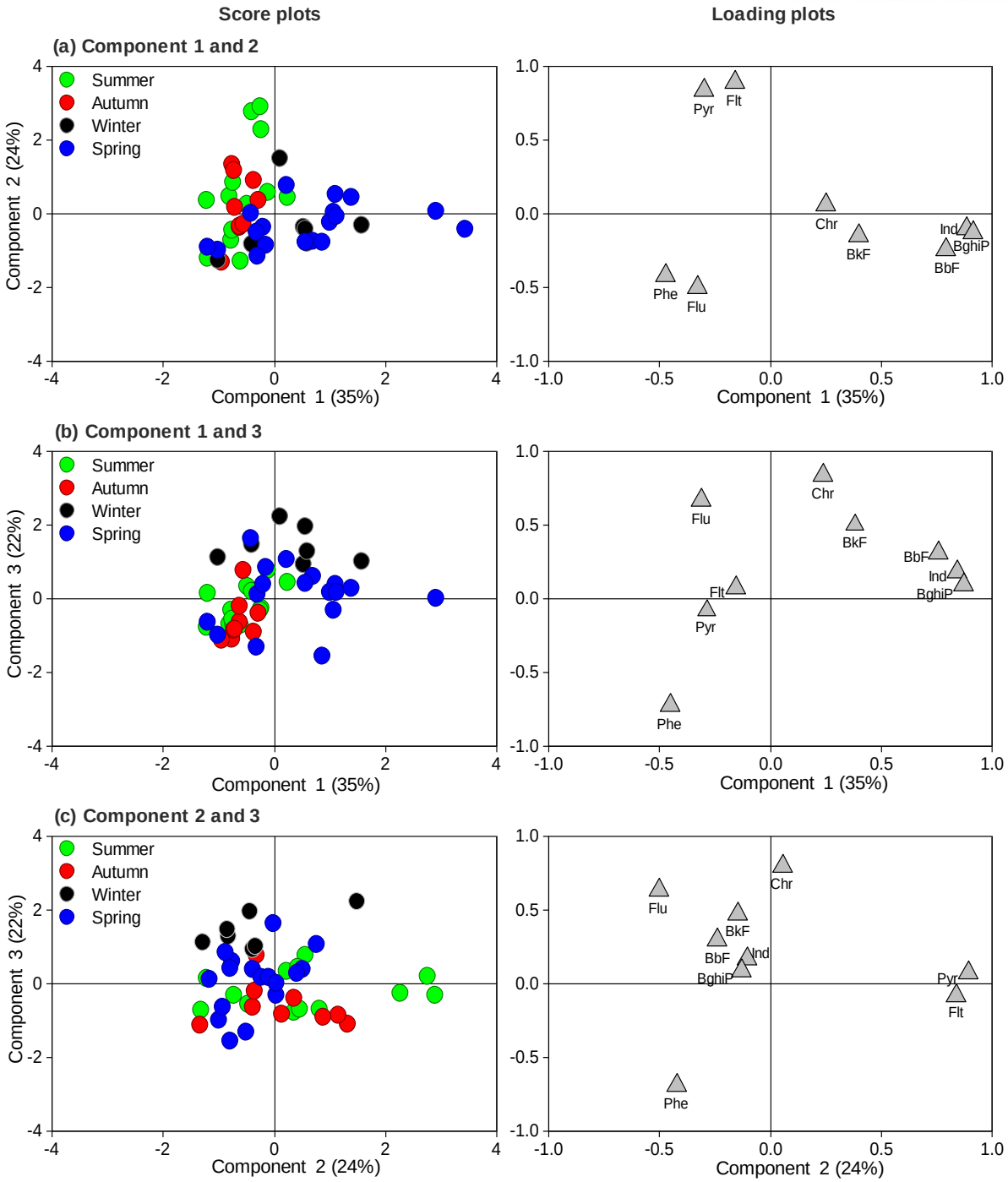

Figure 2-11. Score and loading plots of the total (gas + particle) PAHs corresponding to principal components (a) 1 and 2, (b) 1 and 3, and (c) 2 and 3.

The winter samples were well separated from those of summer or autumn, as denoted by their locations at the bottom (Figure 2-11a), upper right (Figure 2-11b), and upper left (Figure 2-11c) side of the score plots. The winter samples showed relatively high fractions of heavy PAHs (i.e., Chr, BkF, BbF, Ind, and BghiP), with Chr, BkF, and BbF known as markers for coal

combustion (Ravindra et al., 2008; Zou et al., 2015) and coke ovens (Yang et al., 1998; Zou et al., 2015). Additionally, pyrogenic PAH patterns are characterized by the HMW PAHs (Stogiannidis and Laane, 2015), suggesting that pyrogenic sources (e.g., traffic emission, coal combustion, and biomass burning, etc.) were significant in winter. The spring samples were similar to those of summer, autumn (Figure 2-11b, c), and winter (Figure 2-11a), suggesting that this season could be influenced by mixed sources.

2.3.4.3. Positive matrix factorization (PMF)

The PMF was applied to provide more quantitative information on source apportionment and to compare with the results from PCA and DR. Figure 2-12 shows the results of PMF modeling. Three to five PMF factor numbers were tested based on previous studies investigating the PAH emission sources in Ulsan (Dong and Lee, 2009; Kwon and Choi, 2014a). After comparing the $Q_{robust/expected}$ ratio while increasing factor numbers (Brown et al., 2015), a solution with four factors was selected. The uncertainty of each PMF solution was also checked to validate the number of factors chosen (US-EPA, 2014). The detailed results and discussion are shown in Table A1-1 and Text A1-1 in Appendix 1.

The results demonstrated that factor 1 could represent gasoline and heavy oil combustion. This factor accounted for 18% of the total measured data and was dominated by Flt, Pyr, BbF, Chr, Ind, and BghiP (Figure 2-12a). Heavy oil combustion (Li et al., 1999) and gasoline emissions (Ravindra et al., 2008) are represented by Flt, Pyr, Flu, and Ind markers. With the exception of the higher value observed in January, most of the sampling months showed comparable contributions from factor 1. Cold condensation and low air dispersion in winter might result in greater contributions from factor 1 in winter. In addition, summer and autumn (June-October) showed higher levels of factor 1 than spring (March-May). This may reflect the contribution of heavy oil (i.e., bunker A and bunker C) combustion in the industrial complexes (KEEI, 2014) transported by the main seasonal wind.

Factor 2 comprised 25% of the total measured data and denoted coal combustion and coke ovens, with Phe, Flu, BbF, Chr, Ind, and BghiP being the dominant species of this factor. The primary markers for coal combustion (Zou et al., 2015) and coke ovens (Yang et al., 1998) were recognized as Phe, Flu, Chr, and BbF. Winter (January and February) showed relatively high fractions of factor 2 (Figure 2-12a) because of an increase in fossil fuel burning for residential heating and also an enhanced long-range transport of PAHs from the outside of

South Korea (Figure 2-8) (Lee and Kim, 2007). Interestingly, the samples from June also have a great proportion of factor 2 (Figure 2-12a), probably due to the effect of southeasterly seasonal winds bringing PAHs emitted from industrial activities, such as non-ferrous production via coke oven operations (Kwon and Choi, 2014a). In fact, relatively high concentrations of SO_2 were observed in June (Figure 2-3) and are thought to be mostly derived from fossil fuel burning (coal and heavy oil in Ulsan).

Factor 3, accounting for 16% of the total measured PAHs, represents biomass burning sources. This factor showed high contributions of Phe, Ant, BaA, Chr, BbF, and BaP. Among them, BaA and BaP are typically released from biomass burning (Stogiannidis and Laane, 2015) and Phe and BaA are known as source markers for straw combustion (Lu et al., 2009). Results from summer (June-August) and autumn (September and October) showed higher contributions from factor 3 compared with the other seasons. As the sampling site is in a semi-rural area, open burning and post-harvest combustion might explain the greater contributions of biomass burning during summer and autumn, respectively.

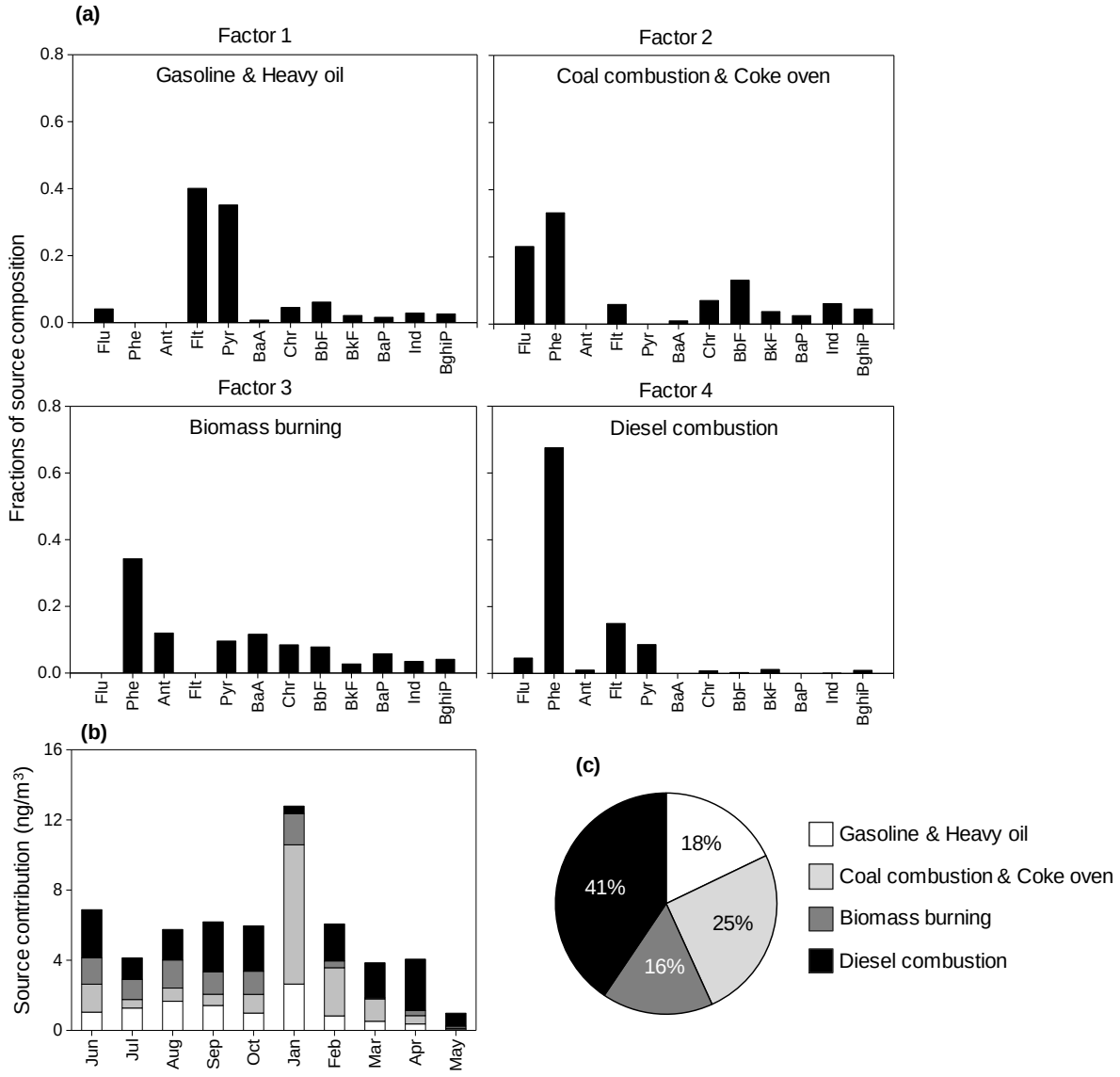

Figure 2-12. PMF results: (a) PAH profiles of each factor/source, (b) source contributions for each sampling month, and (c) source contributions over the sampling period.

Factor 4 explained 41% of the total PAHs and represented diesel combustion. Factor 4 was contributed by the highest fraction of Phe, followed by Flt, Pyr, Flu, and BbF (Figure 2-12a). Emissions from diesel combustion are reported to be enriched in Phe, Flt (Stogiannidis and Laane, 2015), and BbF (Ravindra et al., 2008). The spring season, especially April, exhibited higher levels of factor 4 than the other seasons (Figure 2-12b). In fact, concentrations of NO_2 were greater in spring than those in summer and autumn (Figure 2-3). This might suggest a stronger contribution of exhaust from transportation activities in spring, leading to the greater levels of factor 4. Moreover, the amount of PAHs released from heavy-diesel vehicles was

reported to be greater than that released from light-gasoline vehicles (Kwon and Choi, 2014a). This could potentially explain the higher contribution (41%) from diesel combustion over the sampling events (Figure 1-12c).

2.4. Conclusion

The results of this study demonstrate a seasonal variation in PAH concentrations and phase distributions. Winter and spring experienced the highest and lowest PAH concentrations, respectively. The concentrations of gaseous PAHs, which mostly depend on local emission sources, were greater than those of particulate ones. The heavy or 5- and 6-ring PAHs contributed to a greater proportion of PAHs in winter, whereas light or 3- and 4-ring PAHs were more prominent in summer and autumn. In addition, the highest and lowest fractions of particulate PAHs were observed in winter and summer, respectively. The gas/particle partitioning of PAHs in spring and winter exhibited different behavior, i.e., the higher contributions of the particulate PAHs.

The emission sources of PAHs also varied seasonally. Pyrogenic related emissions (e.g., coal combustion) were proposed as the primary emission sources in winter. The DRs suggested other types of pyrogenic (e.g., petroleum combustion) and petrogenic sources for summer and autumn. Moreover, the results from PCA and PMF supported these findings and additionally revealed the contribution of traffic emission/diesel combustion and industrial fuel oil (i.e., bunker C) combustion. These sources seasonally impacted the samples measured at the sampling site as a result of the predominant wind patterns. Spring was characterized by mixed emission sources, including diesel and coal combustion or biomass burning.

Ulsan has huge industrial complexes such as petrochemical and non-ferrous industries which are considered to be noticeable emission sources of PAHs. Therefore, long-term investigations on PAHs in multimedia environmental compartments of Ulsan are essential. This study contributes to the understanding of seasonal variation in atmospheric PAHs and provides comparable results across three source identification methods: DRs, PCA, and PMF. Thus, this approach can be used in future studies on the source–receptor relations of atmospheric PAHs

.

Chapter 3: Identification of source areas of polycyclic aromatic hydrocarbons in Ulsan, Korea using hybrid receptor models and conditional bivariate probability function

Abstract

In this study, source areas of atmospheric polycyclic aromatic hydrocarbons (PAHs), monitored in Ulsan, South Korea between June 2013 and May 2014, were identified using hybrid receptor models, including potential source contribution function (PSCF) and concentration weighted function (CWT), and the conditional bivariate probability function (CBPF). The PSCF and CWT were modified by adopting trajectory segments within the mixing layers. Especially, 'fraction-weighted trajectory' (FWT), a combination of gas/particle partitioning of PAHs with the hybrid receptor model, is firstly introduced in this study to improve the source identification of organic compounds. The hybrid receptor models and CBPF suggested that the particulate PAHs in Ulsan could be more affected by distant emission sources in the spring and winter, such as long-range transport from northeastern China, northern China, and North Korea. In contrast, the gaseous PAHs were affected by local emissions mostly throughout the year. In addition, the FWT would discriminate the local and distant sources more effectively, especially in summer and fall when the local sources increased their contribution. Moreover, the source areas validated by the modified PSCF and CWT could be more suitable than those confirmed by the conventional ones, demonstrating that the transport altitude of the air parcels should be considered for the identification of source areas.

3.1. Introduction

In the atmosphere, PAHs exist in gaseous or particulate phases depending on their molecular weights and meteorological conditions (e.g., ambient temperature and humidity). The physiochemical properties of the gaseous and particulate PAHs (e.g., mobility, half-life, and volatility) are relatively different. Therefore, the atmospheric transport of the gaseous and particulate PAHs can also differ from each other. In particular, the particulate PAHs tend to have longer atmospheric half-lives (Mackay et al., 2006b) and can be removed from the air during their transport through dry and wet deposition (Keyte et al., 2013b). The dry deposition settles down the particulate PAHs by gravity (Shiraiwa et al., 2017), therefore, it mainly affects coarse particle-bound PAHs. In addition, the wet deposition removes the gaseous PAHs and fine/ultrafine particle-bound PAHs when precipitation (i.e., rainfall or snowfall) occurs.

The PAHs are originated from two main sources, including pyrogenic (i.e., combustion process) and petrogenic (e.g., heavy oil) sources. To identify emission sources of the atmospheric PAHs, hybrid receptor models, associating the backward air trajectory with PAH concentrations at the receptor site, can be used (Simmonds et al., 1997). Several techniques were developed based on this approach, e.g., residence time analysis (RTA) (Ashbaugh, 1983), potential source contribution function (PSCF), and concentration weighted function (CWT) (Fleming et al., 2012). Because the air parcels can traverse several areas prior to arriving at the receptor site, these techniques have been adopted to investigate the transport of air pollutants over non-local scale (e.g., a trans-boundary transport of pollutants over thousands of kilometers) (Polissar et al., 2001). Apart from the hybrid receptor models, conditional probability function (CPF) can also be used to determine directions of emission sources by associating the pollutant concentrations with wind direction (Wimolwattanapun et al., 2011). It is, therefore, mostly applied for the determination of source areas at the local scale (Kim and Hopke, 2004). More recently, the CPF was upgraded into the conditional bivariate probability function (CBPF) by combining the CPF with wind speed at the receptor site. Thus, not only directions of emission sources but also source types (i.e., ground common, stack, and distant sources) can be deduced (Uria-Tellaetxe and Carslaw, 2014).

South Korea locates in Northeast Asia, one of the most PAH-polluted areas over the world (Inomata et al., 2017). As locating downwind of the Asian monsoon system (Tamamura et al., 2007), a contribution of upwind sources in China to air pollution in South Korea has been widely investigated. For instance, the PSCF and a multivariate receptor model were applied to

demonstrate that northeastern and eastern China (i.e., Beijing, Hebei, Tianjin, and Shanghai), and/or North Korea could contribute to an increase of particulate matters and particulate PAHs in the air of Seoul, South Korea, especially in winter (Jeong et al., 2011; Jeong et al., 2017; Kim et al., 2016a). Additionally, PSCF considering a vertical dispersion of air pollutants was introduced and also verified that biomass burning in northeastern China (i.e., Beijing, Tianjin, and Liaoning), northern China (i.e., Liaoning), and/or North Korea (i.e., Pyongyang) could contribute to the particulate PAHs in Seoul (Kim et al., 2016b). Most of the previous studies focused on the transport of particulate PAHs; however, the PAHs occur in both gaseous and particulate phases, and their phase distribution can differ seasonally depending on the meteorological conditions (i.e., ambient temperature and humidity). Therefore, a consideration of both gaseous and particulate PAHs for locating their emission sources is essential.

The main purpose of this study is to identify emission source areas of PAHs in Ulsan, South Korea regarding the regional and local scale by using the PSCF, CWT, and CBPF analyses. Especially, unlike the conventional PSCF and CWT adopting the entire paths of air trajectories (Fleming et al., 2012), the PSCF and CWT used in this study were modified by considering the mixing layer along the trajectory routes to more reflect the realistic transport of air pollutants. A comparison between the conventional and modified PSCF and CWT is also provided to understand the influence of transport altitudes on the identification of source areas. Especially, a combination of PAH gas/particle partitioning and hybrid receptor model (i.e., CWT) is firstly introduced in this study to improve the application of such a model for identifying source areas of organic compounds.

3.2. Materials and methods

3.2.1. Receptor site and PAH data

This study used monitoring data for gaseous and particulate PAHs measured in Ulsan, one of the largest industrial cities in the southeast of South Korea. The industrial areas of Ulsan, comprising of petrochemical, non-ferrous, shipbuilding, and auto-mobile complexes, locate in the east of the city and are shown in Figure 3-1. Under an influence of the Asian monsoon system, prevailing wind directions in Ulsan are the southeast and northwest for summer/fall and winter/spring, respectively. During the winter and spring, the northwesterly winds blow from several upwind areas (e.g., China, North Korea, and western areas of South Korea) to Ulsan, causing this city to become a receptor area. Hence, a trans-boundary transport of air

pollutants can occur in Ulsan especially in winter and spring.

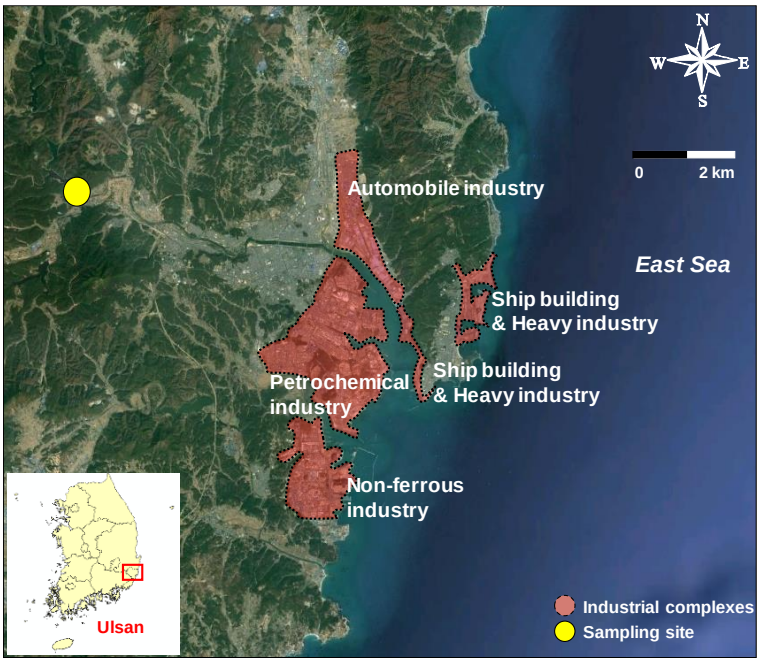

Figure 3-1. Location of the sampling site and industrial areas in Ulsan, South Korea.

Data on the gaseous and particulate PAHs (16 US EPA priority PAHs, except for naphthalene, acenaphthene, and acenaphthylene) were obtained from Chapter 2. The PSCF, CWT, and CBPF of the Σ_{13} PAHs in the gaseous, particulate, and total (gas + particle) phases were calculated to identify source areas of each PAH phase. The atmospheric PAHs were sampled once a week using a high-volume air sampler (Sibata, HV-700F, Japan) from June 2013 to May 2014, except for November and December 2013 because the samples were lost. The sampling campaign, therefore, covered 48 days and was separated into four seasons, including summer (June–August 2013), fall (September–October 2013), winter (January–February 2014), and spring (March–May 2014). The sampling site was at the Ulsan National Institute of Science and Technology (UNIST) in Ulsan, South Korea (35°34'18.32"N, 129°11'20.46"E). More details on the sampling can be found in Chapter 2.

3.2.2. Backward air trajectory

The backward air trajectories of 48 sampling days were obtained using the Hybrid Single-Particle Lagrangian Integrated Trajectory Model (HYSPLIT 4) adopting the GDAS1 (Global Data Assimilation System) meteorological data. To evaluate the PAH transport from outside of South Korea to the receptor site in Ulsan, the total run time for the backward air masses was set as 120 hours (5 days). The trajectories were obtained hourly for 24 hours from 11:00 a.m.

local time for each sampling day. Data on the atmospheric mixing height and several meteorological conditions (i.e., rainfall level, air pressure, and solar radiation) at each trajectory segment were also obtained using the HYSPLIT 4 model and GDAS1 data. The starting height of trajectories was set at 10% to 90% of the atmospheric mixing height at the sampling site. A reason for this selection is to increase a resolution for the hybrid receptor model (Jeong et al., 2011). In addition, after emitted the pollutants are well dispersed and mixed within the mixing layer, thus, the consideration of mixing height could more reflect a realistic transport of air pollutants (Stojić and Stanišić Stojić, 2017). A total of 10,368 backward trajectories (48 sampling days × 9 starting heights × 24 hours/day) were used for one sampling year. Particularly, the number of trajectories regarding each sampling season was 3,456, 2,595, 2,376, and 1,944 for the spring, summer, fall, and winter, respectively.

Recently, the hybrid receptor models considering the transport altitudes of air parcels (i.e., within the mixing layer or under a pre-defined height) were reported to improve the identification of source areas of air pollutants (Kim et al., 2016b; Stojić and Stanišić Stojić, 2017). Following this approach, this study also considers the altitude of each trajectory segment to more reflect the realistic transport of the atmospheric PAHs. Moreover, the residual layer, which is the mixing layer of the previous day (Kolev et al., 2007), was also considered. The residual layer is at top of the mixing layer, especially during the night and low air-temperature days, and the height of the residual layer was assumed to be half of the mixing height (Kolev et al., 2007). In this study, only trajectory segments within the residual and mixing layers were used for further calculation. The endpoint selection was performed using SAS 9.4 software (SAS Institute Inc., USA).

3.2.3. Hybrid receptor models and the vertical dispersion of air pollutants

3.2.3.1. PSCF reflecting the vertical dispersion of air pollutants ($PSCF^m$)

In the conventional PSCF ($PSCF^c$), the entire transport path of trajectory is used (Hopke et al., 1993) for the identification of source areas. However, the modified PSCF in this study adopted the only trajectory within the residual and mixing layers. The modified PSCF ($PSCF^m$) was calculated following the below equation:

$$PSCF_{ij}^{m} = \frac{m_{ij}}{n_{ij}} \tag{3-1}$$

where $PSCF_{ij}^{m}$ is the potential source contribution function reflecting the vertical transport of

air parcels. m_{ij} denotes the number of times the air parcels traversed cell (i,j) when the PAH concentrations were higher than the threshold value. Since there is no fixed threshold for the PAH concentration, three thresholds, including 50th, 75th, and 90th percentiles of the Σ_{13} PAH concentrations, were tested for the PSCF^m, then the most appropriate threshold was chosen for further calculation. n_{ij} is the number of times the trajectories passed through the cell (i,j). As the low n_{ij} can lead to the high PSCF^m, a weighting function was multiplied by the PSCF^m to reduce this uncertainty. In this study, two weighting functions were checked to understand the influence of the function on the PSCF^m results. The first function (W_1) was referred from previous studies (Jeong et al., 2011; Kim et al., 2016a; Wang et al., 2016), and the second function (W_2) was created by halving the previous value to get the following one. The more appropriate weighting function for the PAH dataset was then selected for further calculation. The weighting functions W_1 and W_2 are described below.

$$W_1 = \begin{cases} 1, & 2s \le N \\ 0.7, & s \le N < 2s \\ 0.42, & 0.5s \le N < s \\ 0.17, & N \le 0.5s \end{cases} \qquad W_2 = \begin{cases} 1, & 2s \le N \\ 0.5, & s \le N < 2s \\ 0.25, & 0.5s \le N < s \\ 0.12, & N \le 0.5s \end{cases} \tag{3-2}$$

where s is the average number of trajectory endpoints per cell. The s values calculated for each sampling season are shown in Table A2-1 in Appendix 2. N represents the total number of trajectory endpoints in each grid cell.

3.2.3.2. CWT reflecting the vertical dispersion of air pollutants (CWT^m)

The PSCF is a relatively straightforward approach for locating the source areas of air pollutants; however, it cannot clearly distinguish areas showing strong, moderate, and weak emission (Hsu et al., 2003b). In addition, the source areas associated with concentrations slightly lower than the threshold can be neglected in the PSCF. Therefore, the concentration-weighted trajectory reflecting the vertical transport of air parcels (CWT^m) was also performed to confirm the source areas of PAHs. The modified CWT (CWT^m) was estimated based on the below equation.

$$CWT^m_{ij} = \frac{1}{\sum_{l=1}^{M} \tau_{ijl}} \times \sum_{l=1}^{M} (C_j \times \tau_{ijl}) \tag{3-3}$$

where M is the total number of backward trajectories. τ_{ijl} is the number of endpoints in the cell (i,j) for trajectory l, having its transport route within the mixing layer. C_j denotes the PAH concentrations at the sampling site. To prevent uncertainty stemmed from the low value of τ_{ijl},

the weighting functions were also applied for the CWT^m as described in Section 3.2.2.1.

Moreover, comparisons between the conventional and modified PSCF and CWT were also performed to evaluate the influence of vertical transport on the determination of source areas. The conventional and modified PSCF and CWT were calculated for the 0.5° × 0.5° grid cells over the domain of 110°–140°E and 25°–50°N (Figure 3-2).

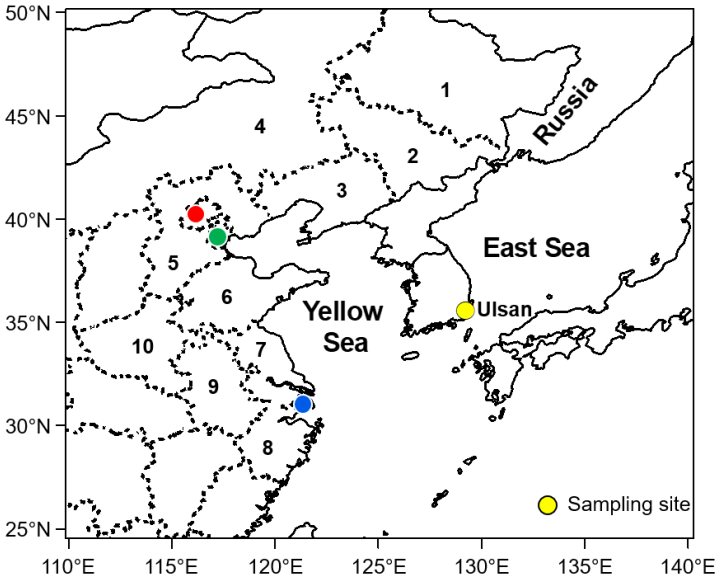

Figure 3-2. The geographical domain used in this study. The numbers denote several areas in China, including Heilongjiang (1), Jilin (2), Liaoning (3), Inner Mongolia (4), Hebei (5), Shandong (6), Jiangsu (7), Zhejiang (8), Anhui (9), and Henan (10). The red, green, and blue circles represent Beijing, Tianjin, and Shanghai, respectively.

The threshold and weighting functions used for the conventional and modified PSCF and CWT were the same. Geographically, areas showing high PSCF or CWT values can be regarded as source areas (Fleming et al., 2012). In this study, TrajStat (Wang et al., 2009) was used to calculate the conventional and modified PSCF and CWT. ArcGIS 10.5 (ESRI, USA) was applied to plot the PSCF and CWT maps.

3.2.4. Application of gas/particle partitioning for the identification of source areas

The particulate PAHs can be more persistent than the gaseous ones because of their longer half-lives and lower mobility (Mackay et al., 2006b). Therefore, the particulate PAHs are expected to more contribute to trans-boundary transport by near-surface winds in Northeastern Asia (Kim et al., 2016a; Tamamura et al., 2007; Wang et al., 2016; Zhang et al., 2017b). The

atmospheric PAHs occur in both gaseous and particulate phases, and these phases can transform into each other during their transport in the atmosphere. In particular, the gas-phase PAHs can undergo nucleation, condensation, and coagulation to form the particle-bound species (Zhang et al., 2015). Moreover, the PAHs bound to aerosols can also desorb to exist in the gaseous phase (Keyte et al., 2013b). Thus, a consideration of gas/particle partitioning of PAHs, instead of the concentrations, is expected to improve the identification of their source areas.

In this study, fractions of the particulate PAHs, calculated as a ratio of the particulate to the total (gas + particle) concentrations, were used as input data for the hybrid receptor model (i.e., CWT) to identify source areas of the PAHs. The calculation procedure was the same as the CWT^m and was named as a "fraction-weighted trajectory" (FWT). In general, areas with higher FWT values indicate their greater effect on the particulate PAHs at the receptor site.

3.2.5. Trajectory cluster analysis

Trajectories simulated from the HYSPLIT 4 were clustered into several groups based on their similar directions and lengths (Fleming et al., 2012) using the Trajstat software (Wang et al., 2009). In general, the distance between two trajectories is calculated based on the Euclidean distance following equation 3-4.

$$d_{12} = \sqrt{\sum_{i=1}^{n} [X_1(i) - X_2(i)]^2 + [Y_1(i) - Y_2(i)]^2} \quad (3\text{-}4)$$

where d_{12} is the Euclidean distance between two backward trajectories. X_1, X_2 and Y_1, Y_2 are the latitudes and longitudes of these trajectories, respectively. The number of clusters was then identified using the eyeball method; the number of clusters would be selected based on a variation of the total spatial variance (TSV) computed among the trajectory endpoints. A dramatical change of the TSV suggests a suitable number of clusters (Wang et al., 2009).

3.2.6. Regional transport contribution

The study domain was divided into 8 sectors, 45 degrees each. The percentage of regional transport contributions in each sector was calculated as below (Wang et al., 2016).

$$T_j\,(\%) = (C_j - C_b)/C_j \times 100 \quad (3\text{-}5)$$

where T_j is a contribution of regional transport. C_j is concentration-weighted trajectory in sector j. C_b is local background concentration, which is a sum of the lowest concentrations in each

sector

3.2.7. Conditional bivariate probability function (CBPF)

The hybrid receptor models, such as PSCF and CWT, mostly determine the source areas at a non-local scale (i.e., trans-boundary transport) (Polissar et al., 2001) because the air parcels considered for the calculation would pass several areas prior to arriving at the receptor site. Hence, to focus on the identification of source areas at a local scale, the conditional bivariate probability function (CBPF) was also performed in the current study.

The CBPF provides information on source directions and source types based on wind dependency. For example, the great CBPF probability at low and high wind speed suggests common ground-level and stack sources, respectively (Uria-Tellaetxe and Carslaw, 2014). The low wind speed mainly distributes atmospheric pollutants in a small area (i.e., local scale), whereas the high wind speed increases the dispersion of pollutants and contributes to their transport to distant areas. Therefore, the low and high wind speed associated with the great CBPF probability can also be indicative of local and non-local emission sources, respectively (Perrone et al., 2018; Zhou et al., 2019). The CBPF was calculated based on the below equation.

$$\mathrm{CBPF}_{\Delta\theta,\Delta u}=\frac{\mathrm{m}_{\Delta\theta,\Delta u}|\mathrm{C}\geq x}{\mathrm{n}_{\Delta\theta,\Delta u}} \tag{3-6}$$

where $\Delta\theta$ and Δu are the wind sector and wind speed, respectively. C is the concentration of Σ_{13} PAHs which is higher than the threshold x within the wind sector $\Delta\theta$ and wind speed Δu. $\mathrm{m}_{\Delta\theta,\Delta u}$ is the number of samples in the wind sector $\Delta\theta$ and wind speed Δu having concentrations higher than the threshold x. $\mathrm{n}_{\Delta\theta,\Delta u}$ denotes the total number of samples in the corresponding wind sector and wind speed interval. The threshold x for the CBPF calculation was the same as that of the PSCF^m described in Section 3.2.2.1. Data for the wind speed and wind direction in the study area were obtained from the Korean Meteorological Administration (https://web.kma.go.kr). The R program, freely downloaded from https://www.r-project.org, and the open-source tool Openair (Carslaw and Ropkins, 2012) were applied to calculate and plot the CBPF.

3.3. Results and discussion

The modified PSCF^m and CWT^m using two weighting functions (i.e., W_1 and W_2) and three

thresholds (i.e., 50th, 75th, and 90th percentiles of the Σ_{13} PAHs) were compared to select the optimal weighting function and concentration threshold for further calculation. As a result, the 75th percentile of Σ_{13} PAHs and the weighting function W_1 were chosen. More details on this comparison can be seen in Text A2-1 in Appendix 2. Additionally, the PSCF^m and CWT^m confirmed the relatively similar source areas for the gaseous, particulate, and total PAHs. This observation could be because the same backward trajectories were used as input data for the PSCF and CWT. Moreover, these techniques apply a similar approach for identifying source areas, which is based on the movement of air parcels and PAH concentrations at the receptor site.

3.3.1. Seasonal source areas of the gaseous PAHs

Long-range transport of the gaseous PAHs in South Korea, to the best of my knowledge, has not been well investigated in previous studies. This limitation could be because the gaseous PAHs have shorter atmospheric half-lives compared to the particulate ones (Mackay et al., 2006b), and the frequent reaction of the gaseous compounds to free radicals (Keyte et al., 2013b). However, the effect of the monsoon system and the suitable weather conditions (e.g., less precipitation, low solar radiation, and high air pressure) might contribute to the long-range transport of the gaseous PAHs in Northeast Asia. A discussion on this issue is provided in the following sections.

3.3.1.1. Source areas of the gaseous PAHs in spring

In the spring, both PSCF^m and CWT^m highlighted that the gaseous PAHs in Ulsan could be contributed by those originating from northeastern China (i.e., Heilongjiang, Jilin, and Liaoning) and North Korea (Figures 3-3a and 3-4a). The gaseous PAHs coming from these areas could account for the highest contribution (47.6%) among the transported PAHs. Moreover, the air parcels from these areas accounted for approximately 45% of the total trajectories in spring (Figure 3-5a) and mostly appeared in March and April when an increase of active fire and thermal anomalies was observed (Figures 3-6a and 3-6b). The gaseous PAHs formed during the combustion process in these areas could be then transported to the receptor site in Ulsan by the surface-wind. In addition, the lower rainfall levels along the routes of trajectories crossing northeastern China (i.e., Heilongjiang, Jilin, and Liaoning) and the East Sea in spring (Figure 3-7a) could limit wet deposition of the gaseous PAHs. Added to this, atmospheric half-lives of some PAHs that are dominant in the gaseous phase (i.e., Phe, Pyr, and

Flt) (Nguyen et al., 2018) range from 55 to 170 h (Mackay et al., 2006b). Meanwhile, the air parcels could spend approximately 72 h (Kim et al., 2016a) to traverse northeastern China (i.e., Heilongjiang, Jilin, and Liaoning) and the East Sea before arriving in Ulsan. Thus, the gaseous PAHs originated from those areas might be long-range transported to the study area.

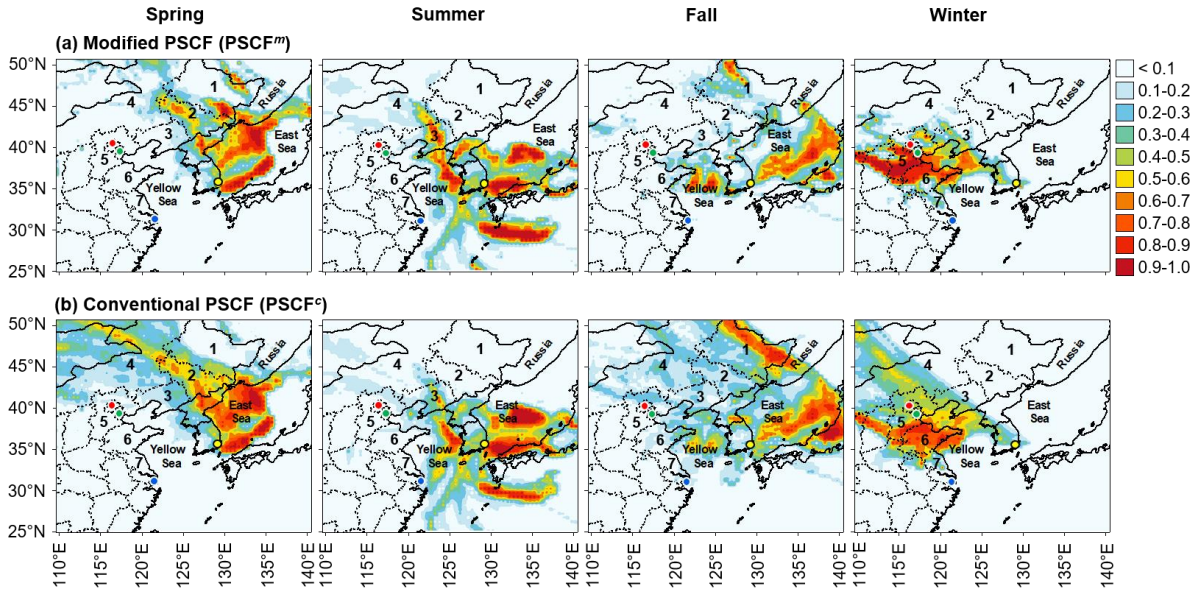

Figure 3-3. PSCF of the gaseous PAHs shown in (a) modified and (b) conventional approaches in four seasons. Names of several Chinese provinces and cities marked by numbers and color circles are shown in Figure 3-2.

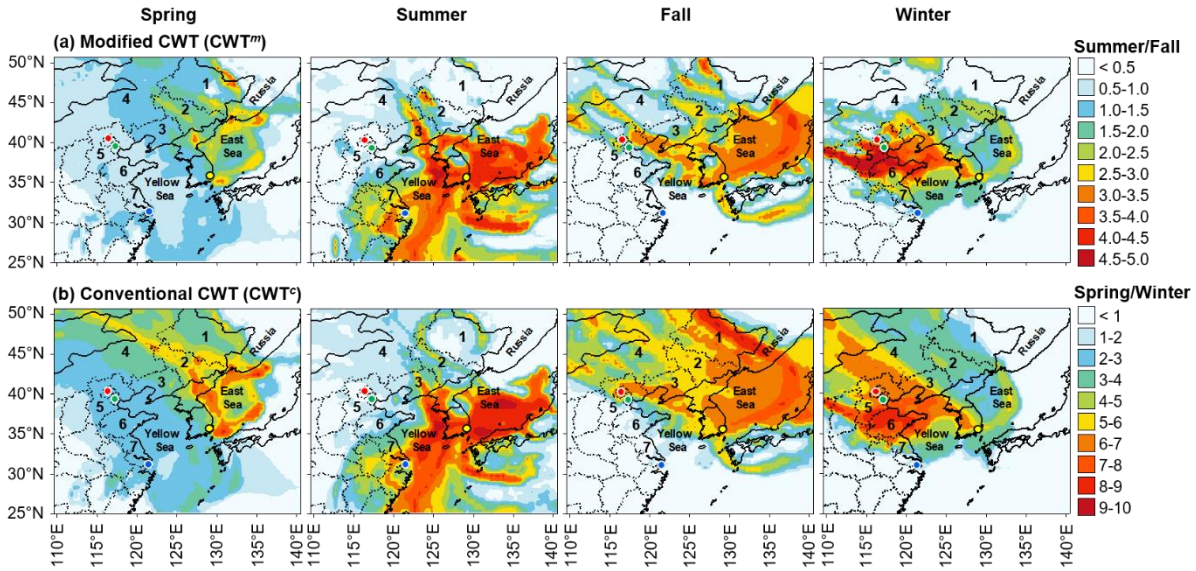

Figure 3-4. CWT of the gaseous PAHs shown in (a) modified and (b) conventional approaches in four seasons.

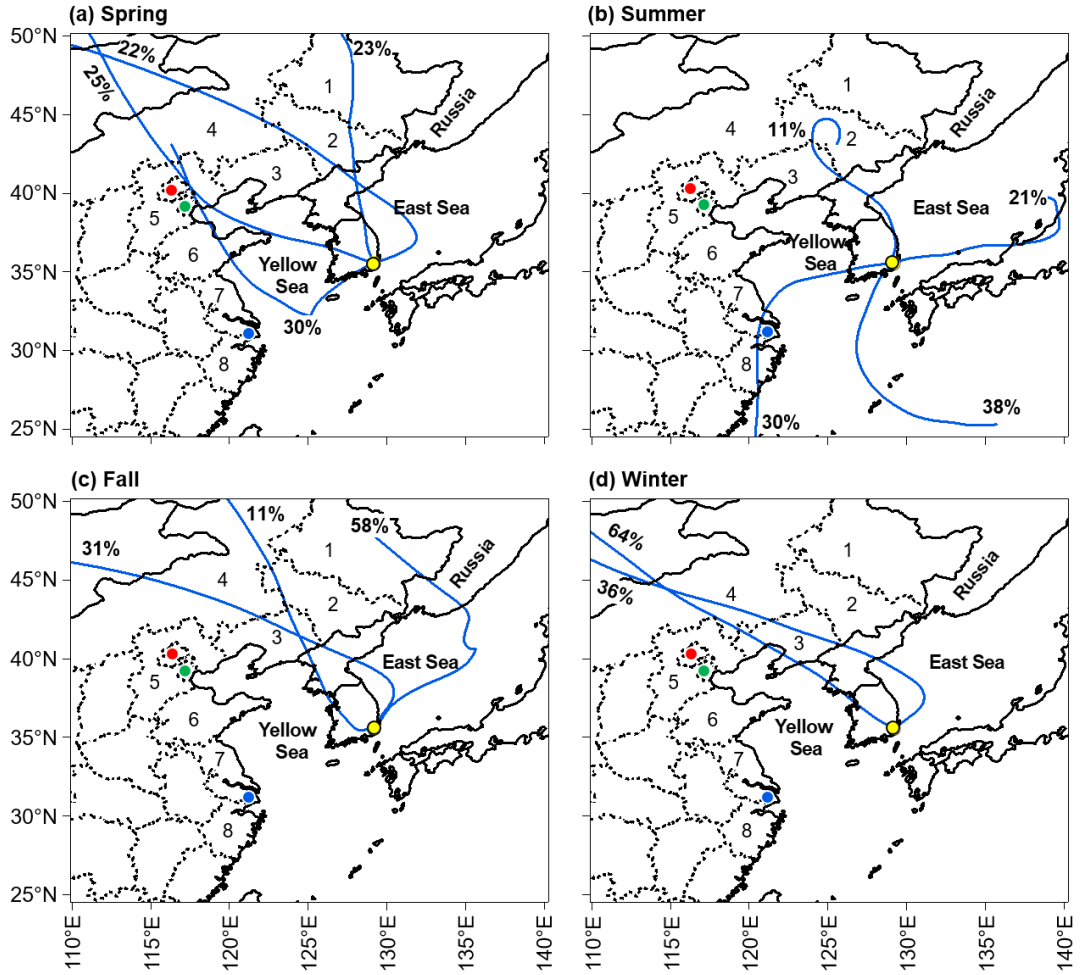

Figure 3-5. Trajectory cluster analysis in the (a) spring, (b) summer, (c) fall, and (d) winter. The percentage numbers denote the contribution of each cluster.

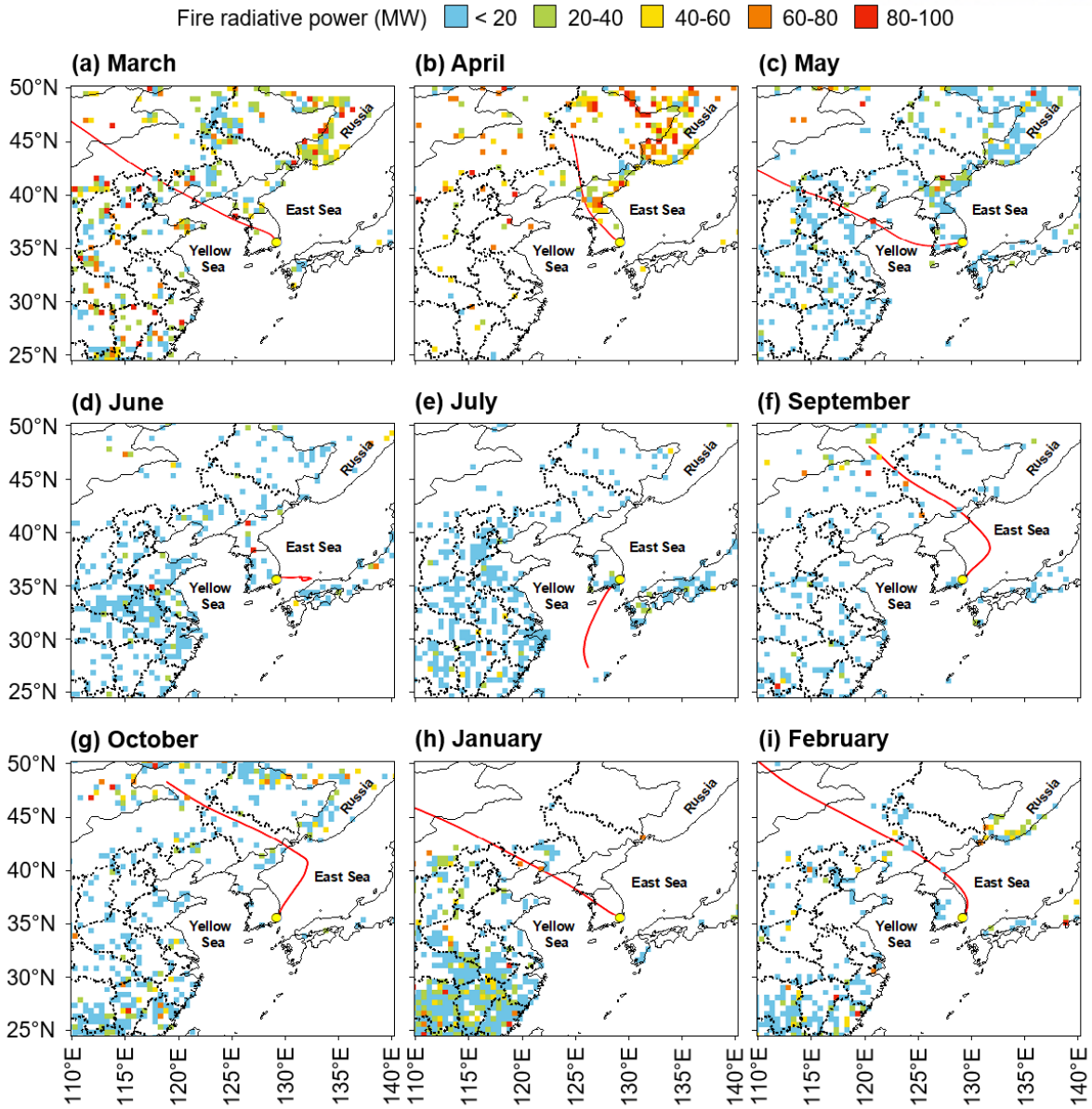

Figure 3-6. Locations of active fire and thermal anomalies over Northeast Asia in (a) March, (b) April, (c) May, (d) June, (e) July, (f) September, (g) October, (h) January, and (i) February. The red lines are the monthly mean air trajectories in the corresponding months. Data were obtained from the MODIS Collection 6 Near real-time Hotspot (https://earthdata.nasa.gov/firms).

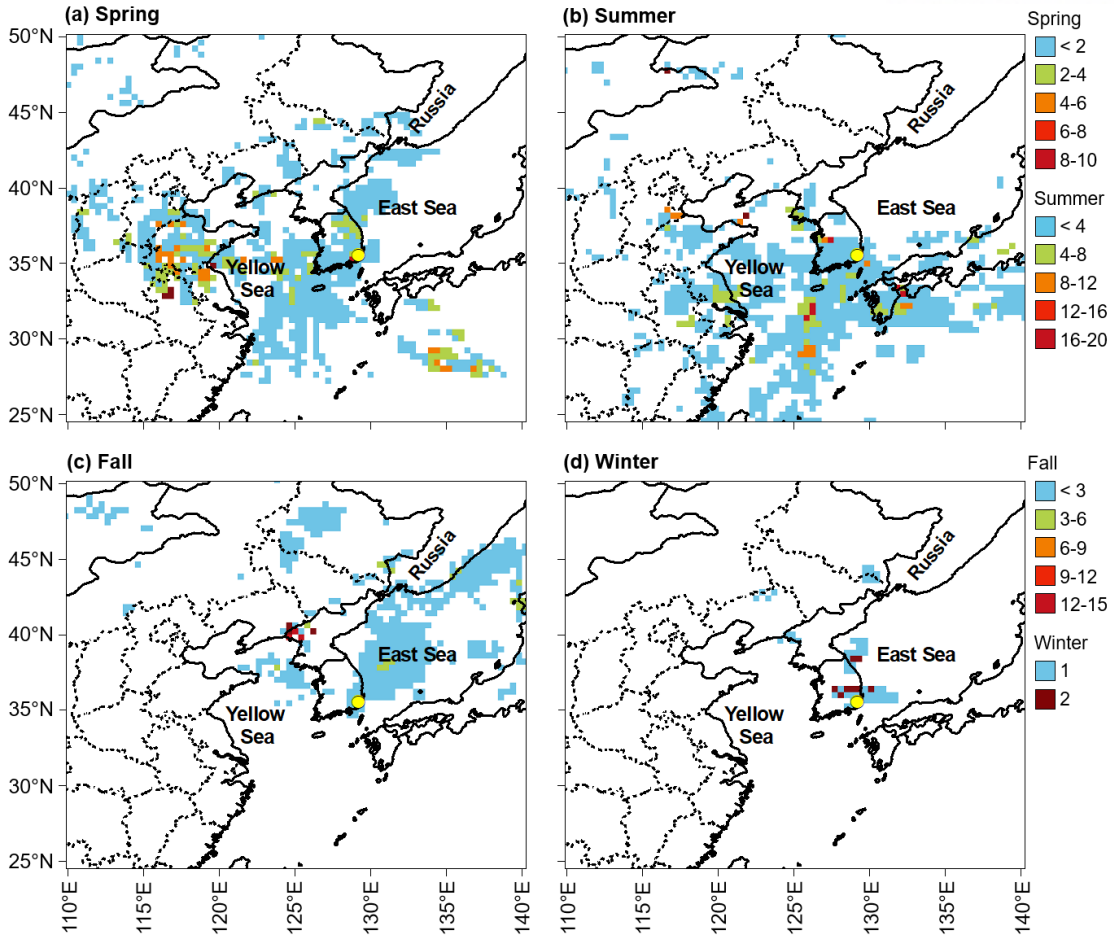

Figure 3-7. Rainfall levels (mm/h) along the backward air trajectories in the (a) spring, (b) summer, (c) fall, and (d) winter. Data were obtained from the HYSPLIT 4 model and GDAS 1 meteorological data.

This finding is also supported by the CBPF plot, suggesting that the gaseous PAHs in Ulsan could be derived from both common ground level (e.g., vehicle exhaust) and distant (e.g., long-range transport) sources (Figure 3-8a). These emission sources could be at the north of the sampling site and associated with the low to high wind speeds (2–6 m/s) for the local and distant sources, respectively. Moreover, the high probabilities of these emission sources (0.8–1.0) could suggest their comparable contributions (Uria-Tellaetxe and Carslaw, 2014) to the gaseous PAHs in Ulsan during the spring.

3.3.1.2. Source areas of the gaseous PAHs in summer and fall

In summer and fall, the CBPF plots for the gaseous PAHs showed high probabilities at relatively low wind speed (< 3 m/s) (Figures 3-8b and 3-8c), reflecting that the gaseous species could be primarily derived from local emission. Particularly, the dispersion of PAHs under such wind speed conditions could be within a relatively small area (e.g., a few kilometers). In addition, the prevailing wind in Ulsan during summer and fall is the southeasterly wind, blowing from the southeast of the city and passing over the industrial and urban areas prior to reaching the sampling site (Figure 3-1). Especially, the petrochemical and non-ferrous industrial complexes in Ulsan have been mentioned to be the important emission sources of PAHs due to coal/coke combustion and heavy oil usage for their operation (Choi et al., 2012b; Nguyen et al., 2018). Hence, the gaseous PAHs derived from such industrial activities and other sources in the urban area (e.g., vehicle exhaust) could obviously affect the sampling site.

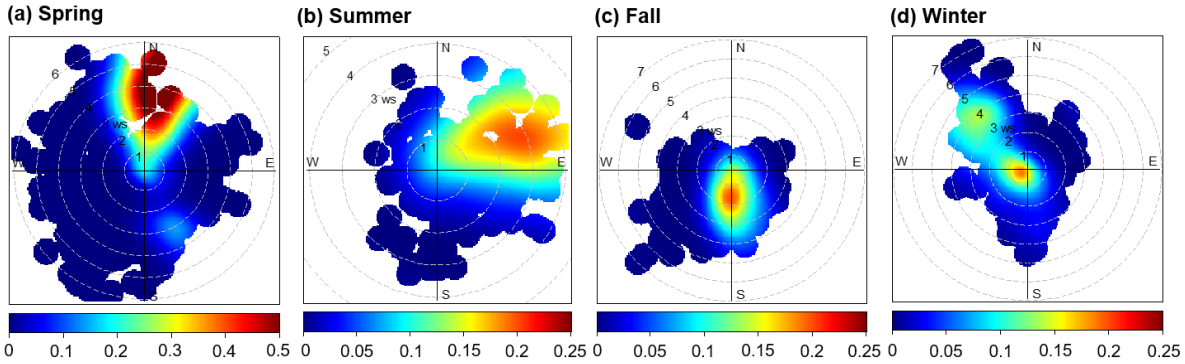

Figure 3-8. CBPF plots for the gaseous PAHs in (a) spring, (b) summer, (c) fall, and (d) winter.

Additionally, the PSCF^m and CWT^m suggested that the gaseous PAHs in Ulsan could also be affected by emission sources in eastern China in the summer (i.e., Jiangsu, Shanghai, and Zhejiang), and northeastern China (i.e., Hebei and Jilin) as well as North Korea in the fall (Figures 3-3 and 3-4). However, the greater rainfall levels (Figure 3-7) and solar radiation in summer and fall could promote the wet deposition and photochemical degradation of the gaseous PAHs during their transport, leading to the insignificant influence of the regional emissions on the gaseous PAHs in Ulsan. This finding is also in line with that confirmed by the CBPF results mentioned above. The effect of air pollutants from the upwind (i.e., China and North Korea) to the downwind areas (i.e., South Korea and Japan) was also reported to weaken in summer and fall due to the Asian monsoon system (Bhardwaj et al., 2019; Inomata et al., 2017; Zhang et al., 2011b). The regional areas suggested by the PSCF^m and CWT^m could be

due to the trailing effect (Hsu et al., 2003a), locating upwind of the emission sources as source areas. The trailing effect could be stemmed from the equal distribution of weighting functions along the routes of trajectories (Hsu et al., 2003b).

3.3.1.3. Source areas of the gaseous PAHs in winter

In winter, the PSCF^m and CWT^m revealed that northern China (i.e., Hebei, Tianjin, and Shandong) and northeastern China (i.e., Jilin and Liaoning) might contribute to the increase of gaseous concentrations in Ulsan (Figures 3-3d and 3-4d) and accounted for 92.3% of the transported PAHs. The CBPF analysis also suggested a distant emission source with medium wind speed (3-4 m/s) toward the northwest of the sampling site (Figure 3-8d). The gaseous PAHs coming from this direction would be contributed by those emitted from the regional sources through trans-boundary transport as described above. The combustion process, such as coal combustion for heating (Figures 3-6h and 3-6i), was expected to be one of the main emission sources of the gaseous PAHs in these areas. Additionally, the CBPF plot for the gas phase in winter also validated the common ground source (e.g., vehicle emission) at the northwest (Figure 3-8d) associating with the low wind speed (< 1 m/s). Because the probability of this source (0.25) was higher than that of the distant source (0.1–0.15), the influence of the local sources on the gaseous PAHs might be more important in Ulsan during the winter.

3.3.2. Seasonal source areas of the particulate PAHs

3.3.2.1. Source areas of the particulate PAHs in spring

In spring, the particulate PAHs derived from northern China (i.e., Hebei, Beijing, and Tianjin), northeastern China (i.e., Inner Mongolia, Jilin, and Liaoning), and North Korea could contribute to the particulate PAHs in Ulsan, South Korea (Figures 3-9a and 3-10a). Northern China (i.e., Hebei, Beijing, and Tianjin) could more contribute to the transported PAHs (40.5%) and were more highlighted in the CWT^m (Figure 3-10a) determining source areas based on the residence time of air trajectories. Therefore, intensities (i.e., strong, moderate, and weak) of the emission sources can be distinguished by the CWT (Fleming et al., 2012). The PSCF, on the contrary, only provides the probability of an area associated with the above-threshold concentrations. For this reason, the emission source areas might be more obviously seen in the CWT.

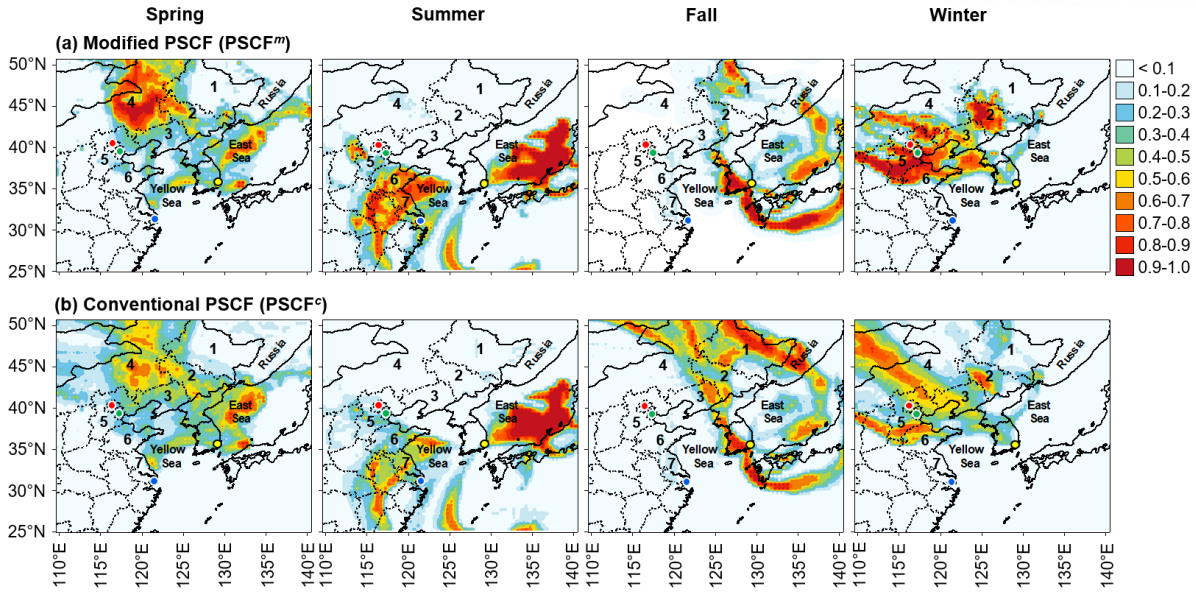

Figure 3-9. PSCF of the particulate PAHs shown in (a) modified and (b) conventional approaches in four seasons.

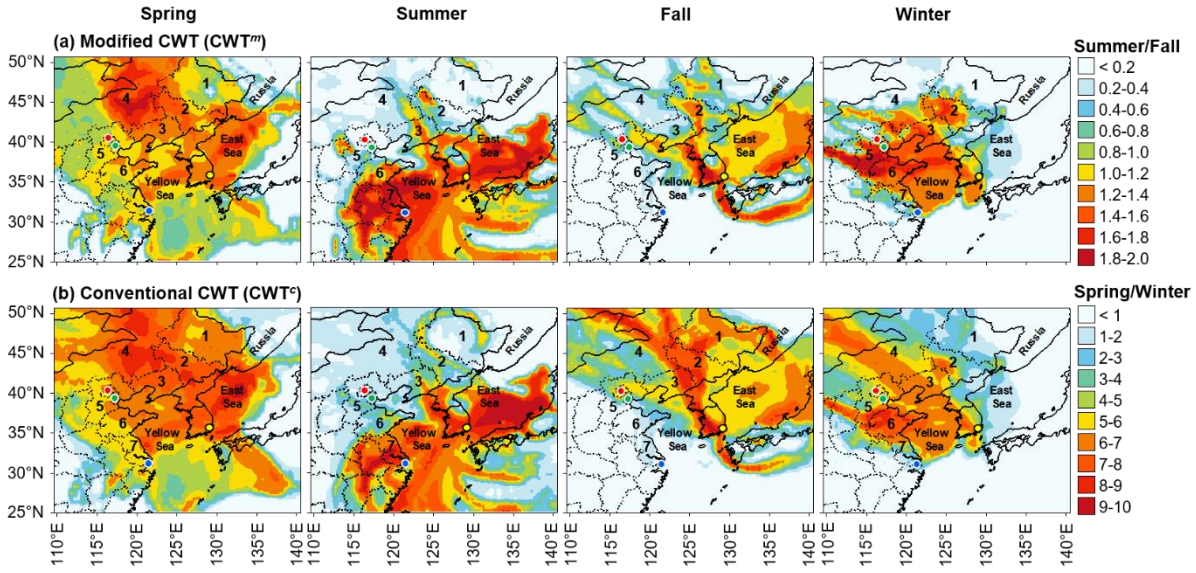

Figure 3-10. CWT of the particulate PAHs shown in (a) modified and (b) conventional approaches in four seasons.

In addition, the outflow of particulate PAHs originated from China could be high in northern China (i.e., Beijing, Tianjin, and Hebei) (Zhang et al., 2011a) and might be reflected through the higher amount of aerosol, the sorbents for particulate PAHs, during spring (Figure 3-11). The particulate PAHs could be then brought to the downwind areas (i.e., Ulsan) by the westerly winds. In addition, during the spring, air parcels coming from north of China (i.e., Hebei,

Beijing, and Tianjin) showed the higher contribution (55%) (Figure 3-5a); therefore, the particulate PAHs from these areas might have more contribution to those at the receptor site. Previous studies (Inomata et al., 2017; Inomata et al., 2012) also showed that northern China (35º–40ºN, including Shandong, Hebei, Beijing, and Tianjin), rather than northeastern China (> 40ºN, including Liaoning, Jilin, and Heilongjiang), could more contribute to the particulate PAHs in South Korea.

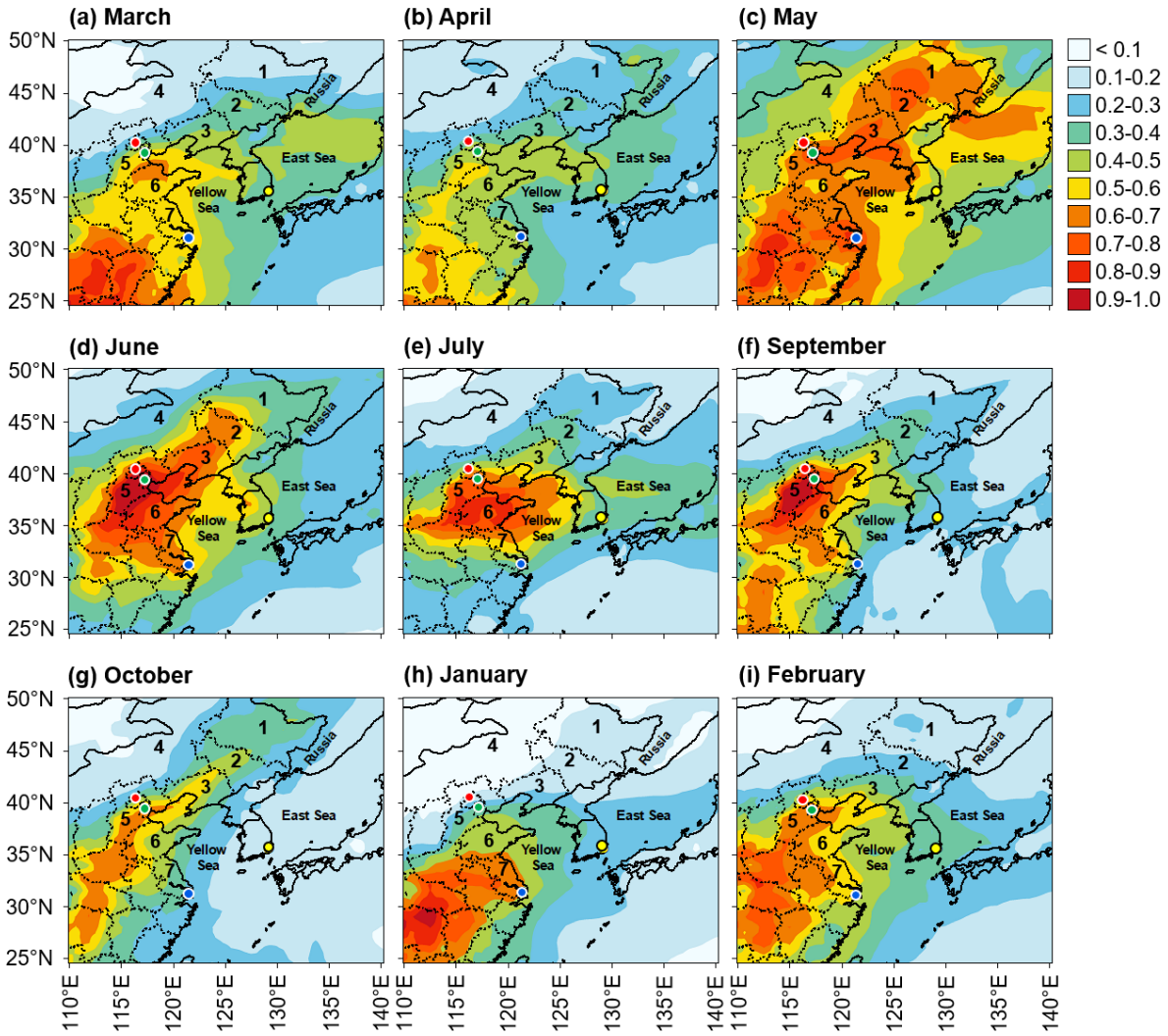

Figure 3-11. Aerosol optical depth (AOD) observed in Northeast Asia during the study period: (a) March, (b) April, (c) May, (d) June, (e) July, (f) September, (g) October, (h) January, and (i) February. Data were obtained from the Modern-Era Retrospective analysis for Research and Applications, version 2 (MERRA-2).

Moreover, the CBPF analysis also confirmed the emission source at the northwest with high wind speed (5–6 m/s). As the high wind speed would enhance the dispersion of air pollutants,

this source was expected to be the non-local or distant source (Masiol et al., 2019), such as long-range transport from outside of South Korea and/or transport from other areas in South Korea passed by the air trajectories before reaching the receptor site (Figures 3-9a and 3-10a).

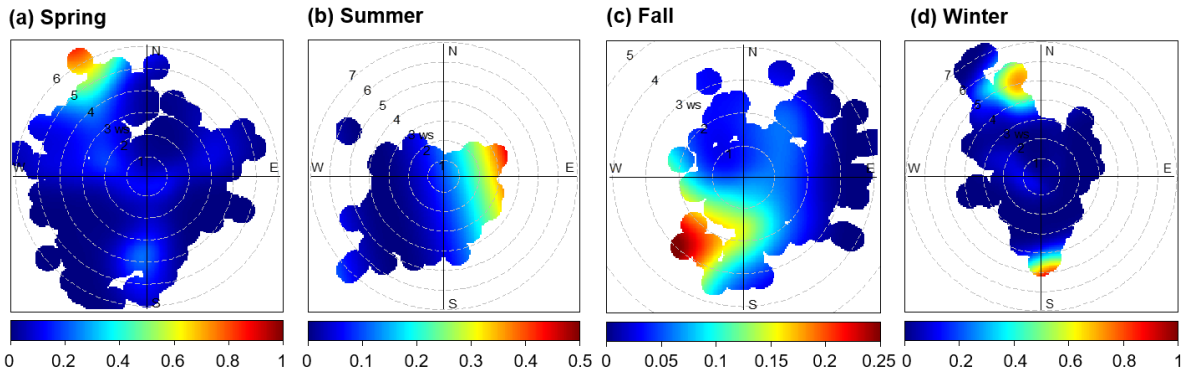

Figure 3-12. CBPF plots for the particulate PAHs in (a) spring, (b) summer, (c) fall, and (d) winter.

3.3.2.2. Source areas of the particulate PAHs in summer and fall

In summer and fall, local emission could more affect the particulate PAHs in Ulsan because the CBPF plots of these seasons showed high probabilities at relatively low (< 3 m/s) wind speed (Figures 3-12b and 3-12c). The low wind speed reduces the dispersion of air pollutants and leads to local residents of the pollutants. In addition, the primary local emission sources in the summer and fall were expected to be possibly the industrial areas located in the eastern Ulsan, including the petrochemical and non-ferrous industrial complexes (Figure 3-1). As mentioned in Section 3.3.1.2, these industrial areas were reported to mainly contribute to the PAHs in Ulsan during summer and fall due to the monsoon system (i.e., prevailing southeasterly wind).

Regarding the hybrid receptor models, the PSCF^m and CWT^m highlighted that emission sources from eastern China (i.e., Shanghai, Anhui, and Jiangsu) for summer (Figures 3-9b and 3-10b), western South Korea for fall, and western Japan for summer and fall (Figures 3-9c and 3-10c) could contribute to the particulate PAHs in Ulsan. However, the higher rainfall levels and solar radiation in summer and fall (Figure 3-7) could reduce the influence of these areas on the PAHs in Ulsan through wet deposition and photochemical degradation. As a result, the local emissions could be more important for the particulate PAHs in summer and fall. This observation is the same as that for the gaseous PAHs and also in line with those from previous studies (Inomata et al., 2017; Zhang et al., 2011b).

3.3.2.3. Source areas of the particulate PAHs in winter

In winter, both $PSCF^m$ and CWT^m validated north of China (i.e., Hebei, Tianjin, and Beijing) could be the source areas of the particulate PAHs in Ulsan (Figures 3-9d and 3-10d). These areas could contribute to 77% of the transported particulate PAHs in Ulsan during winter. An increase in PAHs emitted from combustion (i.e., coal/biomass combustion for heating) (Figure 3-6) combined with the greater aerosol levels in those areas during winter, especially in February (Figure 3-11j), could lead to higher levels of the particulate PAHs by coagulation and/or condensation (Indarto et al., 2010). Moreover, the particulate PAHs, especially the 4- to 6-ring species, mainly sorb to organic matters of fine particles having aerodynamic diameter lower than 1 μm (Park et al., 2007). Such particles can be removed from the air by wet deposition (i.e., in-cloud and below cloud deposition) (Baek et al., 1991b). However, an absence of rainfall when air parcels passed over north of China in winter (Figure 3-7) could lead to the long-range transport of particulate PAHs emitted from these areas.

The CBPF plot of the particulate phase was also checked to more clarify the effect of non-local and local emission sources on the particulate PAHs in Ulsan. Two sources with high wind speed (5–6 m/s) located in the south and northwest of the sampling site were identified (Figure 3-12d). The source at the south was expected to be stack emission (Uria-Tellaetxe and Carslaw, 2014) in the industrial complexes at the east and southeast of Ulsan. Noticeably, the prevailing wind direction in Ulsan during winter is northwesterly, leading to a transport of PAHs derived from the industrial area to the East Sea (Figure 3-1). However, the low mixing height and an increase of the particulate PAHs in Ulsan during winter (Nguyen et al., 2018) could promote the horizontal dispersion of PAHs within the local scale. The other source at the northwest could be a distinct source and might have a contribution from the regional emissions (e.g., long-range transport from northern China). The high probabilities (> 0.8) of the distant and local sources suggest their simultaneous influence on the particulate PAHs in Ulsan during the winter.

3.3.3. Application of gas/particle partitioning for the identification of source areas

The fraction-weighted trajectory (FWT) of each sampling season is illustrated in Figure 3-13. Generally, particulate PAHs in Ulsan could be transported from the areas showing the greater FWT values. In the spring, both northeastern China (i.e., Jilin, Liaoning, and Heilongjiang) and

northern China (i.e., Hebei, Beijing, Tianjin, and Shandong) were suggested as source areas for the particulate PAHs in Ulsan. Interestingly, the north of China (i.e., Hebei, Beijing, and Shandong) were neglected and moderately highlighted as source areas for the particulate PAHs by the PSCF^m and CWT^m, respectively (Figures 3-9a and 3-10a). An explanation could be that the PAH concentrations declined by high rainfall events (Figure 3-7a) when the air parcels crossed over the north of China and the Yellow Sea. However, mass fractions of the particulate PAHs at the receptor site were still high, leading to the greater FWT in northern China, especially in Hebei, Beijing, and Tianjin.

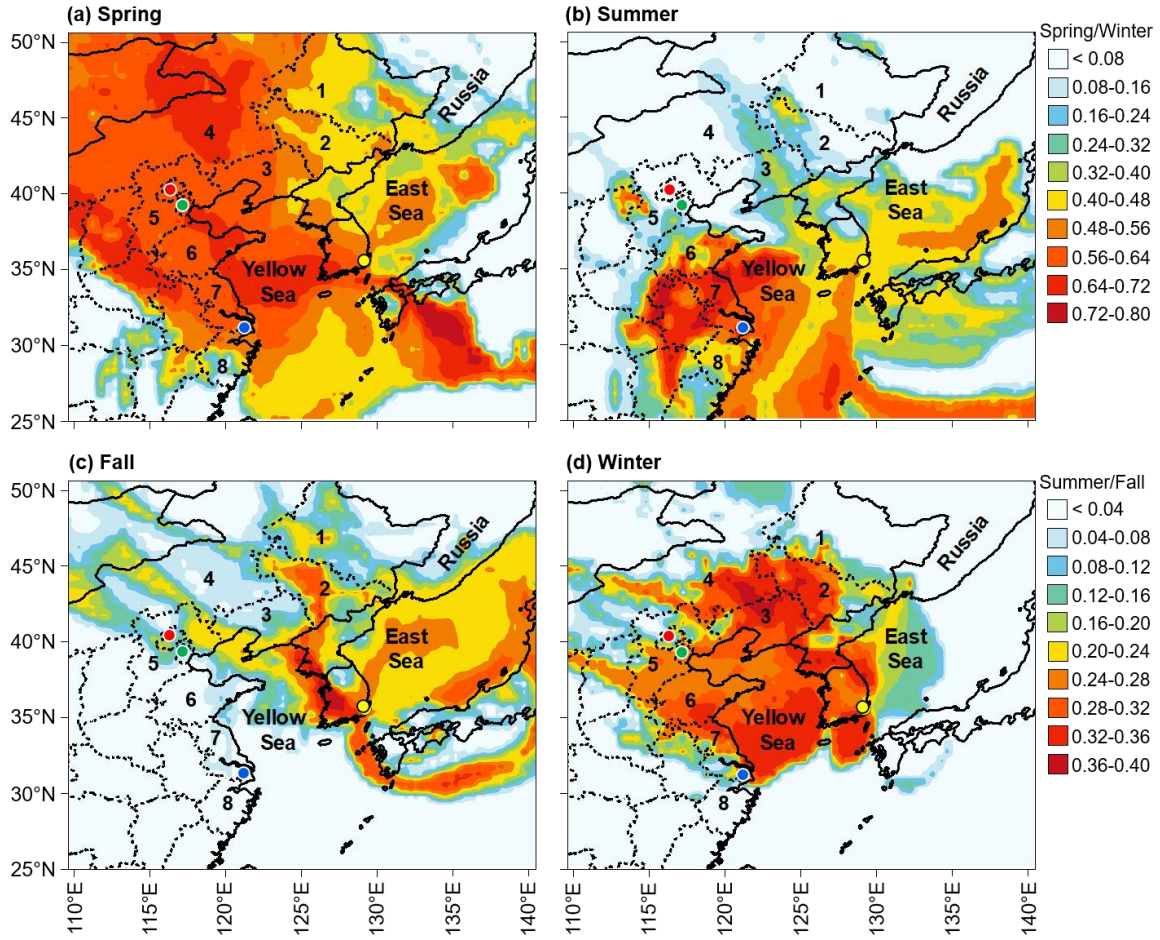

Figure 3-13. Fraction-weighted trajectory (FWT) values in the (a) spring, (b) summer, (c) fall, and (d) winter. The CWT^m was calculated for the ratio of the particulate to the total (gas + particle) concentrations.

In summer, the FWT values were high in eastern China (i.e., Shanghai, Jiangsu, Henan, and Zhejiang), but they obviously declined in the Korean Peninsula (Figure 3-13b). This result suggests that the levels of particulate PAHs emitted from the regional sources could decline during the atmospheric transport of PAHs. In other words, the local emission sources, rather

than the distant ones, could keep an important contribution to the PAHs in Ulsan in the summer. This observation is also consistent with the discussion in Section 3.3.2.2.

For the fall, the FWT confirmed that the particulate PAHs emitted in western Korea could be brought to the sampling site (Figure 3-13c). Emission sources in this area could be several industrial complexes and large-scale coal power plants located at the west coast and open burning after harvest (Ryu et al., 2004) in the fall. However, the low FWT (< 0.4) in fall suggests a less influence of the non-local sources on the particulate PAHs in Ulsan, which was already mentioned in Section 3.3.2.2.

The emission source areas suggested by the FWT in the winter (Figure 3-13d) were similar to those suggested by the $PSCF^m$ and CWT^m for the particulate PAHs (Figures 3-9d and 3-10d). These areas include northeastern China (i.e., Liaoning and Jilin) and northern China (i.e., Hebei, Beijing, and Tianjin). In addition, the other source areas in South Korea and North Korea were more emphasized in the FWT. Indeed, the west and northwest areas of the Korean Peninsula are upwind of Ulsan in the winter; therefore, air parcels could trap the emitted PAHs in these areas and then brought them to Ulsan. However, emission inventories of PAHs in South Korea were much lower than those in China (Shen et al., 2013), implying a large contribution of the trans-boundary transport of PAHs in Ulsan in winter.

Comparing to the $PSCF^m$ and CWT^m, the FWT could validate more appropriately the source areas of particulate PAHs, which could be more affected by the long-range transport. Especially, the FWT would differentiate the source scale (i.e., local and distant sources) more effectively in summer and fall, when the local sources were more important. This result demonstrates that the FWT using both the gaseous and particulate data can more clearly identify the source-receptor relationship.

3.3.4. Comparison of the modified and conventional hybrid receptor models

The areas of PAH emissions identified by the conventional hybrid receptor models (i.e., $PSCF^c$ and CWT^c), using the entire pathway of air trajectory, were compared to those suggested by the modified ones (i.e., $PSCF^m$ and CWT^m), using the selected trajectory segments. This comparison was performed for the gaseous (Figures 3-3 and 3-4) and particulate (Figures 3-9 and 3-10) PAHs. Prior to being added to the modified $PSCF^m$ and CWT^m, the selection for trajectory segments was performed to keep the vertical transports of trajectories within the mixing and residual layers. Because of this selection, some areas determined as emission sources by the conventional $PSCF^c$ and CWT^c were neglected by the modified $PSCF^m$ and CWT^m, in case the vertical transport of trajectory segments was above the mixing and residual layers in those areas.

The neglected areas were relatively similar between the PSCF and CWT, and they were Inner Mongolia and Mongolia for spring and winter as well as northeastern China (i.e., Heilongjiang and Jilin) for summer and fall (Figures 3-3, 3-4, 3-9, and 3-10). The air parcels crossing these areas, especially Inner Mongolia and Mongolia, had lower pressure than those in the surrounding areas (Figure 3-14). This observation indicates that the air parcel in northeastern China and Mongolia could be lifted to a higher altitude under the influence of several meteorological factors. For instance, an expansion of cold surges from Mongolia and Serbia (Liang et al., 2005; Zhang et al., 2011b) associated with the low-pressure system in northeastern China (i.e., Inner Mongolia, Jilin, and Liaoning) in winter, and warm conveyor belt in spring (Mu et al., 2018; Zhang et al., 2011a). After being lifted to the upper atmospheric layer, PAHs could be brought to the Pacific Ocean (Zhang et al., 2011b) and have an insignificant effect on the downwind areas in Northeast Asia, such as the Korean Peninsula. Moreover, Asian dust mainly derived from deserts in Mongolia and China (Sun, 2002), the non-PAH polluted areas. They could contain PAHs after passing through some polluted areas (Tamamura et al., 2007), such as industrial areas in northeastern China. The PAHs in these polluted regions could be trapped by near-surface winds and reached the downwind areas, including South Korea. Therefore, the source areas validated by the modified hybrid receptor models can be more reasonable compared to those suggested by the conventional ones.

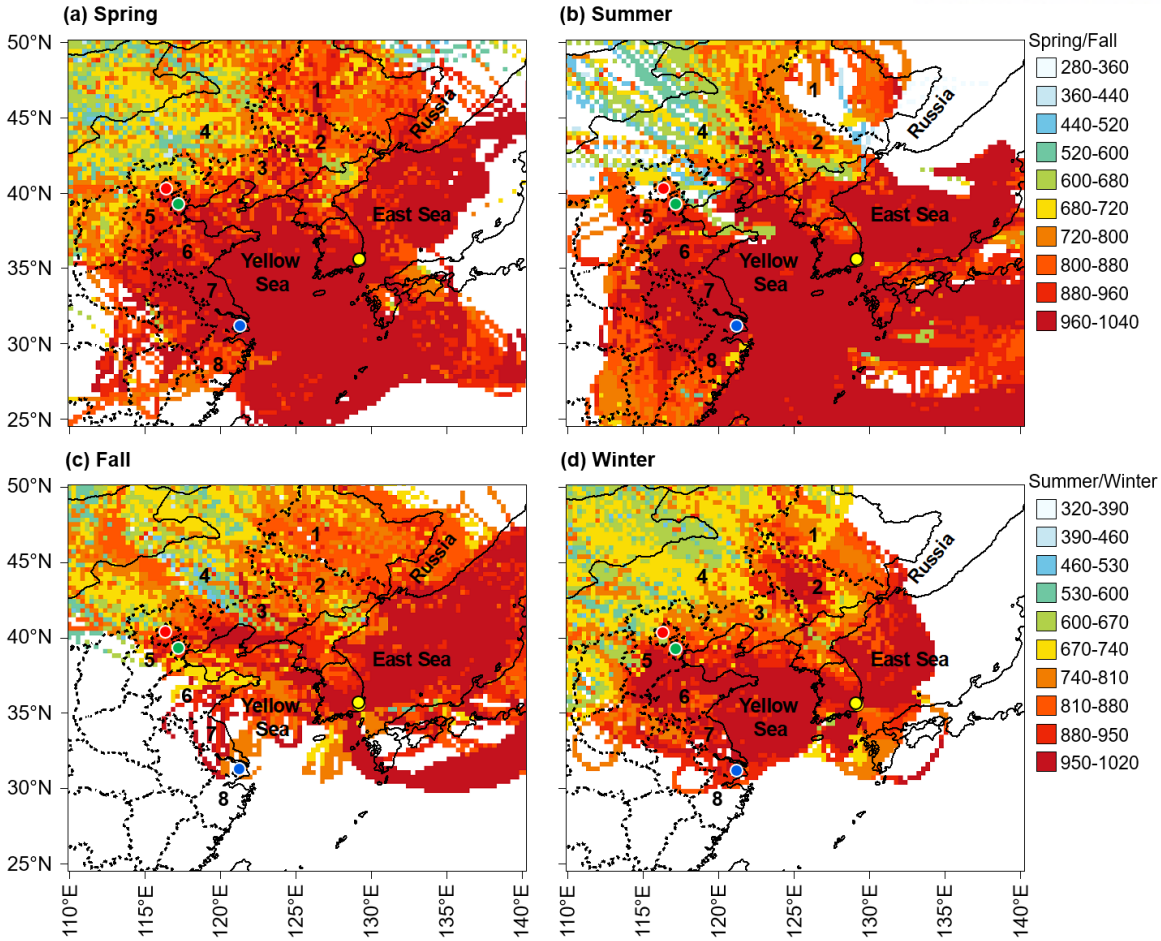

Figure 3-14. Air pressure (hPa) along the transport routes of backward air trajectories in the (a) spring, (b) summer, (c) fall, and (d) winter. Data were simulated from the HYSPLIT model adopting the GDAS meteorological data.

3.4. Conclusion

The hybrid receptor models (i.e., PSCF and CWT) and the CBPF analysis were applied to identify the local and non-local source areas of the gaseous and particulate PAHs in Ulsan, South Korea. Especially, the PSCF and CWT used in this study were modified by selecting trajectory segments within the mixing layer for the identification of more reliable source areas. The particulate PAHs in Ulsan could be more affected by the long-range transport (i.e., from northeastern China and/or North Korea), whereas the gaseous PAHs were mostly contributed by the local emissions (i.e., industrial and vehicle emissions). Particularly, in summer and fall, the effects of the local emission sources on the gaseous and particulate PAHs could be more important than those of the outside sources (i.e., trans-boundary transport from China). However, the opposite trend was observed for the PAHs in the spring and winter. That is, PAHs

originated from northern China (i.e., Hebei, Beijing, and Tianjin), northeastern China (i.e., Liaoning and Jilin), and North Korea could contribute to those at the receptor site.

In addition, the fraction-weighted trajectory (FWT) was firstly introduced in this study to improve the identification of emission source areas for organic compounds. The source areas highlighted by the FWT could be more appropriate than those suggested by the modified $PSCF^m$ and CWT^m, especially in summer and fall when the local emissions increased their contribution. Moreover, the modified $PSCF^m$ and CWT^m in this study could suggest the more suitable source areas of PAHs compared to the conventional ones. In particular, some areas in northeastern China (i.e., Inner Mongol and Heilongjiang) and Mongolia were neglected in the modified $PSCF^m$ and CWT^m because the air parcels in these areas could be lifted to the upper atmospheric layer, leading to the small effect of PAHs from those areas to the receptor site. Therefore, it is essential to consider the trajectory altitude when applying the hybrid receptor models for the better identification of source areas.

Chapter 4: Spatial distribution, temporal variation, and phase distribution of polycyclic aromatic hydrocarbons in runoff and surface water

Abstract

This study aims to investigate spatial distribution, temporal variation, and phase distribution of polycyclic aromatic hydrocarbons (PAHs) in runoff and surface water affected by the runoff discharges. The samples were collected at semi-rural, residential, and industrial sites of Ulsan, South Korea from April to October 2016. The target compounds were the 16 US EPA priority PAHs. The industrial site showed the highest PAH concentrations in the runoff and surface water due to its higher PAH levels in several environmental media. The runoff PAHs reached their highest concentrations in April, which could be strongly affected by the long dry period and the lower rainfall amount prior to the runoff sampling events. The phase distributions of PAHs were relatively similar among the sampling sites, which were the dominance of the dissolved PAHs (i.e., 2- to 4-ring species). In addition, contributions of the particulate PAHs in the runoff and surface water collected before the runoff events increased noticeably in May, mostly due to an effect of rainfall conditions. In July, PAHs in the surface water more distributed in the dissolved phase due to an effect of the higher water temperature. Regarding source identification, PAHs in the runoff and surface water could share the similar emission sources in most of the sampling periods, which were both petrogenic and pyrolysis sources. Additionally, the PAHs in the runoff of July could be also originated from coal/coke/heavy oil combustion as a result of industrial emission and local advection. The results from this study could contribute to the understanding of PAH behaviors and emission sources in the overland runoff and surface water.

4.1. Introduction

The PAHs are frequently detected in the environment (e.g., atmosphere, water, sediment, and soil) (ATSDR, 1990) because they are semi-volatile compounds that can be transferred among the environmental compartments. Once emitted from emission sources to the atmosphere, the PAHs can undergo wet and dry deposition to settle down on surface layers (e.g., soils and impervious surfaces). Then, rainfall-runoff can wash off the PAHs deposited on those surface layers and bring them to water bodies (e.g., streams, rivers, and lakes). In the water layer, the PAHs can be dissolved into the water and sorb to suspended solids within the water layer to form dissolved and particulate phases, respectively (Srogi, 2007). This process depends on several conditions, such as water temperature (Miller et al., 1998), concentrations of the suspended solids, and solubility of the PAH compounds (Srogi, 2007). In particular, the PAHs having low octanol/water partition coefficient (K_{OW}) and high solubility (i.e., naphthalene, acenaphthylene, and acenaphthene) tend to be distributed into the dissolved phase. On the other hand, species with higher K_{OW} values and lower solubility (i.e., benzo(g,h,i)perylene, indeno(1,2,3-c,d)pyrene, and benzo(a)pyrene) tend to sorb to organic matter of the suspended solids and be distributed in the particulate phase (Hwang and Foster, 2006). Additionally, the particulate PAHs can settle down onto the bottom sediment of the water bodies and be regarded as the sediment PAHs, which can also be re-distributed into the water layers under an effect of turbulence caused by inflow, such as rainfall and runoff discharge. Moreover, the PAHs dissolved in the water can evaporate into the atmosphere through the air-water exchange (Gigliotti et al., 2002a).

The overland runoff formed during rainfall or snowmelt has been regarded as one of the important sources to cause pollution for water bodies (Angrill et al., 2017; Parajulee et al., 2017). The PAHs in runoff discharge have been studied widely, but previous studies mostly focused on the runoff flowing over several types of impervious surfaces, such as pavements (Mahler et al., 2014), airport runway (Sulej et al., 2011), and highways (Lau et al., 2009). The consideration of these impervious surfaces may not entirely reflect the PAHs in runoff discharge because during the rainfall PAHs can be washed off from both the impervious surfaces and the soils (Petruzzelli et al., 2002; Shi et al., 2017; Zand et al., 2010). Moreover, the washout of PAHs accumulated in the soils can depend on several variables, such as soil infiltration capacity (Wang et al., 2006) affecting formation of the overland flow and soil texture controlling the dominant PAH species in the soils (Amellal et al., 2001; Li et al., 2010).

Therefore, a study on PAHs in runoff flowing over the soils is essential, as this runoff type can receive PAHs washed off from both the soils and surrounding impervious surfaces.

The runoff discharges can flow into water bodies (e.g., streams and rivers) during and after the rainfall. After receiving inflow from runoff and rainfall, the phase distribution of PAHs in the water bodies can be changed (e.g., increase of the particulate phase), partially depending on PAHs of the inflow. In addition, the PAHs in the water layer can be exchanged to become those in the air and sediment through multi-media transport (Cui et al., 2016; Gigliotti et al., 2002b). Thus, a study on the effect of inflow (e.g., runoff and rainfall) on the PAHs in water bodies is also necessary.

This study aims to investigate spatial distribution and temporal variation of PAHs in overland runoff and surface water of several water bodies receiving the runoff discharges. In addition, distribution coefficients of PAHs between the dissolved and particulate phases were also calculated to understand the behavior of PAHs in the study area. Moreover, emission sources of the PAHs in runoff and surface water were also identified. Results from this study can contribute to the understanding of PAHs from non-point pollution sources (e.g., runoff discharges) and PAH behaviors in the surface water affected by the inflow from runoff and rainfall.

4.2. Materials and methods

4.2.1. Study area and sampling method

PAHs in the runoff and surface water at three sampling sites (i.e., semi-rural, residential, and industrial sites) in Ulsan city, South Korea (Figure 4-1) were monitored from April to October 2016. Geographical information of the sampling sites is provided in Table 4-1.

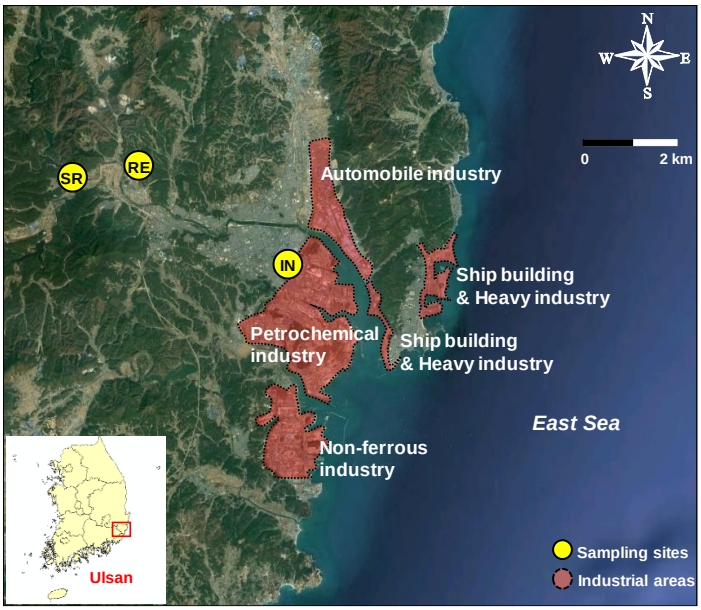

Figure 4-2. Locations of the semi-rural (SR), residential (RE), and industrial (IN) sampling sites in Ulsan, South Korea. The industrial areas are shaded in red color.

Table 4-1. Geographical information of the sampling sites in Ulsan, South Korea. The runoff, surface water, and soil samples were collected at each site.

Site	Area	Latitude	Longitude	Type of water body
Surface water sampling sites				
SR	Semi-rural	35°34'39.92"N	129°11'18.80"E	Stream*
RE	Residential	35°35'36.73"N	129°13'46.67"E	River*
IN	Industrial	35°32'2.00"N	129°21'3.47"E	Stream**
Runoff sampling sites				
SR	Semi-rural	35°34'37.21"N	129°11'06.82"E	-
RE	Residential	35°35'55.38"N	129°14'11.76"E	-
IN	Industrial	35°32'1.75"N	129°21'7.08"E	-
Soil sampling sites				
SR	Semi-rural	35°34'36.73"N	129°11'06.96"E	-
RE	Residential	35°34'55.64"N	129°14'09.27"E	-
IN	Industrial	35°32'01.66"N	129°21'06.80"E	-

*Upstream and **downstream of the Taehwa river in Ulsan, South Korea, respectively.

In each sampling period, the number of five runoff samples (1 L per sample) was taken at the semi-rural, residential, and industrial sites after the rainfall had started for 2.0–2.5 h. Overall, the number of 60 samples were collected over the whole study period. The interval between the sub-runoff samples were 10–15 min. The polypropylene buckets were used to collect the

runoff samples at the points where the runoffs flew into water bodies (i.e., streams and rivers). The samples were then transferred to pre-cleaned brown glass bottles and stored at 4 ºC until analysis.

For the sampling of surface water at each site, before and after the runoff events, surface water samples of water bodies receiving the runoff discharges were collected at a depth of 50 cm from the water surface (n = 24, 12 for each of the before and after runoff). The water samples (1 L per sample) were also taken using polypropylene buckets and contained in pre-cleaned brown glass bottles, then stored at 4 ºC. The detail on the sampling periods can be seen in Table 4-2.

Table 4-2. Information on the runoff and surface water sampling days.

April 2016							May 2016						
2	**3**	4	5	6	7	8	**17**	18	19	20	21	22	23
9	10	11	12	13	14	**15**	**24**	25	26	27	28	29	**30**
July 2016							**September 2016**						
19	20	21	22	23	24	**25**	**23**	24	25	26	27	**28**	29
26	27	28	29	30	31	**01**	30	01	02	03	**04**	05	06

Runoff sampling days
Sampling days for the soils and surface water (before the runoff events)
Sampling days for surface water (after the runoff events)

In addition, prior to the runoff events, soil samples surrounding the target water body at each sampling site were also collected to investigate the influence of soil properties (i.e., size of soil sands and soil organic carbon) on the PAHs in runoffs. At each site, three sub-soil samples (5 cm depth from the soil surface) were collected and mixed together for one final sample. The soil samples were kept at -4 °C until analysis.

4.2.2. Chemical analysis and QA/QC

The target compounds of this study are 16 US EPA PAHs, including naphthalene (Nap), acenaphthylene (Acy), acenaphthene (Ace), fluorene (Flu), phenanthrene (Phe), anthracene (Ant), fluoranthene (Flt), pyrene (Pyr), benzo(a)anthracene (BaA), chrysene (Chr), benzo(b)fluoranthene (BbF), benzo(k)fluoranthene (BkF), benzo(a)pyrene (BaP), benzo(g,h,i)perylene (BghiP), indeno(1,2,3-c,d)pyrene (Ind), and dibenzo(a,h)anthracene

(DahA). The runoff and surface water samples (500 mL per sample) were filtered using glass microfiber filters (GFF, pore size: 0.7 μm, diameter: 47 mm, Whatman, USA) to be separated into two phases, including dissolved phase containing the samples passing through the GFFs and particulate phase containing the remained samples on the GFFs. Prior to the filtration, the GFFs were baked at 400 °C for 4 h to remove organic contaminants. Noticeably, the dissolved phase could comprise both truly dissolved and colloidal PAHs, as the colloidal particles smaller than 0.7 μm could pass through the filters.

The target PAHs were extracted three times using liquid-liquid extraction equipment with 100 mL of dichloromethane/n-hexane (9:1) for the dissolved phase and sonication extraction with 20 mL of n-hexane/acetone (9:1) for the particulate phase. Prior to the extraction, surrogate standards (naphthalene-d_8, acenaphthene-d_{10}, phenanthrene-d_{10}, chrysene-d_{12}, and perylene-d_{12}) were added to the samples to check recoveries of the target chemicals. The extracted PAHs in the dissolved phase were then dehydrated using sodium sulfate anhydrous and were eluted with 30 mL dichloromethane. Meanwhile, the extracted PAHs in the particulate phase were cleaned up in glass funnels containing 5 g of silica gel (activated at 130 °C for 4 h) and 5 g of sodium sulfate. Next, they were eluted with 60 mL of n-hexane/dichloromethane (1:1). The samples were then concentrated by a TurboVap II (Caliper, USA) and a nitrogen evaporator (MGS-2200, Eyela, Japan) to 0.5 mL. Then, they were transferred to gas chromatography (GC) vials, spiked with internal standard (p-terphenyl-d14) and analyzed using a chromatograph coupled to a mass spectrometer (GC-MS, Agilent 7890 GC-5975C MS, USA). The operation conditions of the instrument can be seen in Section 2.2 of chapter 1.

The method blanks (n = 16, 8 for each of the dissolved and particulate phases) were also considered. PAHs in the blank samples were extracted and analyzed using the same method as for the real samples. Average recoveries of the dissolved PAHs were 46.5%, 49%, 59%, 75.7%, and 88.7% for naphthalene-d_8, acenaphthene-d_{10}, phenanthrene-d_{10}, chrysene-d_{12}, and perylene-d_{12}, respectively. Those of the particulate PAHs were 47.2%, 49.4%, 55.6%, 72.7%, and 83.2% for naphthalene-d_8, acenaphthene-d_{10}, phenanthrene-d_{10}, chrysene-d_{12}, and perylene-d_{12}, respectively. Method detection limits (MDL) of the dissolved and particulate PAHs were individually calculated as a multiplication between the Student's t value for a 99% confidence interval (3.14) and the standard deviation of 7 replicate spiked samples. The MDLs were 0.03–0.84 ng/L and 0.03–0.23 ng/L for the dissolved and particulate PAHs, respectively. Other parameters, such as concentrations of total suspended solids (TSS), dissolved organic

carbon (DOC) of the samples, and size of the soil sands were also quantified to understand the effect of those parameters on the PAHs in the runoffs and surface water. The TSS concentrations in runoff and surface water samples were quantified based on the gravimetric method (Rice et al., 2017). In particular, the samples (500 mL per sample) were filtrated with pre-weighted glass microfiber filters (GFF, pore: 0.7 μm, diameter: 47 mm) to separate the suspended solids in the samples. The GFFs were then dried to remove water and then weighted again. The TSS concentrations can be calculated based on the weight difference of the GFFs.

The DOC in each sample was analyzed using a TOC-5000 analyzer (Shimadzu, Japan). Prior to the analysis, the samples were filtrated with the GFF (pore: 0.7 μm, diameter: 47 mm), the filtered samples passing through the GFFs were then used for the analysis of DOC.
The soil samples, collected at watersheds receiving the runoff discharges, were classified into various sizes, including < 63 μm, 63–125 μm, 125–250 μm, 250–500 μm, 500–1000 μm, 1000–2000 μm, and > 2000 μm. The classification for soil sands was conducted using a dynamic sieve shaker (SJ-2155, Sinjung, South Korea).

4.2.3. Distribution coefficient between the dissolved and particulate PAHs

The distribution coefficients of PAHs between the dissolved and particulate phases were calculated based on the below equation (Schwarzenbach et al., 2003).

$$K_D = \frac{C_P}{C_D \times TSS} \quad (4\text{-}1)$$

where K_D (L/kg) is the distribution coefficient of PAHs between the dissolved and particulate phases. The higher K_D value indicates the stronger sorption capacity of PAHs to the suspended solids (Schwarzenbach et al., 2003). C_P and C_D (ng/L) denote the concentrations of PAHs in the particulate and dissolved phases, respectively. TSS (mg/L) is the concentration of the total suspended solids in the samples. The obtained K_D was also linearly correlated to the octanol-water partition coefficient (K_{OW}) of the PAHs to understand the hydrophobic properties of the sampled PAHs to the reference octanol/water system. The K_{OW} values of PAH species were obtained from Mackay and Callcott (1998).

4.2.4. Emission source identification and statistical analysis

The emission sources of PAHs in this study were identified using principal component analysis

(PCA). The PCA was performed in the Origin Pro 2017 SR2 (Origin Lab, USA). The varimax and correlation matrix options were selected for the PCA. Additionally, only extracted components having Eigenvalues higher than one were selected for further interpretation. The total (dissolved and particulate) concentration of each PAH compound was normalized by the total concentration of each sample. Especially, only PAHs detected in both dissolved and particulate phases were used for the PCA to ensure the reliability of the analysis. The Origin Pro 2017 SR2 (Origin Lab, USA) was also used to perform statistical analysis and plot graphs.

4.3. Results and discussion

4.3.1. Concentrations of the PAHs

Concentrations of the Σ_{16} PAHs in the runoff and surface water of Ulsan, South Korea are shown in Table 4-3 and Figure 4-2. Regarding the surface water, after receiving the runoff discharges, mean concentration of the total (particulate and dissolved) Σ_{16} PAHs at all sites and periods declined approximately 3.4 times (before runoff: 104.1 ng/L, after runoff: 30.4 ng/L), indicating the dilution effect by inflow from runoff and rainfall. A statistically significant difference of PAH concentrations was also found between the surface water before and after the runoff events. (Mann-Whitney rank-sum test, $p < 0.05$).

Table 4-3. Mean concentrations (ng/L) at all sites and periods of the dissolved and particulate PAHs in the runoff, surface water before and after the runoff events in Ulsan, South Korea.

	Runoff (n=60)		Surface water before the runoff (n=12)		Surface water after the runoff (n=12)	
	Dissolved	Particulate	Dissolved	Particulate	Dissolved	Particulate
Nap	21.440	5.735	<MDL	0.526	<MDL	<MDL
Acy	3.043	0.461	0.375	<MDL	0.480	<MDL
Ace	4.348	0.883	1.247	0.318	0.315	<MDL
Flu	15.371	6.301	10.184	4.100	0.516	1.908
Phe	40.563	12.283	31.954	7.028	1.954	3.083
Ant	5.452	2.624	3.625	3.235	1.933	0.694
Flt	10.355	3.025	11.795	0.926	2.589	0.738
Pyr	8.766	2.736	15.248	0.903	2.324	0.980
BaA	0.693	0.968	0.394	0.442	0.241	0.446
Chr	0.891	1.708	0.588	0.202	0.321	0.262
BbF	1.025	1.750	0.945	0.524	1.161	0.563
BkF	0.592	1.436	0.603	0.242	0.567	0.257
BaP	1.040	1.048	0.666	0.239	0.515	0.227
Ind	0.814	1.864	0.748	1.003	0.635	0.970
DahA	<MDL	1.216	<MDL	<MDL	<MDL	<MDL
BghiP	0.742	1.850	0.570	0.491	0.788	0.486
Σ_{16} PAHs	115.684	45.89	82.772	21.267	18.088	12.326

<MDL: Below detection limit. Half of the MDL was used to calculate concentrations of Σ_{16} PAHs.

4.3.1.1. Spatial distribution of PAHs in the runoff and surface water

The mean concentration of Σ_{16} PAHs at the industrial site (runoff: 272.2 ng/L, surface water before runoff: 185.7 ng/L, and surface water after runoff: 34.2 ng/L) were 1.1–3.2 times higher than those at the semi-rural (runoff: 252.4 ng/L, surface water before runoff: 58.6 ng/L, and surface water after runoff: 26.5 ng/L) and residential (runoff: 131.1 ng/L, surface water before runoff: 67.8 ng/L, and surface water after runoff: 30.5 ng/L) sites. The higher mean concentration at the industrial site could be due to its greater PAH levels in the ambient air (Vuong et al., 2020), soils (Jeon and Oh, 2019; Kwon and Choi, 2014a), and roadside soils (Kim et al., 2019b). The atmospheric deposition and washout during rainfall could bring the PAHs from these environmental media to the runoff and water bodies, resulting in the higher PAH concentrations at the industrial site.

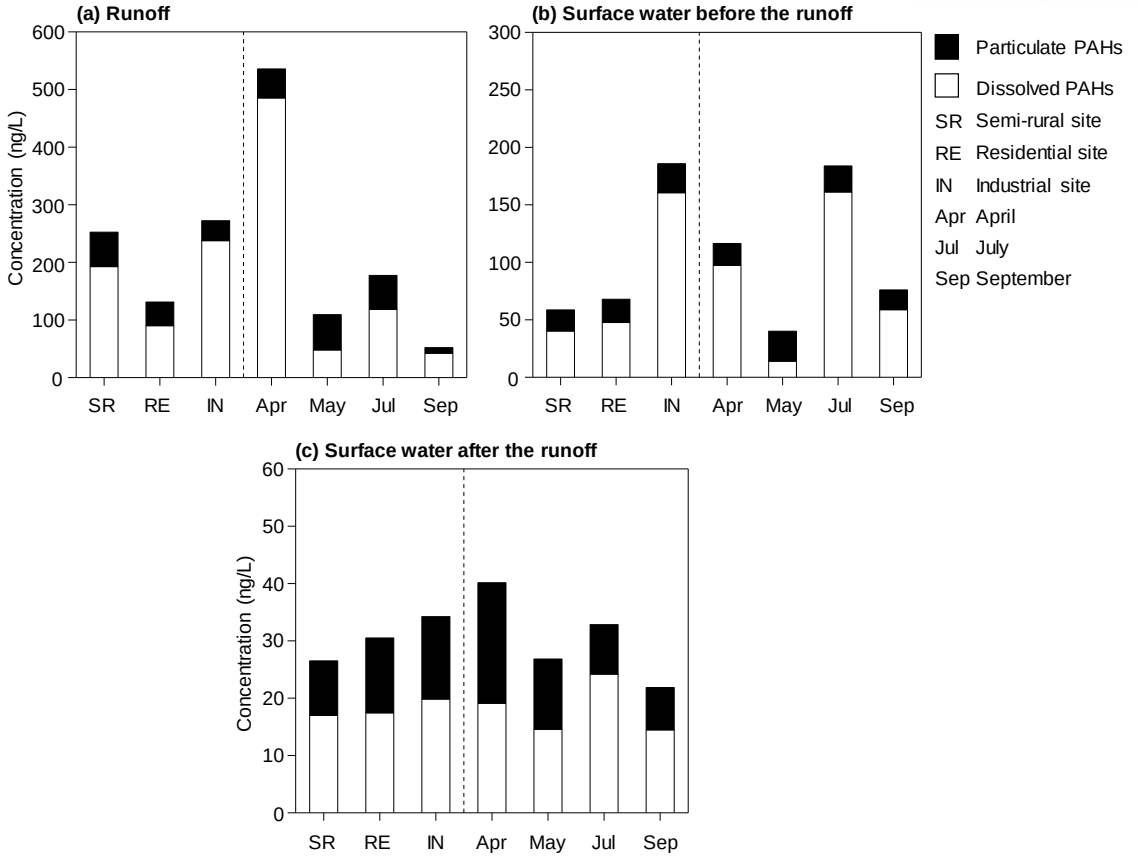

Figure 4-2. Spatial and temporal variations of mean concentrations of Σ_{16} PAHs in the (a) runoff, (b) surface water before the runoff events, and (c) surface water after the runoff events.

Interestingly, regarding the runoff samples, the mean concentration of Σ_{16} PAHs at the semi-rural site (252.4 ng/L) was comparable to that at the industrial site (205.1 ng/L) (Figure 4-2a). This observation might be influenced by several variables of the soils covered by the overland runoff, such as soil PAH levels, soil organic matter (SOM), and sizes of soil sands (Petruzzelli et al., 2002). The soils collected prior to the runoff events at the semi-rural site showed their higher fractions of fine (63–250 μm) and silt (< 63 μm) sands (Figure 4-3). These soil sands could contain a remarkable amount of PAHs (Li et al., 2010; Uyttebroek et al., 2006) due to their large surface area to volume ratios. During the rainfall, the smaller soil sands (i.e., fine and silt sands) could be firstly washed out due to their lighter weights and contribute to the overland runoff, leading to the higher PAH and TSS concentrations in the runoff at the semi-rural site (Figure 4-4).

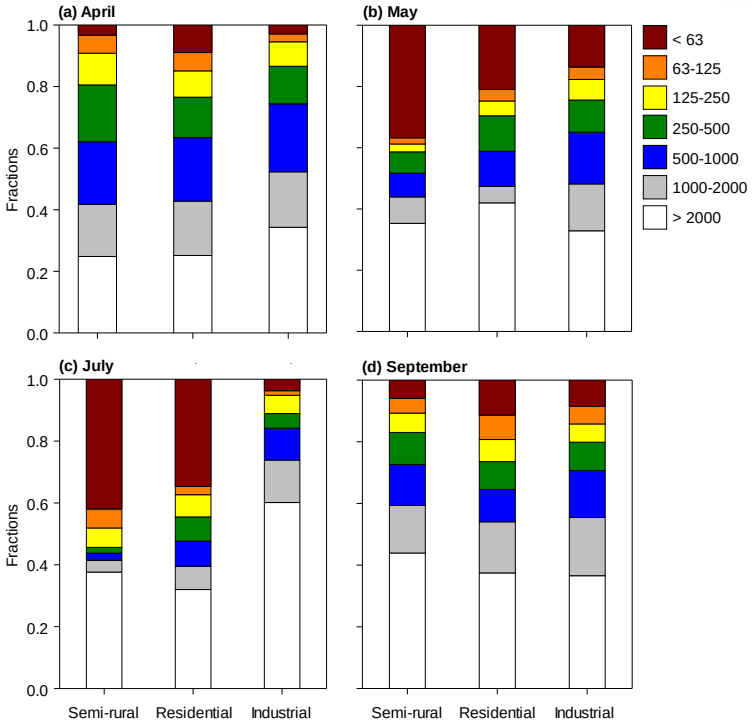

Figure 4-3. Size (μm) fractions of the soils collected at the three sampling sites in (a) April, (b) May, (c) July, and (d) September of 2016.

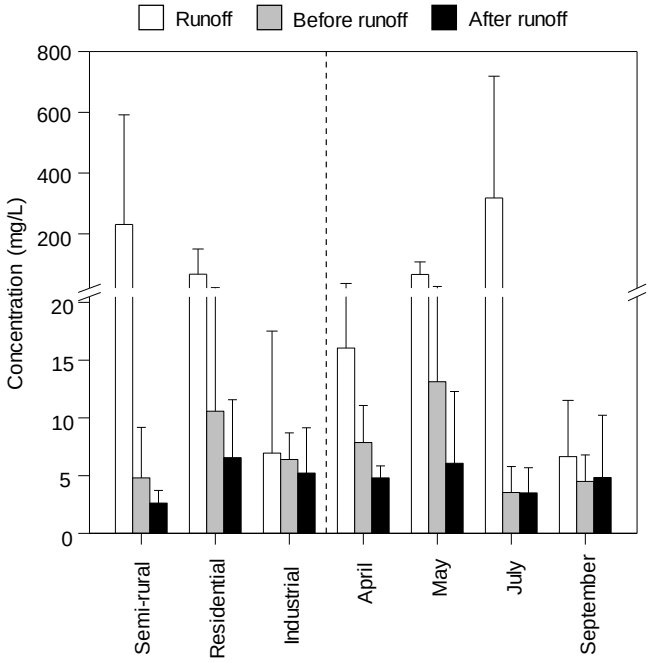

Figure 4-4. Concentrations of the total suspended solids (TSS) in the runoff and surface water before and after the runoff events.

4.3.1.2. Temporal variation of PAHs in the runoff and surface water

Regarding the temporal variation, the runoff PAHs reached their highest concentrations in April (Figure 4-2a) (ANOVA on ranks, $p < 0.05$). The longer dry days and the lower rainfall amount prior to the runoff events in April (Table 4-4) could lead to the more accumulation of PAHs in the atmosphere on the soils and impervious surfaces (e.g., roads, parking plots, and rooftops). An occurrence of runoff during rainfall after the long dry period could wash out the built-up PAHs, resulting in the highest PAH concentrations in the runoff events of April. The highest PAH levels in the first flush and their positive correlation to the antecedent dry period were also reported in previous studies (Gilbreath and McKee, 2015; Nielsen et al., 2015; Parajulee et al., 2017).

Table 4-4. Rainfall amount, rainfall intensity, and rainfall hour at several timelines throughout the study period. Data were obtained from the Korean Meteorological Administration (https://data.kma.go.kr)

	April	May	July	September
A. One month prior to the runoff events				
Dry day number (mm)	25	24	19	15
Rainfall amount (mm/h)	92.2	108.7	135.8	383.5
B. One week prior to the runoff events				
Rainfall amount (mm)	0	0	0	21.7
Rainfall intensity (mm/h)	0	0	0	0.56
Rainfall duration (h)	0	0	0	18
C. Two weeks prior to the runoff events				
Rainfall amount (mm)	164.6	514.5	115.5	1897.6
Rainfall intensity (mm/h)	0.54	1.53	0.43	5.64
Rainfall duration (h)	49	59	54	112
D. During the runoff events				
Rainfall amount (mm)	27.9	47.1	181.2	22.5
Rainfall intensity (mm/h)	3.1	5.2	20.1	3.8
E. 2 days prior to the sampling of surface water (before runoff events)				
Rainfall amount (mm)	0	264.1	0	8.2
Rainfall intensity (mm/h)	0	5.38	0	0.16
Rainfall duration (h)	0	23	0	15
F. From runoff events to the sampling of surface water (after runoff events)				
Rainfall amount (mm)	1296.8	115.9	874.3	325.6
Rainfall intensity (mm/h)	4.48	0.79	5.71	2.50

The lowest PAH concentrations in the runoff were shown in September (Figure 4-2a). The long rainy period and high rainfall amount prior to the runoff sampling events in September (Table 4-4) could induce a more frequent washout of PAHs and a decline of PAH accumulation on the soils and impervious surfaces, resulting in the lower PAH concentrations in the runoff discharge. Additionally, the rainfall amount during the runoff event in September was low (Table 4-4); thus, the runoff flow could be not strong enough to wash off large amounts of soil sands and deposited particles containing PAHs. The lower TSS concentrations in the runoff of September could also support this interpretation (Figure 4-4).

Regarding the surface water before the runoff events, the highest mean concentration of Σ_{16} PAHs was observed in July (Figure 4-2b). The absence of rainfall before the sampling events in July (Table 4-4) might lead to the lower dilution of PAHs in the surface water. After the

runoff events, PAHs in the surface water showed a similar temporal variation as that in the runoff (Figures 4-2a and 4-2b), suggesting that the runoff discharge is an important non-point source of PAHs in the surface water. This issue is more discussed in Section 4.3.4.

4.3.1.3. Comparison of the levels of PAHs

The mean concentrations (dissolved and particulate) of Σ_{16} PAHs measured in this study were compared to those in other areas and countries (Table 4-5). In general, the mean concentrations of Σ_{16} PAHs in the runoff of Ulsan (semi-rural: 252 ng/L, residential: 131 ng/L, and industrial: 272 ng/L) were approximately 0.8–2.9 times higher than those in the industrial (170 ng/L) and urban (100 ng/L) areas of Sweden (Kalmykova et al., 2013) and highways (93.4 ng/L) of the United States (Lau et al., 2009). Additionally, the dissolved concentration of runoff PAHs in this study (semi-rural: 167.1 ng/L, residential: 90.1 ng/L, and industrial: 89.8 ng/L) were 1.8–3.3 times higher than those collected in Gwangan bridge (50.3 ng/L) in Busan, South Korea. The runoff samples collected in Ulsan flew over the soils and could be contributed by PAHs washed out from both the soils and surrounding impervious surfaces, such as pavements and roads, leading to their higher PAH levels compared to the runoffs over impervious surfaces.

Table 4-5. Comparisons of mean concentration (ng/L) of the total (dissolved and particulate) PAHs in the runoff and surface water collected in Ulsan and several areas of other countries.

Area	Place	Country	Concentration	Reference
Runoff				
Rural	Tianjin	China	147×10^3	Shi et al. (2017)
Urban	Gothenburg	Sweden	100	Kalmykova et al. (2013)
Urban	Nantes	France	1994	Lamprea and Ruban (2011)
Urban	Busan	South Korea	50.3[a]	Ok et al. (2011)
Urban	Beijing	China	8300	Zhang et al. (2009)
Highway	Los Angeles	USA	93.4	Lau et al. (2009)
Airport runway	Gdansk	Poland	601	Sulej et al. (2011)
Industrial	Gothenburg	Sweden	170	Kalmykova et al. (2013)
Semi-rural	Ulsan	South Korea	252	This study
Residential	Ulsan	South Korea	131	This study
Industrial	Ulsan	South Korea	272	This study
Surface water				
Rural	Orgeval river	France	72[a,**]	Gateuille et al. (2014)
Suburban	Orge river	France	41[a,**]	Froger et al. (2019)
Suburban	Huaihe river	China	201.5	Liu et al. (2016)
Urban	Pearl river	China	130[*]	Zhang et al. (2012)
Urban	Anacostia river	USA	136	Foster et al. (2000)
Urban	Gao-ping river	Taiwan	430	Doong and Lin (2004)
Industrial	Ulsan bay	South Korea	319.4[*]	Khim et al. (2001a)
Semi-rural	Ulsan	South Korea	28.6[b]	This study
Residential	Ulsan	South Korea	32.6[b]	This study
Industrial	Ulsan	South Korea	90.2[b]	This study

[a] Only dissolved PAHs

[b] Mean concentrations before and after the runoff events

[*] 16 US EPA except for Nap

[**] 16 US EPA except for Nap, Acy, and Ace

Moreover, the mean concentrations of Σ_{16} PAHs collected in the surface water at the semi-rural, residential, and industrial sites of Ulsan were generally lower than those of several areas of other countries: Gao-ping river in urban area of Taiwan (mean: 430 ng/L) (Doong and Lin, 2004), Huaihe river in suburban area of China (mean: 201.5 ng/L) (Liu et al., 2016) and Anacostia river in urban area of the USA (mean: 136 ng/L) (Foster et al., 2000). Especially, the mean concentrations of the surface water PAHs in this study was 3.5–11.2 times lower than those in the Ulsan bay and Taehwa river (mean: 319.4 ng/L) (Khim et al., 2001a). The lower mean concentrations could be because the streams and rivers in this study mostly locate upstream of the Taehwa river and are small scales. In addition, PAH concentrations at the upstream of the Taehwa river could be lower than those at the downstream (Ligaray et al., 2016) surrounding by urban and industrial areas. The water sampling sites in the previous study (Khim et al., 2001a) mostly located downstream, therefore PAH concentrations at these sites

were higher due to the effect of urban and industrial emission.

4.3.2. Phase distribution of PAHs

The phase distributions of PAHs collected in this study are illustrated in Figure 4-5. The dissolved phase, mainly contributed by 2- to 4-ring PAHs (i.e., Nap, Phe, Flt, and Pyr) (Figure 4-6), was dominant, especially for the runoff and surface water before the runoff events (Figures 4-5a and 4-5b). In the water, 5-and 6-rings PAHs having low solubility (Mackay and Callcott, 1998) tend to bind to the suspended solids (SS), distribute in the particulate phase, and settle down to the bottom sediment. On the other hand, the 2- to 4-ring species having higher solubility (Mackay and Callcott, 1998) tend to be dissolved into the water, leading to the predominance of these species in the dissolved phase of the surface water layer. Regarding PAHs in the runoff, they could be originated mainly from wet deposition from the atmosphere and washout from soils and impervious surfaces. The 2- to 4-ring PAHs were more predominant in the wet deposition of Ulsan (Lee and Lee, 2004). Moreover, these species could also be dissolved easier by the runoff during rainfall because of their high solubility and low affinity to soil organic matter (Mackay and Callcott, 1998).

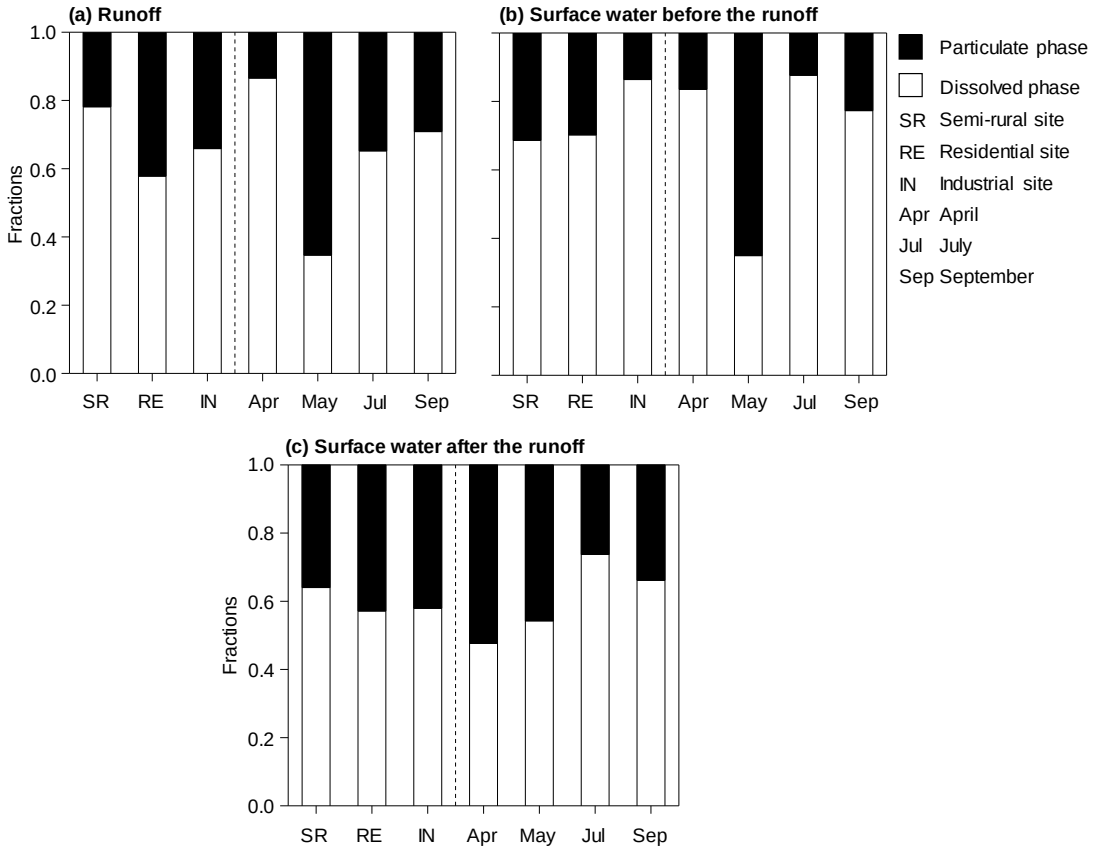

Figure 4-5. Phase distributions of Σ_{16} PAHs in the (a) runoff, (b) surface water before the runoff

events, and (c) surface water after the runoff events.

The particulate phase was mainly contributed by the 3-ring (i.e., Flu, Phe, and Ant), 4-ring (i.e., Flt and Pyr), and 6-ring (i.e., Ind and BghiP) PAHs (Figure 4-6). This observation is also in line with those reported in previous studies (Kalmykova et al., 2013; Niu et al., 2018; Park et al., 2012). The particulate phase showed its higher contribution to the surface water after the runoff events. The contributions of rainfall and runoff discharges to the water bodies could induce more solid-bound PAHs in the water layer, resulting in the increase of particulate phase in the surface water after the runoff events (Figure 4-5c). These particulate PAHs could be directly from the runoff discharges and raindrops. In addition, they might be released from bottom sediments into the overlying layer of the water bodies due to turbulence caused by runoffs and rainfall.

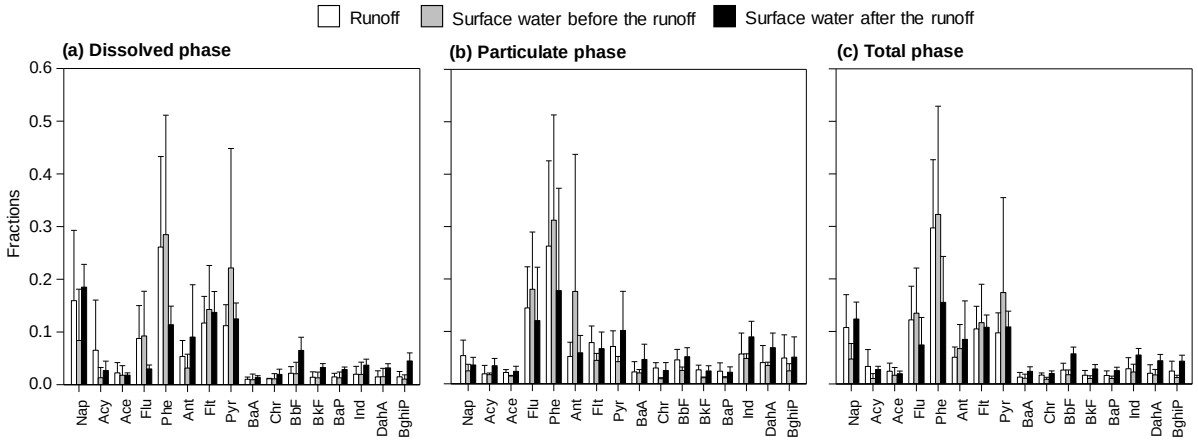

Figure 4-6. Contributions of individual PAHs in the (a) dissolved, (b) particulate, and (c) total phases.

4.3.2.1. Spatial variation of the phase distribution

The phase distributions of PAHs were relatively similar among the semi-rural, residential, and industrial sites, with the dominance of dissolved PAHs (Figure 4-5). Moreover, the dissolved PAHs remarkably increased their contributions in the surface water before the runoff events at the industrial site (Figure 4-5b). The greater DOM in the surface water at the industrial site (Figure 4-7) could promote the solubility of PAHs because they have the strong affinity to the DOM (Chiou et al., 1998), leading to the contribution increase of the dissolved PAHs in water layer at the industrial site. Moreover, the water salinity at the industrial site (mean: 11.6 ‰) was higher than that at the semi-rural (mean: 0.06 ‰) and residential sites (mean: 0.15 ‰). This observation could be because the water sampling site in the industrial area located near

the estuary (Figure 4-1), leading to an effect of seawater on the surface water in this area. Noticeably, the higher salinity could enhance higher concentrations of ions, which could compete with the PAHs to sorb to the SS (Li et al., 2016). As a consequence, PAHs could be desorbed from the SS and increase their contributions in the dissolved phase.

Contributions of the particulate PAHs in the runoff of industrial and residential sites were higher than that of the semi-rural site (Figure 4-5a). This observation can be explained by that the more impervious surfaces (i.e., parking lots, pavements, and roads) in the industrial and residential areas would induce more particle-bound PAHs deposition. On the other hand, the semi-rural site has more soil and vegetation surfaces; therefore, PAHs could strongly sorb to soil organic matter and lead to the lower contribution of particulate PAHs to the runoff (Parajulee et al., 2017).

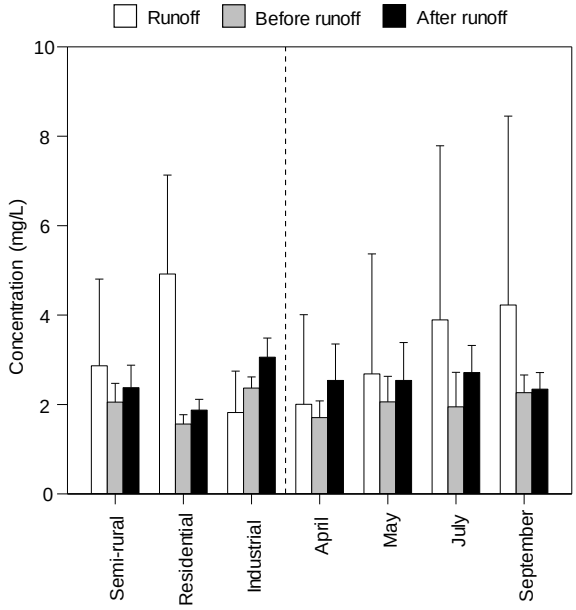

Figure 4-7. Concentrations of the dissolved organic carbon (DOC) in the runoff and surface water before and after the runoff events.

4.3.2.2. Temporal variation of the phase distribution

In May, contributions of the particulate PAHs in the runoff and surface water before the runoff events increased noticeably (Figures 4-5a and 4-5b). The large rainfall amount (1131 mm) and high rainfall intensity (3.36 mm/h) two weeks prior to the sampling of surface water (before runoff events) in May (Table 4-4) could induce more SS in the water bodies through runoffs and resuspension from the bottom sediment. The higher concentrations of SS could result in the greater contribution of particulate PAHs as the SS could act as sorbents for organic

compounds. Indeed, the positive correlation between the concentrations of TSS and particulate PAHs (R = 0.54) was found. In addition, the SS in the runoffs were expected to be mainly contributed by those depositing on the surfaces and leaching from the soils as mentioned previously. The large rainfall amount (514.5 mm) and rainfall intensity (1.53 mm/h) two weeks prior to the runoff events in May (Table 4-4) might decline the soil infiltration rate. Therefore, the overland runoff could be formed more quickly (Wang et al., 2006), and the small soil sands (e.g., fine and silt sands smaller than 250 μm and 63 μm, respectively) could be preferentially washed off due to their lighter weights. These light soil sands could be more polluted by PAHs (Amellal et al., 2001; Uyttebroek et al., 2006), leading to an elevation of the particulate fraction in the runoff of May. In July, PAHs in the surface water more distributed into the dissolved phase (Figures 4-5b and 4-5c). This result can be explained by the desorption of PAHs from the particulate to the dissolved phase (He et al., 1995), stemming from the higher water temperature during this period.

4.3.3. Distribution coefficient between the dissolved and particulate PAHs

The distribution coefficient (K_D) between the dissolved and particulate PAHs in the runoff and surface water are illustrated in Figures 4-8 and 4-9. In general, the K_D increased with molecular weights of the PAHs, reflecting the sorption capacity of the heavy species to the SS. Regarding the runoff, K_D values of the industrial site were higher than those of the others (Figure 4-8a), suggesting that SS in the runoff at the industrial site was more polluted by PAHs. These solids could be mainly washed out from the surrounding surfaces (i.e., soils and impervious surfaces) and could deposit from the atmosphere. The higher PAH concentrations in the soils (Kwon and Choi, 2014a), road soils (Kim et al., 2019b), and air particles (Lee et al., 2018) in the industrial area of Ulsan could contribute to the enrichment of PAHs in the SS of runoff discharges.

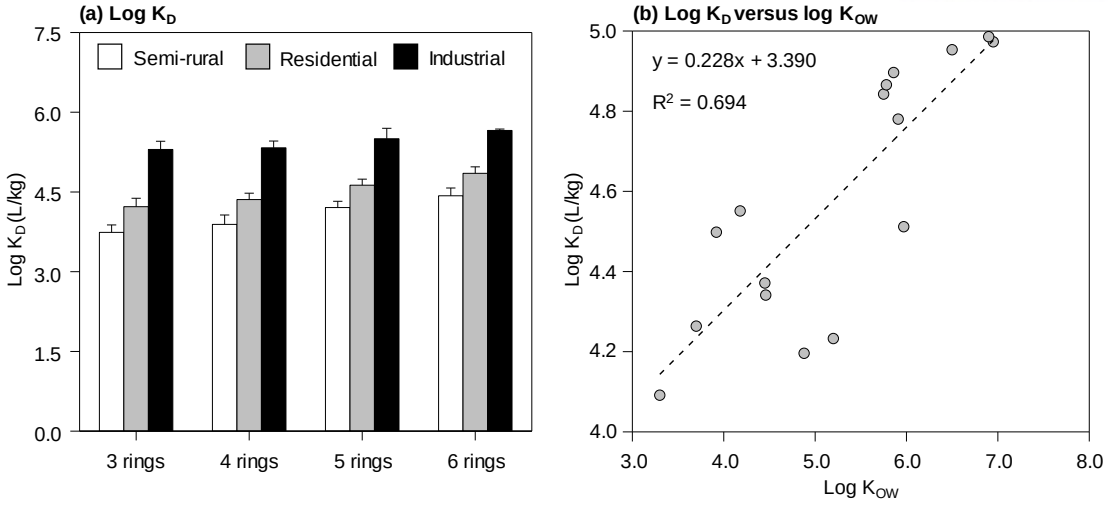

Figure 4-8. K_D values of PAHs (a) in the runoffs collected at three sampling sites and (b) correlation between the K_D of runoffs and K_{OW} for individual PAHs.

The K_D in the surface water showed a reverse trend to those of the runoff (i.e., semi-rural > residential > industrial) (Figure 4-9). The water body at the semi-rural site was shallower than those at the other sites, leading to a frequent release of the particle-bound PAHs in bottom sediments to overlying layers of the water body. The lowest K_D at the industrial site could be because of its higher DOC (Figure 4-7), resulting in the more dissolution of PAHs as described in Section 4.3.1.

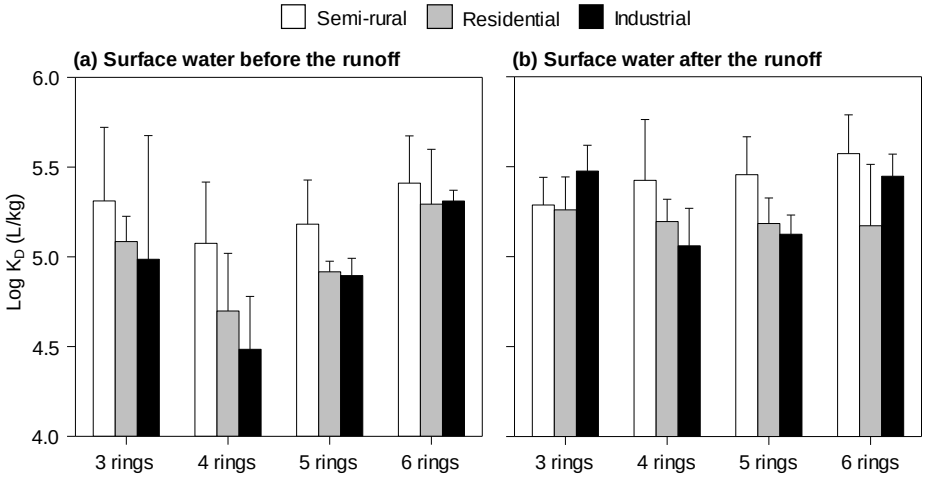

Figure 4-9. Log K_D values of PAHs in the surface water (a) before and (b) after the runoff events.

A strongly positive correlation between the K_D and K_{OW} was found for the PAHs in the runoff discharges (Figure 4-8b), indicating the sorption ability of PAHs would increase with their K_{OW}

values. The slope value derived from this correlation was lower than unity, suggesting an enrichment of the high molecular weight (HMW) PAHs in the dissolved phase, containing both truly dissolved and colloidal PAHs passing through the GFFs. These colloidal-bound PAHs were expected to cause the appearance of HMW PAHs in the dissolved phase. No or relatively low correlation was observed for PAHs in the surface water, which is consistent with that reported in a previous study (Zhang et al., 2017a). An explanation could be because several complicated processes in the water layer (e.g., biological degradation, resuspension, deposition, and photochemical degradation) would strongly and simultaneously affect the partitioning of PAHs in the surface water.

4.3.4. Source identification of the PAHs

The loading and score plots for the identification of PAH emission sources are shown in Figure 4-10. Only PAHs having high detection frequencies in both dissolved and particulate phases (except for Nap, Acy, Ace, and DahA) were considered for the PCA. Two principal components were extracted for each of the runoff and surface water samples. The two principal components accounted for 69.4% (for the runoff) and 76.6% (for the surface water) of the total data variance (Figure 4-10). The score and loading plots were simultaneously used to interpret relations between the PAH species and the samples.

Regarding the runoff discharge, most of the samples of April, May, and September were clustered in the same group locating at the left side and bottom left of the score plot (Figure 4-10a) and were characterized by the 3-ring PAHs (i.e., Flu, Phe, and Ant) as well as 4-ring PAHs (i.e., Flt, and Pyr). These PAHs are the dominant species in diesel emission (Zou et al., 2015) and petrogenic sources (Stogiannidis and Laane, 2015), suggesting that most of PAH species in the runoff of April, May, and September could be mainly originated from the vehicle emission and leaked from the petroleum products (e.g., oil leakage from transportation activities). Moreover, the runoff samples in July were separated into two groups. One group was on the left side of the score plot and overlapped samples of the other sampling periods, indicating the emission sources of PAHs in July could be similar to those in the others. Another group was at the upper right of the score plot and characterized by the 4-ring PAHs (i.e., BaA and Chr), 5-ring PAHs (i.e., BbF, BkF, and BaP), and 6-ring PAHs (i.e., Ind and BghiP) (Figure 4-10a), which could be the PAH markers from coal and coke combustion (Stogiannidis and Laane, 2015; Zou et al., 2015). Hence, PAHs in the runoff of July could be originated from

both petrogenic (e.g., leakage from petroleum products) and pyrogenic (e.g., diesel emission and coke/coal combustion) sources. The industrial area of Ulsan was mentioned to emit higher fractions of several PAH compounds, such as BaA, Chr, BbF, Ind, and BghiP (Lee et al., 2018), due to industrial combustion of coke, coal, and heavy oil (Kwon and Choi, 2014a; Nguyen et al., 2018). The PAH advection from the industrial to other areas (i.e., residential and semi-rural areas) due to the monsoon system in the summer (i.e, July) (Clarke et al., 2014) could contribute to an increase of these PAHs in the atmosphere and on the surface areas through deposition over the city. These PAHs could then undergo wet deposition and washout by runoff during rainfall.

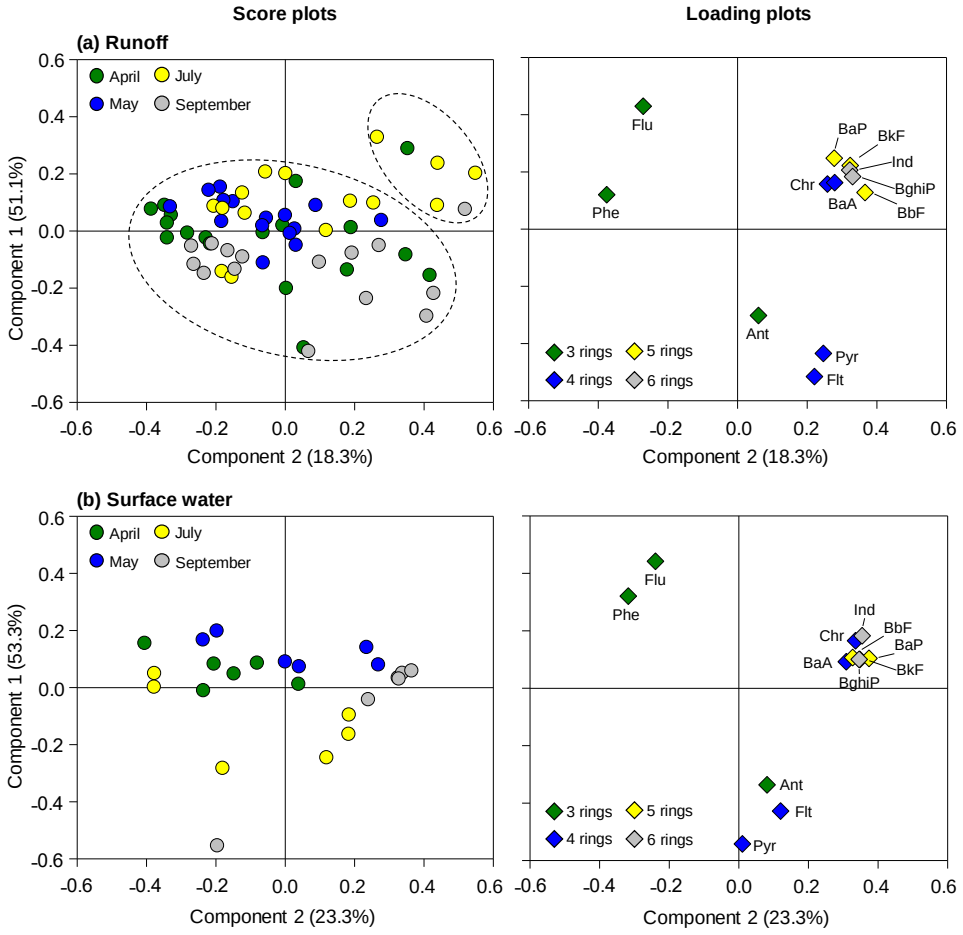

Figure 4-10. Score and loading plots for the (a) runoff and (b) surface water.

The PCA results of the surface water were similar to those of the runoff samples (Figure 4-10b), reflecting the PAHs in runoff and surface water could share the same emission sources. However, the surface water samples of September were mainly characterized by the medium (i.e., BaA and Chr) and heavy PAHs (i.e., BbF, BkF, BaP, Ind, and BghiP) (Figure 4-10b). The

PAHs in water bodies could be contributed from those in the runoff discharges, the atmosphere, and bottom sediments. The PAHs in the runoff of September were mostly characterized by the light species (3- and 4-ring PAHs) (Figure 4-10a). In addition, the deposition PAHs in Ulsan was reported to be dominated by the 2- to 4-ring species (Lee and Lee, 2004). These observations lead to the conclusion that the PAHs in the surface water of September could be re-suspended from the bottom layers of the water bodies. The largest rainfall amount before the sampling of surface water in September (Table 4-4) might lead to the resuspension of the medium and heavy PAHs from bottom to the overlying water layers. This result suggests that rainfall also has an important effect on PAHs in surface water.

4.4. Conclusion

In this study, the spatial distribution, temporal variation, and phase distribution of PAHs in the runoff and surface water collected at the semi-rural, residential, and industrial sites of Ulsan, South Korea were investigated. The highest PAH concentrations were observed at the industrial site due to its higher PAH concentrations in several environmental media (i.e., air, soil, and road soils) affecting the PAHs in runoff discharges and surface water. The concentrations of runoff PAHs were highest in April, mainly due to the strong effect of meteorological conditions prior to the sampling events (i.e., long dry periods and lower rainfall amount).

The dissolved PAHs (i.e., 2- to 4-ring species) were more dominant at all sampling sites. In addition, the particulate PAHs in the runoff and surface water collected before the runoff events increased their contributions noticeably in May, mostly due to an effect of rainfall conditions. Moreover, the higher water temperature in July could enhance the desorption of PAHs and result in an increase in the dissolved phase. Additionally, a positive correlation between the K_D and K_{OW} was found for the PAHs in the runoff discharges, indicating that the sorption ability of PAHs could increase with their K_{OW}. However, a relatively low correlation was observed for PAHs in the surface water, which could be due to an effect of several complicated processes in the water layer (e.g., resuspension, sediment deposition, and degradation).

Regarding the emission source identification, PAHs in the runoff and surface water could be primarily originated from the similar emission sources, which were both petrogenic (e.g., leakage from petroleum products) and pyrolysis (e.g., vehicle emission) sources. Additionally, PAHs in the runoff of July could be also emitted from coal/coke/heavy oil combustion as a result of industrial emissions and local advection. The results from this study could contribute

to the understanding of PAH behaviors in the runoff and surface water affected by the non-point sources. From the basis of this chapter, the exchange of PAHs between multimedia environment (i.e., air-water and air-soil), is investigated in the next chapter.

Chapter 5: Spatial distribution and temporal variation of air-water and air-soil exchange of polycyclic aromatic hydrocarbons

Abstract

This study aims to investigate spatial distribution and temporal variation of direction and magnitude exchange of PAHs between environmental media (i.e., air-water and air-soil) based on the fugacity approach. The study areas were in semi-rural, residential, and industrial areas of Ulsan, South Korea and the study periods were from March to October 2016. Regarding the air-water exchange, most of the PAHs showed net volatilization, indicating that the water could be a source for the atmospheric PAHs. For the air-soil exchange, 3-ring PAHs mainly volatilized from the soils, whereas 4-ring PAHs mostly deposited from the air, suggesting that the soils could act as a sink or source for the atmospheric PAHs depending molecular weights of the compounds. In addition, net volatilization was proved to be strongest in summer, mainly due to the effect of the higher air temperature and lower air concentrations. Moreover, the industrial site showed the highest exchange flux for both the air-water and air-soil exchanges, mainly due to the higher PAH concentrations in the multimedia environment (i.e., air, soil, and water) at this industrial site. Results from this study also revealed that distributions of PAHs in the soils were much higher than those in the air and water, mainly due to the accumulation of PAHs in the soils stemming from their affinity to soil organic matter. However, the atmospheric PAHs in Ulsan should be concerned due to the effect of local advection from industrial emission and long-range transport in this city.

5.1. Introduction

Multimedia transport is a process describing transport behavior and the fate of chemicals, such as polycyclic aromatic hydrocarbons (PAHs) in the environment. After being emitted into the environment, PAHs can transfer among the environmental compartments (i.e., air, soils, and water) under an effect of the 'grasshopper effect', describing the re-emission of deposited semi-volatile chemicals (Semeena and Lammel, 2005). The main emission sources of PAHs include pyrogenic (e.g., biomass burning and fossil fuel combustion) and petrogenic (e.g., petroleum products) sources. In addition, the primary receptor media for PAHs originated from those sources can be the atmosphere. However, the multimedia exchange can lead to the deposition of PAHs from the air to surfaces (i.e., soils, water, and impervious surfaces). Then the re-volatilization of PAHs from such surfaces can cause them to become secondary sources of PAHs in the environment.

To understand the transfer behavior of PAHs between environmental compartments (i.e., air-water and air-soil), the fugacity approach can be used. The term 'fugacity' indicates an escaping tendency (Mackay, 2001) of chemicals from one to another environmental compartment of (e.g., air-water and air-soil) in order to reach equilibrium conditions between them. In more detail, the fugacity approach describes the migration direction of chemicals based on diffusion (i.e., volatilization) and non-diffusion (i.e., deposition and resuspension). Additionally, net equilibrium is established when the fugacities of chemicals in both environmental compartments are equal. This approach has been widely used to investigate the exchange direction of PAHs between the air-water (Gigliotti et al., 2002b; Lammel et al., 2015) and air-soil (Choi et al., 2009; Degrendele et al., 2016). To quantify the transfer magnitude of PAHs between two environmental media, the Whitman two film model can be applied (Thibodeaux, 1996). In this model, the transfer of chemicals is assumed to cross the interface between two environmental media (i.e., air-water and air-soil) and mass transfer can be estimated based on the different concentrations between these media. Following this approach, exchange fluxes of PAHs between the air-water (Fang et al., 2012; Tidwell et al., 2017) and air-soil (Degrendele et al., 2016; Wang et al., 2011a) systems were quantified in several previous studies.

This study aims to understand the exchange of PAHs between the air-water and air-soil of Ulsan city, South Korea. In Ulsan, PAHs in the atmosphere (Choi et al., 2012b; Vuong et al., 2020), soils (Jeon and Oh, 2019; Kim et al., 2019a; Kwon and Choi, 2014a), and surface water (Khim

et al., 2001a; Park et al., 2012) were investigated. Additionally, dry and wet deposition amounts of PAHs in Ulsan were also quantified (Lee and Lee, 2004). However, the exchange of PAHs between the environmental media (i.e., air-soil and air-water) has not been investigated. Hence, a study on the PAH exchange is essential in Ulsan to understand which environmental media (i.e., air, water, and soils) can be a sink or source for the PAHs.

The main objectives of this study are to investigate the spatial distribution and seasonal variation of the PAH exchange between the air-water and air-soil of Ulsan. Based on the results of this study, the noticeable environmental media for PAHs in the study area can be inferred. Moreover, this study can also contribute to an understanding of PAHs (i.e., concentrations and profiles) and their exchange behavior (i.e., exchange direction and magnitudes) in the environment.

5.2. Materials and methods

5.2.1. Air, soil, and surface water sampling

To investigate the exchange of PAHs in the multimedia environment, atmospheric (n = 36), soil (n = 24), and surface water (n = 24) samples were collected at the semi-rural, residential, and industrial sites of Ulsan from March to October of 2016 (Figure 5-1). Since the air, soils, and surface water sampling sites are relatively close to each other, only the air sampling sites are marked in Figure 5-1. The geographical information of the air, water, and soil sampling sites can be seen in Table 5-1.

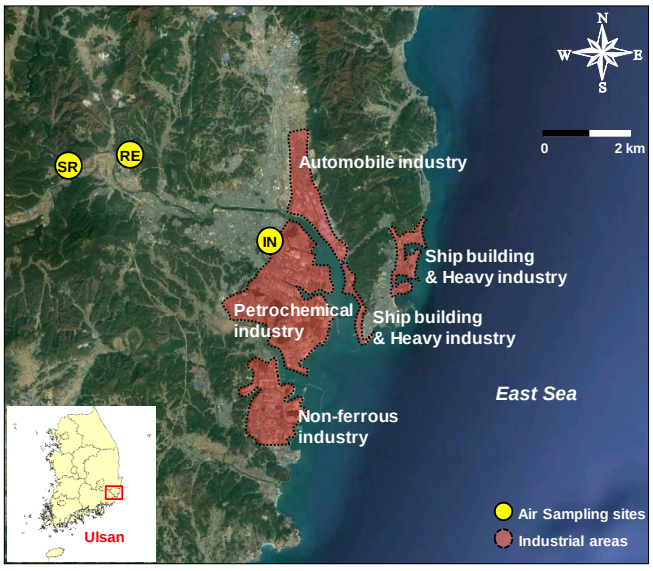

Figure 5-1. Air sampling sites at the semi-rural (SR), residential (RE), and industrial (IN) sites.

Regarding the air sampling, passive air samplers coupled with polyurethane foam (PUF-PAS) were deployed in triplicate at each sampling site. The PUF-PAS mainly captures the gaseous phase of organic chemicals (Klánová et al., 2008), therefore, the air PAHs reported in this study were mainly the gaseous species. The air sampling campaign was divided into four sub-periods: middle spring (March 21–April 22, 2016), late spring (May 17–June 20, 2016), summer (July 1–August 2, 2016), and fall (September 9–October 11, 2016). Prior to the sampling, the PUF disks were cleaned with n-hexane for 24 h to eliminate organic pollutants. Then they were kept in alumina foil and put in polyethylene bags. After the sampling, the PUF disks were stored at -4 °C until analysis.

Table 5-1. Geographical information of the air, soil, and surface water sampling sites at the semi-rural (SR), residential (RE), and industrial (IN) sites in Ulsan, South Korea.

Site	Area	Latitude	Longitude
Air sampling sites			
SR	Semi-rural	35°34'18.32"N	129°11'20.46"E
RE	Residential	35°34'55.88"N	129°14'07.84"E
IN	Industrial	35°32'01.35"N	129°21'07.66"E
Soil sampling sites			
SR	Semi-rural	35°34'36.73"N	129°11'06.96"E
RE	Residential	35°34'55.64"N	129°14'09.27"E
IN	Industrial	35°32'01.66"N	129°21'06.80"E
Surface water sampling sites			
SR	Semi-rural	35°34'37.65"N	129°11'07.16"E
RE	Residential	35°34'55.39"N	129°14'12.62"E
IN	Industrial	35°32'02.08"N	129°21'06.70"E

The surface water and soil samples were collected two times in each sampling period, including middle spring (April 2 and 15), late spring (May 17 and 30), summer (July 19 and August 1), and fall (September 23 and October 4). The sampling method for the surface water and soil samples are described in Section 4.4.2 of chapter 4.

5.2.2. Chemical analysis and QA/QC

The target chemicals in this study were the 16 priority PAHs suggested by the US EPA, except for naphthalene, acenaphthylene, and acenaphthene because these PAHs are blank contamination and potential sampling artifacts, especially for the air samples. The analysis procedures for the air and surface water samples can be seen in Sections 2.2 and 4.2 of Chapters

2 and 4, respectively. Noticeably, regarding the surface water samples, only the dissolved phase passing through the glass microfiber filters (GFFs) was considered for the air-water exchange of PAHs, as the dissolved compounds could mainly volatile from the water into the air whereas the particulate ones tended to deposit onto bottom sediments of water bodies.

Regarding the chemical analysis for the soil samples, the samples were first air-dried at room temperature (22 °C) and sieved to eliminate large particles (larger than 2 mm in diameter). The target PAHs in homogenized soil samples (20 g) were then extracted using Soxhlet extractor for 20 h with 350 mL of n-hexane/acetone. Surrogate standards (phenanthrene-d_{10}, chrysene-d_{12}, and perylene-d_{12}) were added to the samples prior to the extraction to check the recovery efficiency. The extracted compounds were then cleaned up in columns consisting of 2 g of sodium sulfate and 5 g of activated silica gel (130 °C, 4h), and then eluted with 70 mL of dichloromethane/hexane (1:3). The samples were concentrated until 0.5 mL using TurboVap II (Caliper, USA) and nitrogen evaporator (MGS-2200, Eyela, Japan). The samples were then spiked with internal standard (*p*-terphenyl-d_{14}) prior to analyzed using a gas chromatograph coupled to a mass spectrometer (GC-MS, Agilent 7890 GC-5975C MS, USA). The operation conditions of the instrument can be seen in Section 2.2 of chapter 2. In addition, the method blanks (n = 4) were also considered to check contamination during the experiment process and they were treated the same as the real samples.

The average recoveries of surrogate standards were 55.6%–79.7% for the air, 59%–88.7% for the surface water, and 55.6%–79.7% for the soil samples. The method detection limits were calculated as described in the previous chapters and ranged 0.04–0.25 ng/m^3 for the air, 0.03–0.20 ng/L for the surface water, and 0.20–1.30 ng/g for the soil samples. Moreover, to support the calculation of air-soil exchange, total organic carbon (TOC) of the soil samples was identified using the TOC-5000 analyzer (Shimadzu, Japan). The total carbon (TC) and inorganic carbon (IC) contents were quantified, and the TOC was calculated based on different concentrations between the TC and IC.

5.2.3. Calculation of the atmospheric concentration

Atmospheric concentrations of PAHs collected by the PUF-PAS were calculated using this equation.

$$C_A = M/V_{eff} \quad (5\text{-}1)$$

where C_A (ng/m^3) is the atmospheric concentration of the PAH compound. M and V_{eff} denote the amount of PAHs (ng) and effective volume (m^3) collected by the PUF-PAS, respectively. The V_{eff} was estimated for each PAH compound following Herkert et al. (2018). In addition, a detail description of the calculation of V_{eff} can also be seen in the previous study on air PAHs in Ulsan (Vuong et al., 2020).

5.2.4. Calculation of the air-water exchange

The flux magnitude and direction exchange of PAHs between the surface water and atmosphere were calculated using the below equation (Thibodeaux, 1996).

$$F_W = K_{OL} \times (C_{Dis} - C_{Gas}/H') \quad (5\text{-}2)$$

where F_W (ng/m^2/d) is the air-water exchange flux of PAHs. K_{OL} (m/d) is the overall mass transfer coefficient of PAHs between the air and surface water and was calculated following equation (4-3). C_{Dis} and C_{Gas} (ng/m^3) are concentrations of the dissolved and gaseous PAHs, respectively. H' is the dimensionless Henry's law constant, calculated by dividing Henry's law constant at a reference temperature (298 K) by the universal gas constant (R = 8.314 Pa m^3/mol/K) and the air temperature (K). The H' was calculated for each PAH compound and corrected to the sampling temperature following R.Lide (2004). In general, the F_W values higher than one indicate the net volatilization of PAHs from the surface water to the air. In contrast, the F_W lower than one can suggest net deposition. The K_{OL} in equation (5-2) was calculated as follows.

$$1/K_{OL} = 1/K_W + 1/K_A \times H' \quad (5\text{-}3)$$

where K_{OL} (m/d) is the overall mass transfer coefficients of PAHs between the air and surface water. K_W and K_A (m/d) denote the mass transfer of PAHs in water and air, respectively and were estimated as below (Mackay et al., 2006a).

$$K_W = 10^{-6} + 0.0034 \times u_* \times SC_W^{-0.5} \quad (5\text{-}4)$$

$$K_A = 10^{-3} + 0.0462 \times u_* \times SC_A^{-0.67} \quad (5\text{-}5)$$

$$u_* = 0.01 \times (6.1 + 0.63 \times u_{10})^{0.5} \times u_{10} \quad (5\text{-}6)$$

where u_* is friction velocity (m/s) of the PAHs. u_{10} (m/s) is average wind speed during the air sampling campaigns and were obtained from the Korean Meteorological Administration

(https://data.kma.go.kr). SC_W and SC_A (dimensionless) represent water phase and air phase Schmidt number of PAHs and they were estimated using the following equations (Bidleman and McConnell, 1995; Tao et al., 2017).

$$SC_W = 5.42 \times MW + 825.04 \quad (5\text{-}7)$$

$$SC_A = 0.0033 \times MW + 1.85 \quad (5\text{-}8)$$

where MW is molecular weight (g/mol) of the PAHs.

Moreover, fugacity fractions (FR), reflecting the exchange direction of PAHs between the surface water and the air, were also considered in this study.

$$FR = f_A/f_W = C_{Gas} \times R \times T/C_{Dis} \times H' \quad (5\text{-}9)$$

where f_A and f_W (Pa) are the air and water fugacity, respectively. C_{Dis} and C_{Gas} (mol/m^3) are the dissolved and gaseous concentrations of PAHs, respectively. R, T, and H' are defined as mentioned above. The FR values in between 0.3–3.0 suggest phase equilibrium, reflecting a complete transfer of PAHs between the air and surface water. Moreover, the FR higher than 3.0 and lower than 0.3 indicates net deposition and volatilization, respectively (Lammel et al., 2015).

5.2.5. Calculation of the air-soil exchange

The exchange directions of PAHs between the air and soils were determined using the fugacity fraction (*ff*) (Mackay, 2001).

$$ff = f_S/f_S + f_A \quad (5\text{-}10)$$

where f_S and f_A (Pa) are the soil and air fugacity of PAHs, respectively. The *ff* values in between of 0.3 and 0.7 indicate the equilibrium condition, the *ff* values higher than 0.7 suggest net volatilization of PAHs from the soils to the air, and *ff* lower than 0.3 indicates net deposition of PAHs from the air to soils (Harner et al., 2001). The soil and air fugacity were estimated using the below equations (Harner et al., 2001).

$$f_S = C_S \times R \times T/0.411 \times f_{OM} \times K_{OA} \quad (5\text{-}11)$$

where C_S (mol/m^3) is the concentration of PAHs in the soils. T (K) is the atmospheric

temperature. f_{OM} denotes fractions of soil organic matter, estimated by multiplying the soil organic carbon and 1.72 (W.Murphy, 2014). K_{OA} denotes the octanol/air partition coefficient of PAHs, estimated following Lei et al. (2002) and Xiao and Wania (2003). 0.411 is the correlation coefficient constant between the air/soil partition coefficient (K_{SA}) and the K_{OA}. The air fugacity was calculated as below.

$$f_A = C_A \times R \times T \quad (5\text{-}12)$$

where C_A (mol/m^3) is the air concentration of PAHs. R and T are the universal gas constant (8.314 Pa m^3/mol/K) and air temperature (K), respectively. The exchange flux of PAHs between the air and soil was calculated using this equation (Mackay, 2001).

$$F_S = D_{SA} \times (f_S - f_A) \times MW \quad (5\text{-}13)$$

where F_S (ng/m^2/d) is the air-soil exchange flux of PAHs. D_{SA} (mol/Pa/m^2/h) is the transfer coefficient and was calculated as below (Kobližková et al., 2009).

$$D_{SA} = 1/((1+D_{SAB})+ 1/(D_{SAA}+D_{SAL})) \quad (5\text{-}14)$$

where D_{SAB}, D_{SAA}, and D_{SAL} are air boundary layer, soil-air phase diffusion, and soil-water diffusion, respectively. The calculation methods for these variables are reported elsewhere (Kobližková et al., 2009).

5.3. Results and discussion

5.3.1. Concentrations of PAHs in the air, surface water, and soils

The mean concentrations of Σ_{13} PAHs in the air, surface water and soils are illustrated in Figure 5-2. In general, PAH concentrations at the industrial (air: 26.6 g/m^3, surface water: 153.84 ng/L, and soils: 72.16 ng/g) were 2.8 to 4.4 times higher than those at the residential (air: 9.53 g/m^3, surface water: 43.84 ng/L, and soils: 25.02 ng/g) and semi-rural (air: 8.80 g/m^3, surface water: 36.17 ng/L, and soils: 16.43 ng/g) sites (Mann-Whitney rank-sum test, $p < 0.05$). The spatial variations of PAH concentrations were consistent to those in previous studies investigating PAHs in the soil (Jeon and Oh, 2019; Kwon and Choi, 2014a), air (Choi et al., 2012b; Vuong et al., 2020), and surface water (Khim et al., 2001a) of Ulsan. Moreover, these observations could also reflect the concentration gradients of PAHs from the main emission sources (e.g., industrial area) to the receptors (e.g., residential and semi-rural areas) in Ulsan.

The temporal variations of PAHs varied depending on the environmental media. Regarding the air, the mean PAH concentrations reached their lowest values in the summer (mean: 12.43 ng/m^3) (Figure 5-2a), when the air temperature was highest (mean: 25.3 °C). An increase of air mixing height and photochemical reactions during summer could also increase the dispersion and degradation of PAHs (Keyte et al., 2013b), resulting in the decrease of PAH concentrations in this period. However, no statistically significant difference was observed for the atmospheric PAHs among the sampling periods. In fact, the concentrations of PAHs in the air could vary depending on meteorological conditions, such as air temperature and wind speed. The similar mean air temperature (middle spring: 11.8 °C, late spring: 18.9 °C, summer: 25.3 °C, fall: 21.7 °C) and mean wind speed (middle spring: 2.11 m/s, late spring: 1.64 m/s, summer: 1.60 m/s, and fall: 2.19 m/s) among the air sampling periods could, therefore, explain for the non-statistical difference of PAH concentrations during the sampling campaigns.

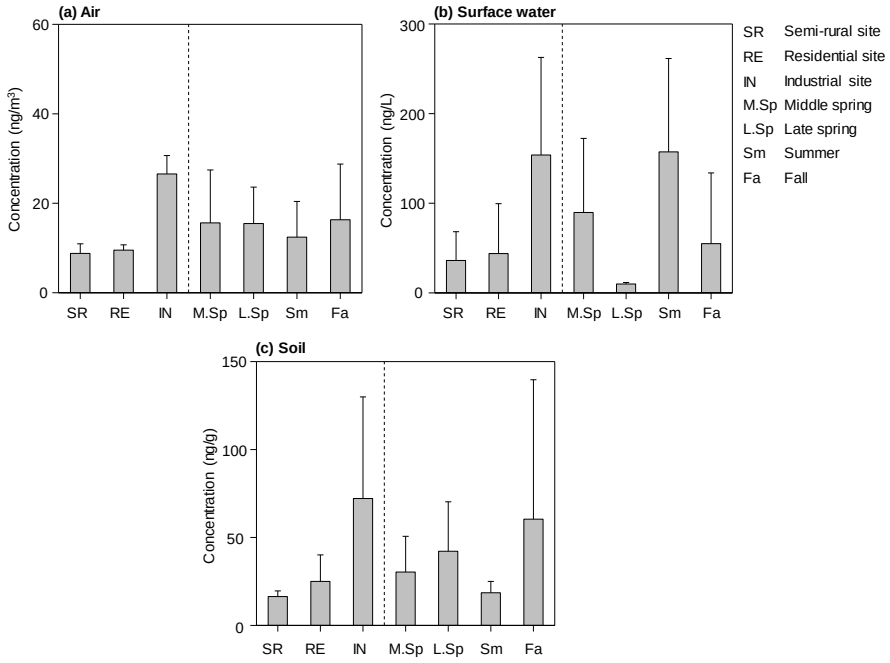

Figure 5-2. Mean concentrations of Σ_{13} PAHs in the (a) air, (b) surface water, and (c) soils at the semi-rural, residential, and industrial sites.

For the surface water, mean concentrations of Σ_{13} PAHs were highest in the summer (88.84 ng/L), followed by middle spring (52.94 ng/L), fall (32.78 ng/L), and late spring (10.33 ng/L) (Figure 5-2b). The highest PAH concentrations in summer could be because of the stronger desorption of PAHs from the particulate to the dissolved phase (Niu et al., 2018), stemming from the higher water temperature during this period. The lowest dissolved concentration was

shown in late spring. In fact, the PAH concentrations in water bodies could be affected by inflows (i.e., rainfall and runoff), the higher rainfall prior to the sampling campaigns in May (Table 4-4 in Chapter 4) could, therefore, lead to the stronger dilution of PAHs in the water and result in the lowest concentrations of dissolved PAHs in the late spring.

The mean concentrations of Σ_{13} PAHs in soils were highest in fall (60.41 ng/g), followed by late spring (42.16 ng/g), middle spring (30.36 ng/g), and summer (18.55 ng/g) (Figure 5-2c). The PAH concentrations in soils could be affected by several variables, including air temperature, controlling the volatilization and deposition of PAHs, and soil organic carbon, affecting the sorption ability of PAHs to the soils (Wang et al., 2011a). The total organic carbon (TOC) of the soils showed the highest concentration in the fall (Figure 4-4). Added to this, the PAH concentrations also showed a relatively strong correlation to the soil organic carbon in fall (R= 0.74), indicating that the PAHs could more bind to organic matter of the soils and result in the highest concentrations of PAHs in this sampling period. Moreover, the lowest PAH concentrations in the summer could be due to the higher air temperature promoting the stronger volatilization of PAHs from the soils (Keyte et al., 2013b). The temporal variations of PAH concentrations in soils corresponding to air temperature were also reported elsewhere (Dumanoglu et al., 2017; Wang et al., 2008).

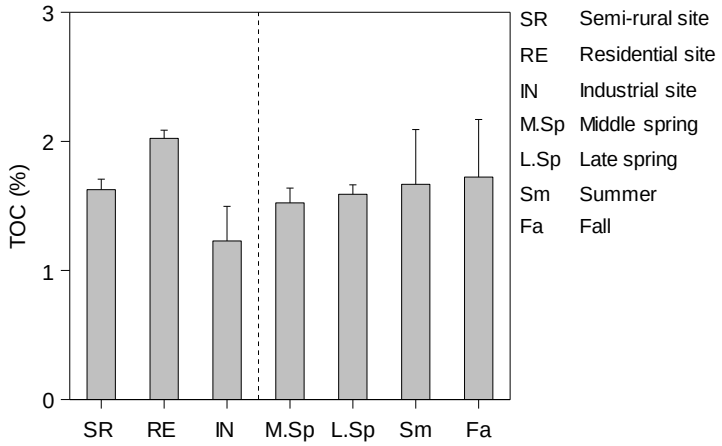

Figure 5-3. Total organic carbon (TOC) at three sites and four sampling periods.

5.3.2. Profiles of PAHs in the air, surface water, and soils

The profiles of PAHs in the air and surface water were relatively similar, with a dominance of 3- to 4-ring PAHs, such as Flu, Phe, Ant, Flt, and Pyr (Figure 5-4). These species have higher volatility and water solubility compared to the 5- to 6-ring PAHs (R.Lide, 2004), resulting in their predominance in the gaseous and dissolved phases. Regarding the surface water, the 4- to 6-ring PAHs (i.e., BaA, Chr, BbF, BkF, and Ind) increased their contributions especially in sampling periods showing higher rainfall amount (i.e., middle spring and fall) (Figure 5-4b). This observation might derive from the contributions of colloidal PAHs passing through the filters for sample filtration. The greater rainfall level could lead to higher concentrations of the TSS in water bodies through runoff and turbulence within the water layer. The TSS could then act as sorbents for the particulate and colloidal PAHs in the water.

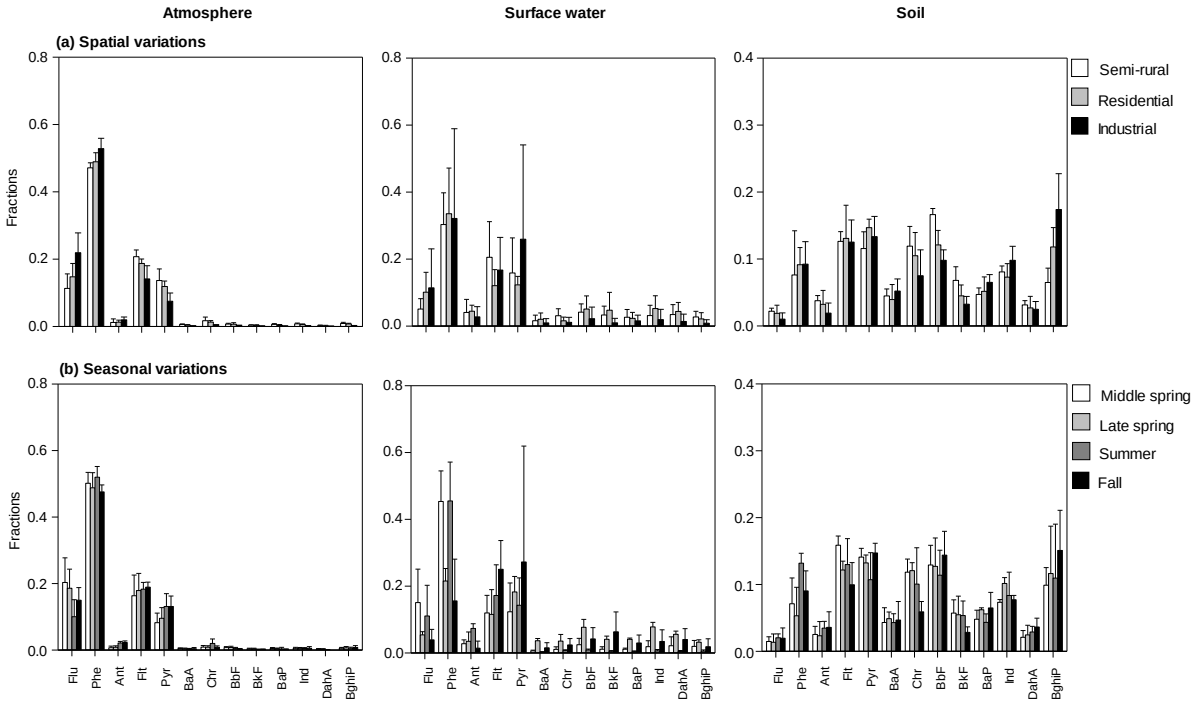

Figure 5-4. Contributions of PAH species in the (a) atmosphere, (b) surface water, and (c) soils at three sampling sites in four periods.

The 4- to 6-ring PAHs (i.e., Flt, Pyr, Chr, BbF, and BghiP) were more dominant in the soils (Figure 5-4). These compounds have lower volatility and higher affinity to soil organic matter compared to the others (R.Lide, 2004), leading to their stronger sorption to the soil particles, and thus, higher contributions in the soils. On the other hand, the 3-ring PAHs (i.e., Flu, Phe, and Ant) have higher volatility and shorter half-lives in the soils (Mackay et al., 2006a).

Therefore, they could be degraded or volatilize easier and had lower contributions. These observations were also in line with those reported in previous studies (Kwon and Choi, 2014a; Shi et al., 2017).

Regarding the spatial distribution and temporal variation, the PAH profiles of the air and soils were relatively similar among the sampling sites and periods, with a dominance of 3- to 4-ring PAHs for the air and 4- to 6-ring PAHs for the soils (Figure 5-4). These observations might be derived from the relatively similar meteorological conditions (i.e., air temperature and wind speed), potential PAH emissions, and organic carbon of the soils among the sampling campaigns. For the surface water, the dissolved PAHs at the industrial site were more dominant by the 3- and 4-ring PAHs (Figure 5-4). The higher DOC at the industrial site (Figure 4-7 in chapter 4) could enhance the fraction of dissolved PAHs, especially the 3- and 4-ring species because they have higher water solubility and stronger affinity to the DOC. Moreover, the surface water in the late spring showed an increase of the 5- to 6-ring PAHs (Figure 5-4). As the heavy PAHs could primarily bound to particles or solids, this result could be derived from the higher rainfall amount in the late spring, leading to the higher colloidal-bound PAHs as mentioned previously.

5.3.3. Air-water and air-soil exchange of PAHs

In this study, only the gaseous PAHs having the ability to directly undergo the exchange between multimedia environment (i.e., air-water and air-soil) were considered. The PUF-PAS for collecting the air PAHs mostly captures the gaseous compounds (Melymuk et al., 2011). However, some portions of the particle-bound PAHs (i.e., 5- and 6-ring species) could also be trapped due to inefficient filtration for atmospheric particles of the PAS protective chamber (Melymuk et al., 2011). As the 3- and 4-ring PAHs (i.e., Flu, Phe, Ant, Flt, Pyr, BaA, and Chr) collected by the PUF-PAS are believed to be primarily in the gaseous phase (Nguyen et al., 2020), these species were selected for the consideration of air-water and air-soil exchange of PAHs.

5.3.3.1. Air-water exchange of the PAHs

The exchange flux and fugacity ratios (FR) for the air-water exchange of PAHs are shown in Figure 5-5. Generally, most of the PAHs, except for Phe, mainly volatilized from surface water to the air, reflecting that surface water could be a source for the gaseous PAHs in Ulsan.

However, no correlations were found between the exchange flux or FR and the air concentrations, indicating that the volatilization from surface water could insignificantly contribute to the air PAHs. Interestingly, Phe mainly showed the net deposition, which could be due to its high concentration in the air promoting the escaping tendency to the other environmental media (Mackay, 2001), such as surface water.

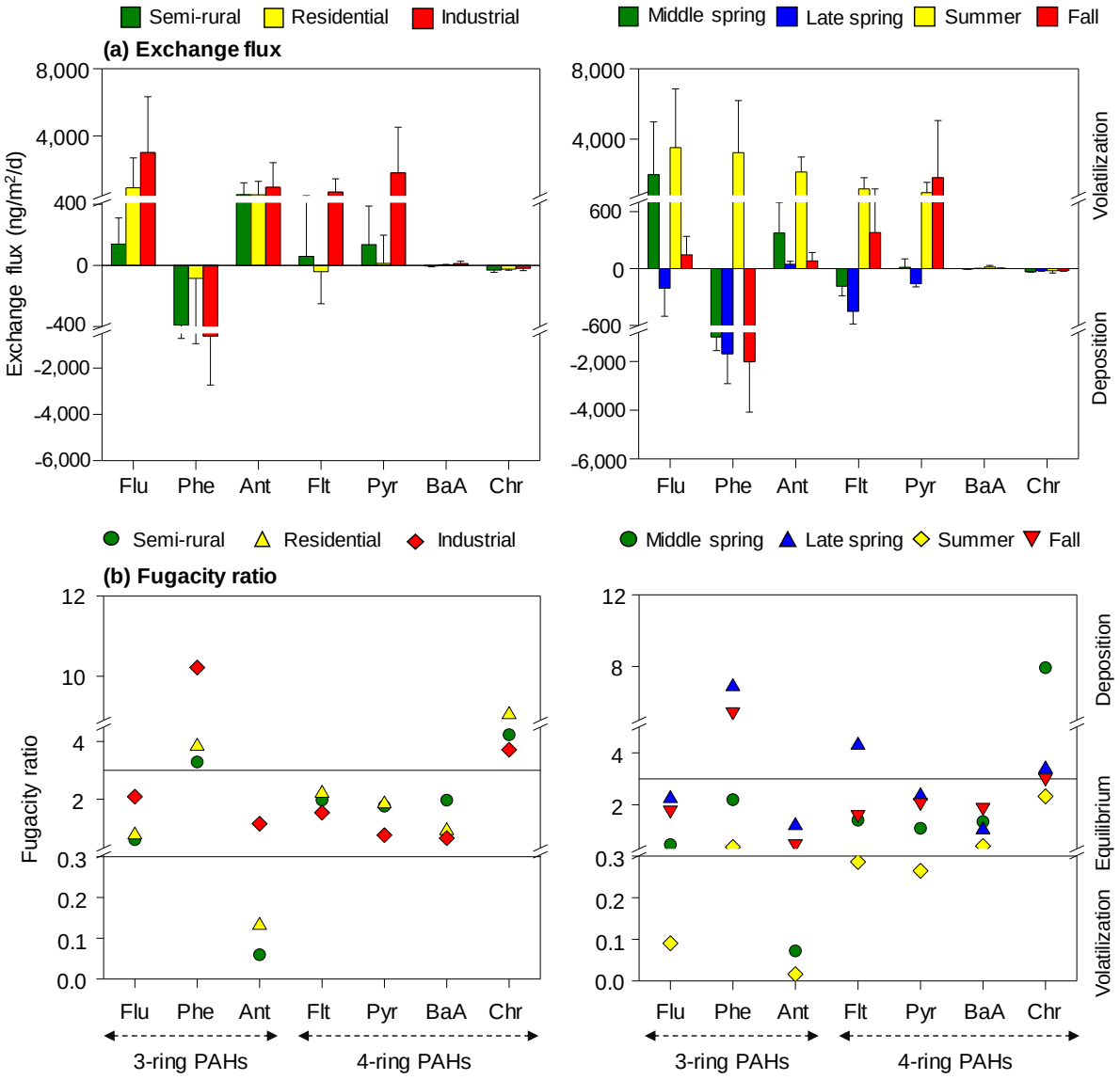

Figure 5-5. Air-water exchange of PAHs shown in (a) exchange flux and (b) fugacity ratio.

However, the FR revealed that the net volatilization was more evident for the 3-ring PAHs (i.e., Flu and Ant) and the phase equilibrium was mainly observed for the 4-ring species (i.e., Flt, Pyr, BaA, and Chr) (Figure 5-5b). The relative difference in determining the transfer direction of PAHs between the exchange flux and FR could stem from the uncertainty of the calculation.

In particular, uncertainty from the temperature-corrected Henry's law constant was considered in the FR approach, leading to the definition of net equilibrium (i.e., 0.3 < FR < 3.0) (Lammel et al., 2015). Moreover, the uncertainty from the calculation of exchange flux could be mainly from the overall mass transfer coefficients of PAHs between the air and surface water (Fang et al., 2012), however, net equilibrium is not defined in this approach.

Regarding the spatial distribution, the exchange fluxes of PAHs were highest in the industrial (mean: 807.5 ng/m^2/d), followed by the residential (mean: 295.2 ng/m^2/d), and the semi-rural (mean: 141.9 ng/m^2/d) sites (Figure 5-5). This observation could be because of the higher PAH concentrations in the air and surface water of the industrial and residential sites (Figure 5-2), leading to their higher exchange fluxes. For the temporal variation, the net volatilization was mostly strongest in summer (Figure 5-5), when the air and water temperature were highest during the sampling campaigns. The higher water temperature in summer could result in higher concentrations the dissolved PAHs through desorption (He et al., 1995). Moreover, the low concentrations of gaseous PAHs in summer (Figure 5-2a) could more promote the escaping tendency of PAHs from the surface water to the air to establish their equilibrium conditions between these environmental media (Mackay, 2001).

In addition, the exchange fluxes of PAHs in late spring and fall were relatively low compared to those in the other periods (Figure 5-5). These results could be because of the higher gaseous concentrations in late spring and fall, leading to weaker volatilization from surface water. In fact, the temporal variations of PAH exchange, stemming from the different concentrations of PAH in the air and surface water, were also reported in previous studies (Fang et al., 2012; Lohmann et al., 2011).

5.3.3.2. Air-soil exchange of the PAHs

The exchange flux and fugacity fractions (*ff*) for the air-soil exchange of PAHs are illustrated in Figure 5-6. Generally, the net transfer of PAHs between the air and soils varied depending on their molecular weights. In particular, the 3-ring PAHs (i.e., Flu, Phe, and Ant) mostly experienced net volatilization, suggesting that the soils could be a secondary source of these species in the air. The 3-ring PAHs have high volatility and low affinity to the soil particles; thus, they could mainly experience net volatilization from the soils to the air. However, contributions from the soils could be unnoticeable because there were no correlations between the atmospheric concentrations and the exchange flux or fugacity fractions. The 4-ring PAHs

(i.e., Flt, Pyr, BaA, and Chr) mainly showed net deposition (Figure 5-6), reflecting that the soils could be a sink for these compounds. These observations were also in line with those reported in previous studies (Bozlaker et al., 2008; Dumanoglu et al., 2017). Moreover, the exchange fluxes of PAHs between the air-soil (-0.94 to 68.29 ng/m^2/d) were much lower than those of the air-water (-364.06 to 1358.94 ng/m^2/d). This result can be because solid particles of the soils might block or slow down the diffusion of PAHs between the air and soils (Mackay, 2001), resulting in their lower mass transfer compared to the air-water system.

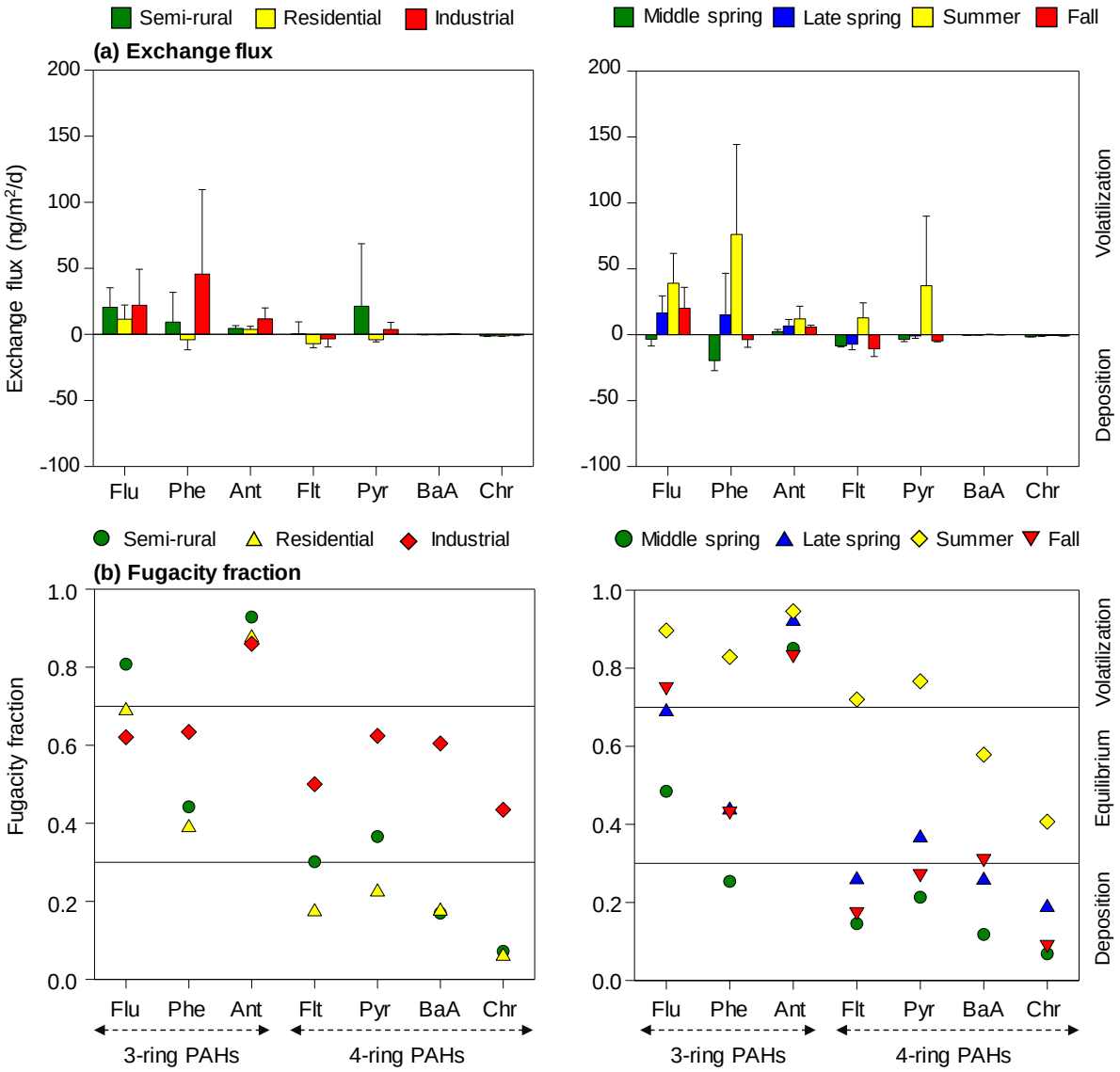

Figure 5-6. Air-soil exchange of PAHs shown in (a) exchange flux and (b) fugacity ratio.

The air-soil exchange behaviors of PAHs also showed their spatial distributions. In particular, the exchange fluxes and *ff* values of almost PAHs at the industrial site were higher than those at the other sites (Figure 5-6). Additionally, they were mostly higher than 0.7 (i.e., Ant) and between 0.3 to 0.7 (i.e., Flu, Phe, Flt, Pyr, BaA, and Chr), suggesting the net equilibrium and volatilization of these species, respectively. The highest PAH concentrations in both the air and soils of the industrial site might lead to the equilibrium conditions of the PAHs, reflecting the delay of mass transfer between the air and soils.

For the seasonal variations, the exchange fluxes and *ff* values in summer were higher than those in the other sampling periods (Figure 5-6). Moreover, statistically significant differences were also found between the exchange fluxes or *ff* of summer and those of the other seasons (Mann-Whitney rank-sum test, $p < 0.05$). The higher air temperature and the lower atmospheric concentrations of PAHs in the summer could enhance the escape of PAHs from soils to the air. In addition, the lowest flux and *ff* values were shown in the middle spring, however, no statistical differences were observed between the flux or *ff* of middle spring and those of the late spring or fall. As the air-soil partitioning could be strongly affected by meteorological conditions, such as air temperature (Wang et al., 2011a), this observation could be because of the relatively similar air temperature in the middle spring to those in late spring and fall. Regarding the 3-ring PAHs (i.e., Flu, Phe, and Ant), they mostly experienced net volatilization or equilibrium during the sampling campaigns. However, for the 4-ring PAHs (i.e., Flt, Pyr, BaA, and Chr), they reached the equilibrium condition or volatilization in the summer and shifted to net deposition in the other seasons, especially in the middle spring when the air temperature was lowest during the study period. This result also reflected a sensitivity of the medium PAHs (i.e., 4-ring PAHs) to the air temperature as reported in previous studies (Bozlaker et al., 2008; Degrendele et al., 2016; Wang et al., 2011a).

5.3.4. Distribution of PAHs among environmental media

The distributions of PAHs among the air, surface water, and soils were calculated and shown in Table 5-2. The areas for air, surface water, and soils of Ulsan were adopted from the Korean Statistical Information Service (http://kosis.kr/search) and were 1059, 108.16, and 261.67 km^2, respectively. In addition, the depth for air, surface water, and soils were assumed to be 1000, 1, and 0.05 m, respectively. The distributions of PAHs in each environmental media were calculated by multiplying the PAH concentrations in each media and the media volume.

Table 5-2. Percentage distributions of PAHs among the air, surface water, and soils.

PAHs	Air	Water	Soil
3 to 6 rings	1.01	0.03	98.96
3 rings	6.46	0.16	93.39
4 rings	0.64	0.03	99.33
3 and 4 rings	1.84	0.05	98.11

As shown in Table 5-2, the PAHs mostly distributed in the soils, followed by the air and surface water. However, it should be noted that the air and water PAHs considered in this study were primarily in the gaseous and dissolved phases, respectively. Therefore, a consideration of PAHs in both gaseous and particulate phases for the air, as well as dissolved and particulate phases for the surface water, could increase the distributions of PAHs in these environmental media. The highest fractions of PAHs in the soils (over 90%) could be because the PAHs have the affinity to bind to the soil organic matter, leading to their accumulation in the soils. Meanwhile, PAHs in the air and surface water could be washed out and degraded easier by several processes, such as photochemical reaction, deposition, and advection.

In the soil, the heavy PAHs having higher toxicity are more dominant due to their less mobility and stronger sorption to organic matters of soil particles. Additionally, these heavy species tend to more accumulate in the soils and mostly undergo soil-water exchange through overland runoff. In the water, they would deposit onto bottom sediments rather than dissolve in the water due to their low water solubility (Mackay et al., 2006a). Moreover, the heavy PAHs have less ability to undergo air-soil exchange to become the atmospheric chemicals because of their low vapor pressure (Mackay et al., 2006a). Since the heavy species are more toxic, their low distributions in the air and their strong accumulation in the soil might contribute to low cancer risk for human health through inhalation intake and dermal absorption. However, the re-suspension of soil particles containing the heavy PAHs (e.g., road dust) from soils to the air under strong wind speed could affect human health and this issue should be considered regarding human health risk assessment for the soil PAHs.

The distribution of PAHs in the air was the second highest, however, the atmospheric PAHs should be paid attention because the original sources of these compounds (i.e., biomass burning and fossil fuel combustion) would emit them directly into the air. Especially, for Ulsan city, the petrochemical and non-ferrous industrial activities are believed to be the noticeable source of PAHs because their production processes can have coke/coal/heavy oil combustion, one of the

emission sources of PAHs. In addition, the monsoon system in Ulsan, especially during summer, could bring PAHs emitted in the industrial area to the others (i.e., urban and residential areas) (Nguyen et al., 2018). Moreover, as South Korea locates downwind of other countries in the Northeast Asia (i.e., China and North Korea), the monsoon system, especially in winter and spring (Inomata et al., 2017), could also bring PAHs originated from upwind areas (i.e., China and western areas of South Korea) to Ulsan and contribute to the local pollution. Therefore, although the PAHs were demonstrated to secondly distribute in the air, the atmospheric PAHs in Ulsan should be preferentially studied.

5.4. Conclusion

The spatial distributions and seasonal variations of magnitude and direction exchange of PAHs between the air-water and air-soil were investigated. For the air-water exchange, net volatilization was mostly observed for the PAHs, suggesting that the water could be a secondary source of the air PAHs. Regarding the air-soil system, the exchange of PAHs could vary depending on their molecular weight. In particular, the 3-ring PAHs mainly showed net volatilization and equilibrium, whereas the 4-ring PAHs mostly experienced net deposition. Additionally, the exchange fluxes of PAHs between the air-water and air-soil were highest at the industrial site, mostly due to its higher PAH concentrations in the multimedia environment (i.e., air, soil, and water). Regarding the temporal variation, the net volatilization was strongest in the summer due to the effect of the higher air temperature and the lower air concentrations.

The distributions of PAHs among the multimedia environment revealed that PAHs could primarily distribute in the soils, followed by the air and water. However, the main emission sources of PAHs (i.e., biomass burning and fossil fuel combustion) would emit them directly into the air, in addition, the monsoon system in Ulsan could seasonally affect the atmospheric PAHs in this city. Therefore, a study on PAHs in the air of Ulsan should also be preferable.

Chapter 6: Conclusion

In summary, this dissertation has two main objectives, including to investigate the seasonal/spatial concentrations, profiles, phase distribution, and exchange of PAHs and to identify the emission sources of PAHs regarding source types (i.e., petrogenic or pyrogenic source) and source areas (i.e., local or regional source). Based on the results of this dissertation, four main conclusions were drawn as below.

Conclusion 1: Seasonal variations, phase distribution, and source identification of the atmospheric PAHs.

The concentrations and profiles of PAHs in the atmosphere of Ulsan were demonstrated to vary seasonally. In particular, the total (gas + particle) concentrations of PAH were highest and lowest winter and spring, respectively. Moreover, the concentrations of gaseous PAHs were higher than those of particulate PAHs mostly throughout the sampling period. The 5- and 6-ring PAHs increased their contributions in winter, mainly because of the lower air temperature and the combustion elevation for heating. The 3- and 4-ring PAHs increased their contributions in summer and fall, mostly because of the desorption stemming from the higher air temperature. Additionally, the gas/particle partitioning of PAHs in spring and winter showed different behavior compared to those in the other seasons, i.e., the higher contributions of the particulate PAHs. The main emission sources of atmospheric PAHs in Ulsan also varied seasonally. In more detail, the pyrogenic sources (e.g., coal combustion) could be the main sources of PAHs in the winter. Other types of pyrogenic (e.g., petroleum combustion) and petrogenic sources were believed to be the main PAH sources in summer and fall. Additionally, the spring could have mixed sources, including diesel and coal combustion or biomass burning.

Conclusion 2: Identification of source areas of the atmospheric PAHs

The atmospheric PAHs in Ulsan were proved to be affected by both local and regional emission sources; however, this influence could vary depending on the PAH phase and the monsoon system. In particular, the particulate PAHs were more affected by the long-range transport (i.e., from northeastern China and/or North Korea), however, the gaseous PAHs could be primarily affected by the local emissions (i.e., industrial and vehicle emissions). Moreover, the effect of trans-boundary transport on the PAHs was more evident in the spring and winter. In summer

and fall, a decrease of the monsoon system activity led to the more important influence of the local emission sources on PAHs.

Conclusion 3: Spatial distribution, temporal variation, and phase distribution of PAHs in runoff and surface water

The PAH concentrations in overland runoff and surface water were higher at the industrial site, mostly due to the higher PAH levels in the multimedia environment of the industrial area. The concentrations of PAHs in the runoff varied temporally depending on several variables, such as rainfall amount and the number of antecedent dry days. The dissolved PAHs were more predominant at most sites throughout the study periods. Moreover, the higher water temperature in summer could induce the desorption of PAHs from the particulate to the dissolved phase and result in an increase of the dissolved PAHs in the surface water. For the source identification, PAHs in the runoff and surface water could have the similar sources, which were a mix of both petrogenic (e.g., leakage from petroleum products) and pyrolysis (e.g., vehicle emission) sources. Additionally, the PAHs in the runoff of July (summer) could be also emitted from coal/coke/heavy oil combustion as a result of industrial emissions and local advection.

Conclusion 4: Spatial distribution and seasonal variation of air-water and air-soil exchange of PAHs

The exchange fluxes of PAHs between the air-water and air-soil were mostly highest at the industrial site because of its higher PAH concentrations in the multimedia environment (i.e., air, soil, and water). The net volatilization was strongest in the summer because of the higher air temperature and the lower air concentrations. In addition, most of the PAHs showed net volatilization from the surface water to the air, reflecting that the water could be a source for the atmospheric PAHs in Ulsan. However, no significant difference was observed between the air concentration and the exchange flux, indicating that the contribution from water could be insignificant for PAHs in the air. Moreover, the soil could be a source and a sink for the air PAHs depending mostly on their molecular weight (i.e., a source for the 3-ring PAHs and a sink for the 4-ring PAHs). However, the volatilization and contribution from the soils could be not important for the atmospheric PAHs. Additionally, the PAHs in Ulsan could primarily distribute in the soils, followed by the air, and the surface water. The highest distribution of

PAHs in the soils could be because these compounds have the affinity to sorb to the soil organic matter and then accumulate in the soils. However, based on the results from previous chapters, it is suggested that the atmospheric PAHs in Ulsan should also concerned because of several reasons, such as the effect of trans-boundary transport and direct emission from the local PAH sources.

Implications

Moreover, this dissertation can contribute to the understanding of PAHs in the multimedia environment, including the air, soils, runoff, and surface water. In more detail, the approaches used for the identification of source types (e.g., petrogenic or pyrogenic source) and source areas (e.g., local source or trans-boundary transport) can be applied in further studies on source-receptor relations of pollutants. Especially, the combination of hybrid receptor model and gas/particle partitioning is firstly introduced in this dissertation and this approach can be applied to study on long-range transport for other organic chemicals. In addition, the PAH behaviors in runoff and surface water, as well as the seasonal variations of multimedia exchange of PAHs can also be more understood. Added to this, results from this dissertation can also support the decision-making related to environmental issues in Ulsan.

Based on the results of this dissertation, further studies can more focus on the soil and atmospheric PAHs in Ulsan. For instance, seasonal monitoring of the soil PAHs, application of other models that consider the reaction of PAHs during transport (e.g., WRF-Chem and CMAQ) to identify the influence of trans-boundary transport on PAHs, and monitoring of other PAH-derivative compounds (i.e., oxygen and nitrogen-containing PAHs) in Ulsan.

Appendix 1

Table A1-1. Summary of PMF and error estimation diagnostics.

Diagnostic	3 factors	4 factors	5 factors	6 factors
$Q_{robust/expected}$	28.9	-0.28	-0.43	-0.17
DISP swaps	0	0	0	69 cases
BS mapping (%)	Factor 1: 98	Factor 1: 100	Factor 1: 97	Factor 1: 98
	Factor 2: 90	Factor 2: 96	Factor 2: 96	Factor 2: 97
	Factor 3: 96	Factor 3: 94	Factor 3: 100	Factor 3: 98
		Factor 4: 99	Factor 4: 96	Factor 4: 75
			Factor 5: 99	Factor 5: 94
				Factor 6: 99
BS-DISP% cases with swaps	9%	38%	86%	No results

Text A1-1. Discussion on the selection of PMF solution.

The results of Q values and uncertainty error estimation of four PMF solutions are shown in Table S3. Three error estimation methods suggested by (US-EPA, 2014) were used, including bootstrapping (BS), displacement (DISP), and bootstrapping with displacement (BS-DISP). In moving from three to four factors, the values of $Q_{robust/expected}$ declined from 28.9 to -0.28. Additionally, a smaller change of $Q_{robust/expected}$, from -0.28 to -0.43, was observed when moving from four to five factors. Change in Q becomes small with increasing factors suggests too many factors were chosen (Brown et al., 2015). Thus, four factors could be a favorable solution.

To support this selection, uncertainty error estimation for all PMF solutions was checked. With a six-factor solution, factor 4 was mapped 75% of the run for the BS, and 69 cases were swapped in the DISP, indicating this solution is not stable (US-EPA, 2014). A five-factor solution had high mapping rates for all factors. However, 86% of cases with swaps were observed in the BS-DISP. Thus, this factor could not be an optimal selection (Brown et al., 2015). For a four-factor solution, all factors were mapped over 90% in BS, and the number of swaps was low (38%), reflecting this solution is acceptable.

Appendix 2

Table A2-1. The average number of trajectory endpoints per cell (*s* value) used for the conventional ($PSCF^c$), using the entire trajectory path for calculation, and the modified PSCF ($PSCF^m$), using the trajectory endpoints within the mixing and residual layers.

Season	Conventional $PSCF^c$	Suggested $PSCF^m$
Summer	60	20
Autumn	20	10
Winter	10	2
Spring	10	2
4 seasons	25	14

Text A2-1. Selection of the optimal weighting function and concentration threshold.

Two weighting functions (W_1 and W_2) and three thresholds, including the 50^{th}, 75^{th}, and 90^{th} percentiles of the Σ_{13} PAHs, were applied to calculate the $PSCF^m$ and CWT^m. In general, the $PSCF^m$ and CWT^m using the weighting functions W_1 and W_2 suggested the relatively similar source areas for the PAHs (Figure A2-1). However, the smaller values of the W_2 obviously declined the output values of the $PSCF^m$ and CWT^m. As the possible source areas are determined based on the higher values of the PSCF and CWT (Hopke et al., 1993), this observation might lead to the inadequate identification of the source areas. Indeed, the $PSCF^m$ and CWT^m using the W_1 determined that PAHs in Ulsan could be transported from China, especially Beijing, Hebei, Tianjin, Liaoning, and Jilin (Figure A2-1a). Nevertheless, these areas were not obviously confirmed by the models using the weighting function W_2, especially the $PSCF^m$ (Figure A2-1b). Hence, for the comprehensive identification of the source areas, the weighting function W_1 was selected for further calculation in this study.

Regarding the threshold for the PSCF calculation, $PSCF^m$ with the 90^{th} percentile of the Σ_{13} PAHs apparently ignored northeastern China (i.e., Jilin and Liaoning) as the source areas of the PAHs in Ulsan (Figure A2-1). These areas, however, were suggested as the PAH sources by the $PSCF^m$ with 75^{th} and 50^{th} percentiles and the CWT^m (Figure A2-1). Therefore, the insufficient identification of source areas regarding $PSCF^m$ with the 90^{th} percentile indicates that this value is an inappropriate threshold.

Moreover, the 50th percentile-PSCF^{m} suggested potential source areas (e.g., Liaoning, Jilin, and mainland Japan). However, these areas were not strongly verified by the 75th percentile-PSCF^{m} and the CWT^{m} (Figure A2-2), reflecting that they might be not the source areas of PAHs in Ulsan. Therefore, the 75th percentile was selected as the threshold for further PSCF calculation in this study.

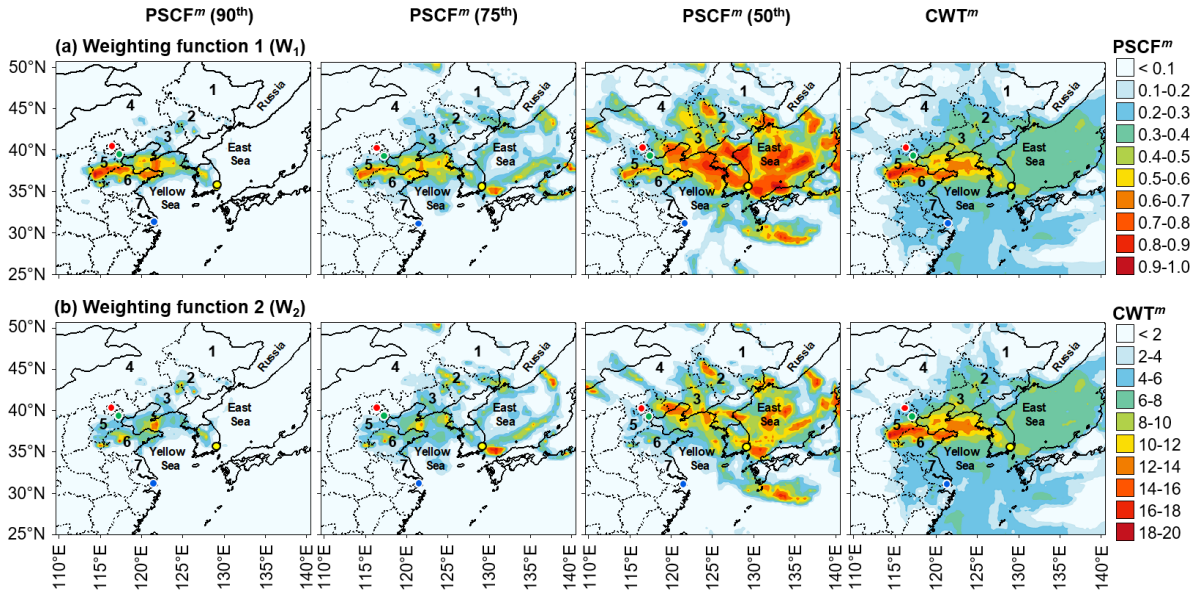

Figure A2-1. Modified PSCF (PSCF^{m}) with the 90th, 75th, and 50th percentiles of the Σ_{13} PAHs and the modified CWT (CWT^{m}) using two weighting functions: (a) W_1 and (b) W_2. The average annual of the total (gas + particle) PAHs were used.

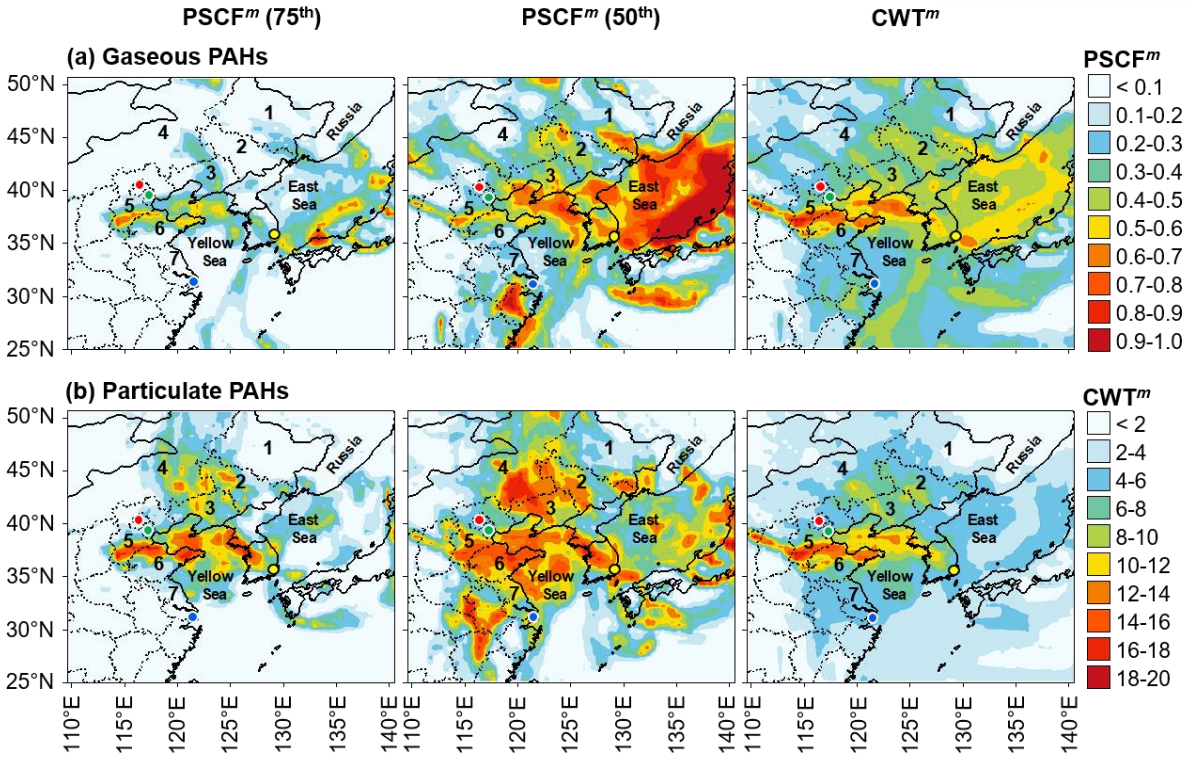

Figure A2-2. Modified PSCF (PSCF^m) using the 75th and 50th percentiles of the Σ_{13} PAHs and the modified CWT (CWT^m) of the (a) gaseous and (b) particulate PAHs. The weighting function W_1 was applied for the calculation. The average annual data were used.

.

References

Albuquerque, M., Coutinho, M., Borrego, C., 2016. Long-term monitoring and seasonal analysis of polycyclic aromatic hydrocarbons (PAHs) measured over a decade in the ambient air of Porto, Portugal. Sci. Total Environ. 543, Part A, 439–448.

Amellal, N., Portal, J.M., Berthelin, J., 2001. Effect of soil structure on the bioavailability of polycyclic aromatic hydrocarbons within aggregates of a contaminated soil. Appl. Geochem. 16, 1611–1619.

Angrill, S., Petit-Boix, A., Morales-Pinzón, T., Josa, A., Rieradevall, J., Gabarrell, X., 2017. Urban rainwater runoff quantity and quality – A potential endogenous resource in cities? J. Environ. Manage. 189, 14–21.

Ashbaugh, L.L., 1983. A statistical trajectory technique for determining air pollution source regions. J. Air Pollut. Control Assoc. 33, 1096–1098.

ATSDR, 1990. Polycyclic aromatic hydrocarbons U.S. Public Health Statement, Atlanta, USA.

Baek, S.O., Field, R.A., Goldstone, M.E., Kirk, P.W., Lester, J.N., Perry, R., 1991a. A review of atmospheric polycyclic aromatic hydrocarbons: sources, fate and behavior. Water Air Soil Pollut. 60, 279–300.

Baek, S.O., Goldstone, M.E., Kirk, P.W.W., Lester, J.N., Perry, R., 1991b. Phase distribution and particle size dependency of polycyclic aromatic hydrocarbons in the urban atmosphere. Chemosphere 22, 503–520.

Bhardwaj, P., Ki, S.J., Kim, Y.H., Woo, J.H., Song, C.K., Park, S.Y., Song, C.H., 2019. Recent changes of trans-boundary air pollution over the Yellow Sea: Implications for future air quality in South Korea. Environ. Pollut. 247, 401–409.

Biache, C., Mansuy-Huault, L., Faure, P., 2014. Impact of oxidation and biodegradation on the most commonly used polycyclic aromatic hydrocarbon (PAH) diagnostic ratios: implications for the source identifications. J. Hazard. Mater. 267, 31–39.

Bidleman, T.F., McConnell, L.L., 1995. A review of field experiments to determine air-water gas exchange of persistent organic pollutants. Sci. Total Environ. 159, 101-117.

Bozlaker, A., Muezzinoglu, A., Odabasi, M., 2008. Atmospheric concentrations, dry deposition and air–soil exchange of polycyclic aromatic hydrocarbons (PAHs) in an industrial region in Turkey. J. Hazard. Mater. 153, 1093-1102.

Brown, S.G., Eberly, S., Paatero, P., Norris, G.A., 2015. Methods for estimating uncertainty in PMF solutions: examples with ambient air and water quality data and guidance on

reporting PMF results. Sci. Total Environ. 518–519, 626–635.

Carslaw, D.C., Ropkins, K., 2012. Openair - An R package for air quality data analysis. Environ. Modell. Softw. 27–28, 52–61.

Cesari, D., Amato, F., Pandolfi, M., Alastuey, A., Querol, X., Contini, D., 2016. An inter-comparison of PM10 source apportionment using PCA and PMF receptor models in three European sites. Environ. Sci. Pollut. R. 23, 15133–15148.

Cheng, J.-O., Ko, F.-C., Lee, C.-L., Fang, M.-D., 2016. Atmospheric polycyclic aromatic hydrocarbons (PAHs) of southern Taiwan in relation to monsoons. Environ. Sci. Pollut. R. 23, 15675–15688.

Cheruiyot, N.K., Lee, W.-J., Mwangi, J.K., Wang, L.-C., Lin, N.-H., Lin, Y.-C., Cao, J., Zhang, R., Chang-Chien, G.-P., 2015. An overview: polycyclic aromatic hydrocarbon emissions from the stationary and mobile sources in the ambient air. Aerosol Air Qual. Res. 15, 2730–2762.

Chiou, C.T., McGroddy, S.E., Kile, D.E., 1998. Partition characteristics of polycyclic aromatic hydrocarbons on soils and sediments. Environ. Sci. Technol. 32, 264–269.

Choi, S.-D., Ghim, Y.S., Lee, J.Y., Kim, J.Y., Kim, Y.P., 2012a. Factors affecting the level and pattern of polycyclic aromatic hydrocarbons (PAHs) at Gosan, Korea during a dust period. J. Hazard. Mater. 227–228, 79–87.

Choi, S.-D., Kwon, H.-O., Lee, Y.-S., Park, E.-J., Oh, J.-Y., 2012b. Improving the spatial resolution of atmospheric polycyclic aromatic hydrocarbons using passive air samplers in a multi-industrial city. J. Hazard. Mater. 241–242, 252–258.

Choi, S.-D., Shunthirasingham, C., Daly, G.L., Xiao, H., Lei, Y.D., Wania, F., 2009. Levels of polycyclic aromatic hydrocarbons in Canadian mountain air and soil are controlled by proximity to roads. Environ. Pollut. 157, 3199-3206.

Choi, S.-L., Shin, S.-H., Chun, H.-H., Jo, W.-K., 2013. Multi-year PAH behaviours in atmospheric particulates according to land-use type. Aerosol Air Qual. Res. 13, 721–729.

Clarke, K., Kwon, H.-O., Choi, S.-D., 2014. Fast and reliable source identification of criteria air pollutants in an industrial city. Atmos. Environ. 95, 239–248.

Cui, S., Fu, Q., Li, T.-x., Ma, W.-l., Liu, D., Wang, M., 2016. Sediment-water exchange, spatial variations, and ecological risk assessment of polycyclic aromatic hydrocarbons (PAHs) in the Songhua river, China. Water 8, 334.

Degrendele, C., Audy, O., Hofman, J., Kučerik, J., Kukučka, P., Mulder, M.D., Přibylová, P., Prokeš, R., Šáňka, M., Schaumann, G.E., Lammel, G., 2016. Diurnal Variations of Air-

Soil Exchange of Semivolatile Organic Compounds (PAHs, PCBs, OCPs, and PBDEs) in a Central European Receptor Area. Environ. Sci. Technol. 50, 4278-4288.

Dong, T.T.T., Lee, B.-K., 2009. Characteristics, toxicity, and source apportionment of polycylic aromatic hydrocarbons (PAHs) in road dust of Ulsan, Korea. Chemosphere 74, 1245–1253.

Doong, R.-a., Lin, Y.-t., 2004. Characterization and distribution of polycyclic aromatic hydrocarbon contaminations in surface sediment and water from Gao-ping River, Taiwan. Water Res. 38, 1733–1744.

Dumanoglu, Y., Gaga, E.O., Gungormus, E., Sofuoglu, S.C., Odabasi, M., 2017. Spatial and seasonal variations, sources, air-soil exchange, and carcinogenic risk assessment for PAHs and PCBs in air and soil of Kutahya, Turkey, the province of thermal power plants. Sci. Total Environ. 580, 920-935.

Fang, M.-D., Lee, C.-L., Jiang, J.-J., Ko, F.-C., Baker, J.E., 2012. Diffusive exchange of PAHs across the air–water interface of the Kaohsiung Harbor lagoon, Taiwan. J. Environ. Manage. 110, 179-187.

Fleming, Z.L., Monks, P.S., Manning, A.J., 2012. Review: Untangling the influence of air-mass history in interpreting observed atmospheric composition. Atmos. Res. 104, 1–39.

Foster, G.D., Roberts, E.C., Gruessner, B., Velinsky, D.J., 2000. Hydrogeochemistry and transport of organic contaminants in an urban watershed of Chesapeake Bay (USA). Appl. Geochem. 15, 901–915.

Froger, C., Quantin, C., Gasperi, J., Caupos, E., Monvoisin, G., Evrard, O., Ayrault, S., 2019. Impact of urban pressure on the spatial and temporal dynamics of PAH fluxes in an urban tributary of the Seine River (France). Chemosphere 219, 1002–1013.

Gateuille, D., Evrard, O., Lefevre, I., Moreau-Guigon, E., Alliot, F., Chevreuil, M., Mouchel, J.-M., 2014. Mass balance and decontamination times of polycyclic aromatic hydrocarbons in rural nested catchments of an early industrialized region (Seine River basin, France). Sci. Total Environ. 470–471, 608-617.

Gigliotti, C.L., Brunciak, P.A., Dachs, J., Glenn IV, T.R., Nelson, E.D., Totten, L.A., Eisenreich, S.J., 2002a. Air—water exchange of polycyclic aromatic hydrocarbons in the New York—New Jersey, USA, Harbor Estuary. Environ Toxicol Chem. 21, 235-244.

Gigliotti, C.L., Brunciak, P.A., Dachs, J., Glenn, T.R., Nelson, E.D., Totten, L.A., Eisenreich, S.J., 2002b. Air-water exchange of polycyclic aromatic hydrocarbons in the New York-New Jersey, USA, Harbor Estuary. Environ. Toxicol. Chem. 21, 235–244.

Gilbreath, A.N., McKee, L.J., 2015. Concentrations and loads of PCBs, dioxins, PAHs, PBDEs, OC pesticides and pyrethroids during storm and low flow conditions in a small urban semi-arid watershed. Sci. Total Environ. 526, 251–261.

Gustafson, K.E., Dickhut, R.M., 1997. Particle/gas concentrations and distributions of PAHs in the atmosphere of Southern Chesapeake bay. Environ. Sci. Technol. 31, 140–147.

Harner, T., Bidleman, T.F., Jantunen, L.M.M., Mackay, D., 2001. Soil—air exchange model of persistent pesticides in the United States cotton belt. Environ. Toxicol. Chem. 20, 1612-1621.

He, Y., Yediler, A., Sun, T., Kettrup, A., 1995. Adsorption of fluoranthene on soil and lava: Effects of the organic carbon contents of adsorbents and temperature. Chemosphere 30, 141-150.

Herkert, N.J., Spak, Scott N., Smith, A., Schuster, J.K., Harner, T., Martinez, A., Hornbuckle, K.C., 2018. Calibration and evaluation of PUF-PAS sampling rates across the global atmospheric passive sampling (GAPS) network. Environmental Science: Processes & Impacts 20, 210–219.

Hopke, P.K., Gao, N., Cheng, M.-D., 1993. Combining chemical and meteorological data to infer source areas of airborne pollutants. Chemometr. Intell. Lab. 19, 187–199.

Hsu, Y.-K., Holsen, T.M., Hopke, P.K., 2003a. Comparison of hybrid receptor models to locate PCB sources in Chicago. Atmos. Environ. 37, 545-562.

Hsu, Y.-K., Holsen, T.M., Hopke, P.K., 2003b. Locating and quantifying PCB sources in Chicago: Receptor modeling and field sampling. Environ. Sci. Technol. 37, 681–690.

Hwang, H.-M., Foster, G.D., 2006. Characterization of polycyclic aromatic hydrocarbons in urban stormwater runoff flowing into the tidal Anacostia River, Washington, DC, USA. Environ. Pollut. 140, 416–426.

Hyeon-Seo, C., Young-Seok, Y., Jeong-Hoon, L., Jeong-Chae, P., Dong-Myung, K., 2012. Distribution Characteristics of Polycyclic Aromatic Hydrocarbons(PAHs) in Riverine Waters of Ulsan Coast, Korea. Journal of the Korean Society of Marine Environment and Safety 18, 398-405.

IARC, 2014. Diesel and Gasoline Engine Exhausts and some Nitroarenes. International Agency for Research on Cancer, Lyon, France.

Indarto, A., Giordana, A., Ghigo, G., Maranzana, A., Tonachini, G., 2010. Polycyclic aromatic hydrocarbon formation mechanism in the “particle phase”: A theoretical study. Phys. Chem. Chem. Phys. 12, 9429–9440.

Inomata, Y., Kajino, M., Sato, K., Kurokawa, J., Tang, N., Ohara, T., Hayakawa, K., Ueda, H., 2017. Source–receptor relationship analysis of the atmospheric deposition of PAHs subject to long-range transport in Northeast Asia. Environ. Sci. Technol. 51, 7972–7981.

Inomata, Y., Kajino, M., Sato, K., Ohara, T., Kurokawa, J.-I., Ueda, H., Tang, N., Hayakawa, K., Ohizumi, T., Akimoto, H., 2012. Emission and atmospheric transport of particulate PAHs in Northeast Asia. Environ. Sci. Technol. 46, 4941–4949.

Jain, S., Sharma, S.K., Choudhary, N., Masiwal, R., Saxena, M., Sharma, A., Mandal, T.K., Gupta, A., Gupta, N.C., Sharma, C., 2017. Chemical characteristics and source apportionment of PM2.5 using PCA/APCS, UNMIX, and PMF at an urban site of Delhi, India. Environ. Sci. Pollut. R., 1–20.

Jamhari, A.A., Sahani, M., Latif, M.T., Chan, K.M., Tan, H.S., Khan, M.F., Mohd Tahir, N., 2014. Concentration and source identification of polycyclic aromatic hydrocarbons (PAHs) in PM10 of urban, industrial and semi-urban areas in Malaysia. Atmos. Environ. 86, 16–27.

Jeon, H.-D., Oh, S.-Y., 2019. Distribution, toxicity, and origins of polycyclic aromatic hydrocarbons in soils in Ulsan, South Korea. Environ. Monit. Assess. 191, 409.

Jeong, U., Kim, J., Lee, H., Jung, J., Kim, Y.J., Song, C.H., Koo, J.-H., 2011. Estimation of the contributions of long range transported aerosol in East Asia to carbonaceous aerosol and PM concentrations in Seoul, Korea using highly time resolved measurements: A PSCF model approach. J. Environ. Monit. 13, 1905–1918.

Jeong, U., Kim, J., Lee, H., Lee, Y.G., 2017. Assessing the effect of long-range pollutant transportation on air quality in Seoul using the conditional potential source contribution function method. Atmos. Environ. 150, 33–44.

Kalmykova, Y., Björklund, K., Strömvall, A.-M., Blom, L., 2013. Partitioning of polycyclic aromatic hydrocarbons, alkylphenols, bisphenol A and phthalates in landfill leachates and stormwater. Water Res. 47, 1317–1328.

KEEI, 2014. Yearbook of Regional Energy Statistics (In Korean), Korea Energy Economics Institute.

Keyte, I.J., Harrison, R.M., Lammel, G., 2013a. Chemical reactivity and long-range transport potential of polycyclic aromatic hydrocarbons - a review. Chem. Soc. Rev. 42, 9333–9391.

Keyte, I.J., Harrison, R.M., Lammel, G., 2013b. Chemical reactivity and long-range transport potential of polycyclic aromatic hydrocarbons – A review. Chem. Soc. Rev. 42, 9333–

9391.

Khalili, N.R., Scheff, P.A., Holsen, T.M., 1995. PAH source fingerprints for coke ovens, diesel and, gasoline engines, highway tunnels, and wood combustion emissions. Atmos. Environ. 29, 533–542.

Khim, J.S., Lee, K.T., Kannan, K., Villeneuve, D.L., Giesy, J.P., Koh, C.H., 2001a. Trace Organic Contaminants in Sediment and Water from Ulsan Bay and Its Vicinity, Korea. Arch. Environ. Contam. Toxicol. 40, 141-150.

Khim, J.S., Lee, K.T., Villeneuve, D.L., Kannan, K., Giesy, J.P., Koh, C.H., 2001b. In Vitro Bioassay Determination of Dioxin-Like and Estrogenic Activity in Sediment and Water from Ulsan Bay and Its Vicinity, Korea. Arch. Environ. Contam. Toxicol. 40, 151-160.

Kim, B.M., Lee, S.-B., Kim, J.Y., Kim, S., Seo, J., Bae, G.-N., Lee, J.Y., 2016a. A multivariate receptor modeling study of air-borne particulate PAHs: Regional contributions in a roadside environment. Chemosphere 144, 1270–1279.

Kim, E., Hopke, P.K., 2004. Comparison between conditional probability function and nonparametric regression for fine particle source directions. Atmos. Environ. 38, 4667–4673.

Kim, I.S., Wee, D., Kim, Y.P., Lee, J.Y., 2016b. Development and application of three-dimensional potential source contribution function (3D-PSCF). Environ. Sci. Pollut. R. 23, 16946–16954.

Kim, J.Y., Lee, J.Y., Choi, S.D., Kim, Y.P., Ghim, Y.S., 2012. Gaseous and particulate polycyclic aromatic hydrocarbons at the Gosan background site in East Asia. Atmos. Environ. 49, 311–319.

Kim, L., Jeon, H.-J., Kim, Y.-C., Yang, S.-H., Choi, H., Kim, T.-O., Lee, S.-E., 2019a. Monitoring polycyclic aromatic hydrocarbon concentrations and distributions in rice paddy soils from Gyeonggi-do, Ulsan, and Pohang. Appl. Biol. Chem. 62, 18.

Kim, S.-J., Park, M.-K., Lee, S.-E., Go, H.-J., Cho, B.-C., Lee, Y.-S., Choi, S.-D., 2019b. Impact of traffic volumes on levels, patterns, and toxicity of polycyclic aromatic hydrocarbons in roadside soils. Environmental Science: Processes & Impacts 21, 174–182.

Klánová, J., Èupr, P., Kohoutek, J., Harner, T., 2008. Assessing the influence of meteorological parameters on the performance of polyurethane foam-based passive air samplers. Environ. Sci. Technol. 42, 550–555.

Kobližková, M., RŮžičková, P., Čupr, P., Komprda, J., Holoubek, I., Klánová, J., 2009. Soil

Burdens of Persistent Organic Pollutants: Their Levels, Fate, and Risks. Part IV. Quantification of Volatilization Fluxes of Organochlorine Pesticides and Polychlorinated Biphenyls from Contaminated Soil Surfaces. Environ. Sci. Technol. 43, 3588-3595.

Kolev, N., Grigorov, I., Kolev, I., Devara, P.C.S., Raj, P.E., Dani, K.K., 2007. Lidar and sun photometer observations of atmospheric boundary-layer characteristics over an urban area in a mountain valley. Bound-Lay. Meteorol 124, 99–115.

Kwon, H.-O., Choi, S.-D., 2014a. Polycyclic aromatic hydrocarbons (PAHs) in soils from a multi-industrial city, South Korea. Sci. Total Environ. 470–471, 1494–1501.

Kwon, H.-O., Choi, S.-D., 2014b. Polycyclic aromatic hydrocarbons (PAHs) in soils from a multi-industrial city, South Korea. Sci. Total Environ. 470-471, 1494-1501.

Lai, I.C., Lee, C.-L., Zeng, K.-Y., Huang, H.-C., 2011. Seasonal variation of atmospheric polycyclic aromatic hydrocarbons along the Kaohsiung coast. J. Environ. Manage. 92, 2029–2037.

Lammel, G., Audy, O., Besis, A., Efstathiou, C., Eleftheriadis, K., Kohoutek, J., Kukučka, P., Mulder, M.D., Přibylová, P., Prokeš, R., Rusina, T.P., Samara, C., Sofuoglu, A., Sofuoglu, S.C., Taşdemir, Y., Vassilatou, V., Voutsa, D., Vrana, B., 2015. Air and seawater pollution and air–sea gas exchange of persistent toxic substances in the Aegean Sea: spatial trends of PAHs, PCBs, OCPs and PBDEs. Environ. Sci. Pollut. R. 22, 11301–11313.

Lamprea, K., Ruban, V., 2011. Characterization of atmospheric deposition and runoff water in a small suburban catchment. Environ. Technol. 32, 1141–1149.

Lau, S.-L., Han, Y., Kang, J.-H., Kayhanian, M., Stenstrom, M.K., 2009. Characteristics of highway stormwater runoff in Los Angeles: Metals and polycyclic aromatic hydrocarbons. Water Environ. Res. 81, 308–318.

Lee, B.-K., Dong, T.T.T., 2010. Effects of road characteristics on distribution and toxicity of polycyclic aromatic hydrocarbons in urban road dust of Ulsan, Korea. J. Hazard. Mater. 175, 540-550.

Lee, B.-K., Lee, C.-B., 2004. Development of an improved dry and wet deposition collector and the atmospheric deposition of PAHs onto Ulsan Bay, Korea. Atmos. Environ. 38, 863–871.

Lee, J.Y., Kim, Y.P., 2007. Source apportionment of the particulate PAHs at Seoul, Korea: impact of long range transport to a megacity. Atmos. Chem. Phys. 7, 3587–3596.

Lee, S.-J., Kim, S.-J., Park, M.-K., Cho, I.-G., Lee, H.-Y., Choi, S.-D., 2018. Contamination characteristics of hazardous air pollutants in particulate matter in the atmosphere of Ulsan,

Korea. Journal of the Korean Society for Environmental Analysis 21, 281–291.

Lei, Y.D., Chankalal, R., Chan, A., Wania, F., 2002. Supercooled Liquid Vapor Pressures of the Polycyclic Aromatic Hydrocarbons. J. Chem. Eng. Data 47, 801–806.

Li, C.-T., Mi, H.-H., Lee, W.-J., You, W.-C., Wang, Y.-F., 1999. PAH emission from the industrial boilers. J. Hazard. Mater. 69, 1–11.

Li, H., Chen, J., Wu, W., Piao, X., 2010. Distribution of polycyclic aromatic hydrocarbons in different size fractions of soil from a coke oven plant and its relationship to organic carbon content. J. Hazard. Mater. 176, 729–734.

Li, R., Feng, C., Wang, D., Li, B., Hu, L., Shen, Z., 2016. Role of salinity in the multiphase redistribution of polycyclic aromatic hydrocarbons (PAHs) in sediment suspension. Environ. Earth Sci. 75, 116.

Liang, Q., Jaeglé, L., Wallace, J.M., 2005. Meteorological indices for Asian outflow and transpacific transport on daily to interannual timescales. J. Geophys. Res-Atmos. 110, D18308.

Ligaray, M., Baek, S.S., Kwon, H.-O., Choi, S.-D., Cho, K.H., 2016. Watershed-scale modeling on the fate and transport of polycyclic aromatic hydrocarbons (PAHs). J. Hazard. Mater. 320, 442-457.

Liu, M., Feng, J., Hu, P., Tan, L., Zhang, X., Sun, J., 2016. Spatial-temporal distributions, sources of polycyclic aromatic hydrocarbons (PAHs) in surface water and suspended particular matter from the upper reach of Huaihe river, China. Ecol. Eng. 95, 143–151.

Lohmann, R., Dapsis, M., Morgan, E.J., Dekany, V., Luey, P.J., 2011. Determining Air−Water Exchange, Spatial and Temporal Trends of Freely Dissolved PAHs in an Urban Estuary Using Passive Polyethylene Samplers. Environ. Sci. Technol. 45, 2655-2662.

Lu, H., Zhu, L., Zhu, N., 2009. Polycyclic aromatic hydrocarbon emission from straw burning and the influence of combustion parameters. Atmos. Environ. 43, 978–983.

Mackay, D., 2001. Multimedia environmental models - The fugacity approach, Second ed. Lewis, Washington, D.C.

Mackay, D., Callcott, D., 1998. Partitioning and physical chemical properties of PAHs, in: Neilson, A.H. (Ed.), PAHs and Related Compounds: Chemistry. Springer Berlin Heidelberg, Berlin, Heidelberg, pp. 325–345.

Mackay, D., Shui, W.Y., Ma, K.-C., Lee, S.C., 2006a. Handbook of physical-chemical properties and environmental fate for organic chemicals.

Mackay, D., Shui, W.Y., Ma, K.-C., Lee, S.C., 2006b. Handbook of physical-chemical

properties and environmental fate for organic chemicals. Volume I: Introduction and hydrocarbons. Taylor & Fancis.

Mahler, B.J., Van Metre, P.C., Foreman, W.T., 2014. Concentrations of polycyclic aromatic hydrocarbons (PAHs) and azaarenes in runoff from coal-tar- and asphalt-sealcoated pavement. Environ. Pollut. 188, 81–87.

Masiol, M., Squizzato, S., Cheng, M.-D., Rich, D.Q., Hopke, P.K., 2019. Differential probability functions for investigating long-term changes in local and gegional air pollution sources. Aerosol Air Qual. Res. 19, 724–736.

Meglen, R.R., 1992. Examining large databases: a chemometric approach using principal component analysis. Mar. Chem. 39, 217–237.

Melymuk, L., Robson, M., Helm, P.A., Diamond, M.L., 2011. Evaluation of passive air sampler calibrations: Selection of sampling rates and implications for the measurement of persistent organic pollutants in air. Atmos. Environ. 45, 1867–1875.

Miller, D.J., Hawthorne, S.B., Gizir, A.M., Clifford, A.A., 1998. Solubility of Polycyclic Aromatic Hydrocarbons in Subcritical Water from 298 K to 498 K. Journal of Chemical & Engineering Data 43, 1043-1047.

Moolgavkar, S.H., Luebeck, E.G., Anderson, E.L., 1998. Estimation of unit risk for coke oven emissions. Risk Anal. 18, 813–825.

Mu, Q., Shiraiwa, M., Octaviani, M., Ma, N., Ding, A., Su, H., Lammel, G., Pöschl, U., Cheng, Y., 2018. Temperature effect on phase state and reactivity controls atmospheric multiphase chemistry and transport of PAHs. Sci. Adv. 4, eaap7314.

Nguyen, T.N.T., Jung, K.-S., Son, J.M., Kwon, H.-O., Choi, S.-D., 2018. Seasonal variation, phase distribution, and source identification of atmospheric polycyclic aromatic hydrocarbons at a semi-rural site in Ulsan, South Korea. Environ. Pollut. 236, 529–539.

Nguyen, T.N.T., Kwon, H.-O., Lammel, G., Jung, K.-S., Kim, D., Lee, M.-I., Choi, S.-D., 2020. Spatially high-resolved monitoring and risk assessment of polycyclic aromatic hydrocarbons in an industrial city. (unpublished).

Nielsen, K., Kalmykova, Y., Strömvall, A.-M., Baun, A., Eriksson, E., 2015. Particle phase distribution of polycyclic aromatic hydrocarbons in stormwater — Using humic acid and iron nano-sized colloids as test particles. Sci. Total Environ. 532, 103–111.

Niu, L., Cai, H., Van Gelder, P.H.A.J.M., Luo, P., Liu, F., Yang, Q., 2018. Dynamics of polycyclic aromatic hydrocarbons (PAHs) in water column of Pearl River estuary (China): Seasonal pattern, environmental fate and source implication. Appl. Geochem. 90, 39–49.

Ok, G.O.N., Kim, D.-H., Im, J.-S., Lee, S.-H., Kim, H.-S., 2011. Release of PAHs through runoff from the Gwangan bridge to the coast in Busan, Korea. Polycycl. Aromat. Comp. 31, 110–122.

Parajulee, A., Lei, Y.D., Kananathalingam, A., McLagan, D.S., Mitchell, C.P.J., Wania, F., 2017. The transport of polycyclic aromatic hydrocarbons during rainfall and snowmelt in contrasting landscapes. Water Res. 124, 407–414.

Park, E.-J., Kwon, H.-O., Oh, J.-Y., Choi, S.-D., 2012. Levels and distribution of polycyclic aromatic hydrocarbons (PAHs) in the Taehwa river, Ulsan, Korea. Journal of the Korean Society for Environmental Analysis 15, 155–162.

Park, S.S., Kim, Y.J., Kang, C.H., 2007. Polycyclic aromatic hydrocarbons in bulk PM2.5 and size-segregated aerosol particle samples measured in an urban environment. Environ. Monit. Assess. 128, 231–240.

Perrone, M.G., Vratolis, S., Georgieva, E., Török, S., Šega, K., Veleva, B., Osán, J., Bešlić, I., Kertész, Z., Pernigotti, D., Eleftheriadis, K., Belis, C.A., 2018. Sources and geographic origin of particulate matter in urban areas of the Danube macro-region: The cases of Zagreb (Croatia), Budapest (Hungary) and Sofia (Bulgaria). Sci. Total Environ. 619–620, 1515–1529.

Petruzzelli, L., Celi, L., Cignetti, A., Marsan, F.A., 2002. Influence of soil organic matter on the leaching of polycyclic aromatic hydrocarbons in soil. J. Environ. Sci. Health B. 37, 187–199.

Polissar, A.V., Hopke, P.K., Harris, J.M., 2001. Source regions for atmospheric aerosol measured at Barrow, Alaska. Environ. Sci. Technol. 35, 4214–4226.

R.Lide, D., 2004. Handbook of chemistry and physics. CRC Press.

Ravindra, K., Sokhi, R., Van Grieken, R., 2008. Atmospheric polycyclic aromatic hydrocarbons: source attribution, emission factors and regulation. Atmos. Environ. 42, 2895–2921.

Rice, E.W., Baird, R.B., Eaton, A.D., 2017. Standard methods for the examination of water and wastewater, 23 ed. American Public Health Association, American Water Works Association, Water Environment Federation.

Ryu, S.Y., Kim, J.E., Zhuanshi, H., Kim, Y.J., Kang, G.U., 2004. Chemical composition of post-harvest biomass burning aerosols in Gwangju, Korea. J. Air Waste Manage. 54, 1124–1137.

Salam, M.A., Shirasuna, Y., Hirano, K., Masunaga, S., 2011. Particle associated polycyclic

aromatic hydrocarbons in the atmospheric environment of urban and suburban residential area. International Journal of Environmental Science & Technology 8, 255–266.

Schwarzenbach, R.P., Gschwend, P.M., Imboden, D.M., 2003. Environmental Organic Chemistry. Wiley.

Semeena, V., Lammel, G., 2005. The significance of the grasshopper effect on the atmospheric distribution of persistent organic substances. Geophys. Res. 32.

Shen, H., Huang, Y., Wang, R., Zhu, D., Li, W., Shen, G., Wang, B., Zhang, Y., Chen, Y., Lu, Y., Chen, H., Li, T., Sun, K., Li, B., Liu, W., Liu, J., Tao, S., 2013. Global atmospheric emissions of polycyclic aromatic hydrocarbons from 1960 to 2008 and future predictions. Environ. Sci. Technol. 47, 6415–6424.

Shi, R., Xu, M., Liu, A., Tian, Y., Zhao, Z., 2017. Characteristics of PAHs in farmland soil and rainfall runoff in Tianjin, China. Environ. Monit. Assess. 189, 558.

Shiraiwa, M., Li, Y., Tsimpidi, A.P., Karydis, V.A., Berkemeier, T., Pandis, S.N., Lelieveld, J., Koop, T., Pöschl, U., 2017. Global distribution of particle phase state in atmospheric secondary organic aerosols. Nat. Commun. 8, 15002.

Simmonds, P.G., Seuring, S., Nickless, G., Derwent, R.G., 1997. Segregation and interpretation of ozone and carbon monoxide measurements by air mass origin at the TOR station Mace Head, Ireland from 1987 to 1995. J. Atmos. Chem. 28, 45–59.

Srogi, K., 2007. Monitoring of environmental exposure to polycyclic aromatic hydrocarbons: a review. Environ. Chem. 5, 169–195.

Stogiannidis, E., Laane, R., 2015. Source characterization of polycyclic aromatic hydrocarbons by using their molecular indices: an overview of possibilities, in: Whitacre, D.M. (Ed.), Reviews of Environmental Contamination and Toxicology. Springer International Publishing, Switzerland, pp. 49–133.

Stojić, A., Stanišić Stojić, S., 2017. The innovative concept of three-dimensional hybrid receptor modeling. Atmos. Environ. 164, 216–223.

Su, Y., Lei, Y.D., Wania, F., Shoeib, M., Harner, T., 2006. Regressing gas/particle partitioning data for polycyclic aromatic hydrocarbons. Environ. Sci. Technol. 40, 3558–3564.

Sulej, A.M., Polkowska, Ż., Namieśnik, J., 2011. Contamination of runoff water at Gdańsk airport (Poland) by polycyclic aromatic hydrocarbons (PAHs) and polychlorinated biphenyls (PCBs). Sensors 11, 11901–11920.

Sun, J., 2002. Provenance of loess material and formation of loess deposits on the Chinese Loess Plateau. Earth Planet Sc. Lett. 203, 845–859.

Tamamura, S., Sato, T., Ota, Y., Wang, X., Tang, N., Hayakawa, K., 2007. Long-range transport of polycyclic aromatic hydrocarbons (PAHs) from the eastern Asian continent to Kanazawa, Japan with Asian dust. Atmos. Environ. 41, 2580–2593.

Tao, Y., Yu, J., Lei, G., Xue, B., Zhang, F., Yao, S., 2017. Indirect influence of eutrophication on air – water exchange fluxes, sinking fluxes, and occurrence of polycyclic aromatic hydrocarbons. Water Res. 122, 512-525.

Tham, Y.W.F., Takeda, K., Sakugawa, H., 2008. Polycyclic aromatic hydrocarbons (PAHs) associated with atmospheric particles in Higashi Hiroshima, Japan: influence of meteorological conditions and seasonal variations. Atmos. Res. 88, 224–233.

Thibodeaux, L.J., 1996. Environmtal chemodynamics: Movement of chemicals in air, water, and soil, 2nd ed. Wiley, New York.

Tidwell, L.G., Blair Paulik, L., Anderson, K.A., 2017. Air-water exchange of PAHs and OPAHs at a superfund mega-site. Sci. Total Environ. 603–604, 676–686.

Tobiszewski, M., Namieśnik, J., 2012. PAH diagnostic ratios for the identification of pollution emission sources. Environ. Pollut. 162, 110–119.

Tomaz, S., Shahpoury, P., Jaffrezo, J.-L., Lammel, G., Perraudin, E., Villenave, E., Albinet, A., 2016. One-year study of polycyclic aromatic compounds at an urban site in Grenoble (France): Seasonal variations, gas/particle partitioning and cancer risk estimation. Sci. Total Environ. 565, 1071–1083.

Unwin, J., Cocker, J., Scobbie, E., Chambers, H., 2006. An assessment of occupational exposure to polycyclic aromatic hydrocarbons in the UK. Ann. Ocuup. Hyg. 50, 395–403.

Uria-Tellaetxe, I., Carslaw, D.C., 2014. Conditional bivariate probability function for source identification. Environ. Modell. Softw. 59, 1–9.

US-EPA, 1995. Compilation of Air Pollutant Emission Factors. Volume I: Stationary Point and Area Sources.

US-EPA, 2014. Positive Matrix Factorization (PMF) 5.0: Fundamentals and User Guide. Environmental Protection Agency, Washington DC, USA.

Uyttebroek, M., Breugelmans, P., Janssen, M., Wattiau, P., Joffe, B., Karlson, U., Ortega-Calvo, J.-J., Bastiaens, L., Ryngaert, A., Hausner, M., Springael, D., 2006. Distribution of the Mycobacterium community and polycyclic aromatic hydrocarbons (PAHs) among different size fractions of a long-term PAH-contaminated soil. Environ. Microbiol. 8, 836–847.

Van-Tuan, V., Byeong-Kyu, L., Mai Tra, N., Ji-Tae, K., 2010. A study on characteristics of organic carbon and polycyclic aromatic hydrocarbons (PAHs) in PM10 at the residential and industrial areas in Ulsan of Korea, International Forum on Strategic Technology 2010, pp. 263–266.

Vu, V.-T., Lee, B.-K., Kim, J.-T., Lee, C.-H., Kim, I.-H., 2011. Assessment of carcinogenic risk due to inhalation of polycyclic aromatic hydrocarbons in PM10 from an industrial city: A Korean case-study. J. Hazard. Mater. 189, 349-356.

Vuong, Q.T., Kim, S.-J., Nguyen, T.N.T., Thang, P.Q., Lee, S.-J., Ohura, T., Choi, S.-D., 2020. Passive air sampling of halogenated polycyclic aromatic hydrocarbons in the largest industrial city in Korea: Spatial distributions and source identification. J. Hazard. Mater. 382, 121238.

W.Murphy, B., 2014. Soil organic matter and soil function - Review of the literature and underlying data. Department of the Environment, Canberra, Australia.

Wang, A., Jin, C., Liu, J., Pei, T., 2006. A modified Hortonian overland flow model based on laboratory experiments. Water Resour. Manag. 20, 181–192.

Wang, D., Yang, M., Jia, H., Zhou, L., Li, Y., 2008. Seasonal variation of polycyclic aromatic hydrocarbons in soil and air of Dalian areas, China: an assessment of soil–air exchange. J. Environ. Monit. 10, 1076-1083.

Wang, Q., Liu, M., Yu, Y., Li, Y., 2016. Characterization and source apportionment of PM2.5-bound polycyclic aromatic hydrocarbons from Shanghai city, China. Environ. Pollut. 218, 118–128.

Wang, W., Simonich, S., Giri, B., Chang, Y., Zhang, Y., Jia, Y., Tao, S., Wang, R., Wang, B., Li, W., Cao, J., Lu, X., 2011a. Atmospheric concentrations and air–soil gas exchange of polycyclic aromatic hydrocarbons (PAHs) in remote, rural village and urban areas of Beijing–Tianjin region, North China. Sci. Total Environ. 409, 2942-2950.

Wang, W., Simonich, S.L.M., Wang, W., Giri, B., Zhao, J., Xue, M., Cao, J., Lu, X., Tao, S., 2011b. Atmospheric polycyclic aromatic hydrocarbon concentrations and gas/particle partitioning at background, rural village and urban sites in the North China Plain. Atmos. Res. 99, 197–206.

Wang, Y.Q., Zhang, X.Y., Draxler, R.R., 2009. TrajStat: GIS-based software that uses various trajectory statistical analysis methods to identify potential sources from long-term air pollution measurement data. Environ. Modell. Softw. 24, 938–939.

Wei, C., Han, Y., Bandowe, B.A.M., Cao, J., Huang, R.-J., Ni, H., Tian, J., Wilcke, W., 2015.

Occurrence, gas/particle partitioning and carcinogenic risk of polycyclic aromatic hydrocarbons and their oxygen and nitrogen containing derivatives in Xi'an, central China. Sci. Total Environ. 505, 814–822.

Wimolwattanapun, W., Hopke, P.K., Pongkiatkul, P., 2011. Source apportionment and potential source locations of PM2.5 and PM2.5–10 at residential sites in metropolitan Bangkok. Atmos. Pollut. Res. 2, 172–181.

Xiao, H., Wania, F., 2003. Is vapor pressure or the octanol–air partition coefficient a better descriptor of the partitioning between gas phase and organic matter? Atmos. Environ. 37, 2867–2878.

Yang, H.-H., Lee, W.-J., Chen, S.-J., Lai, S.-O., 1998. PAH emission from various industrial stacks. J. Hazard. Mater. 60, 159–174.

Yang, Y., Guo, P., Zhang, Q., Li, D., Zhao, L., Mu, D., 2010. Seasonal variation, sources and gas/particle partitioning of polycyclic aromatic hydrocarbons in Guangzhou, China. Sci. Total Environ. 408, 2492–2500.

Yunker, M.B., Macdonald, R.W., Vingarzan, R., Mitchell, R.H., Goyette, D., Sylvestre, S., 2002. PAHs in the Fraser River basin: a critical appraisal of PAH ratios as indicators of PAH source and composition. Org. Geochem. 33, 489–515.

Zand, A.D., Grathwohl, P., Nabibidhendi, G., Mehrdadi, N., 2010. Determination of leaching behaviour of polycyclic aromatic hydrocarbons from contaminated soil by column leaching test. Waste Manag. Res. 28, 913–920.

Zedeck, M., 1980. Polycyclic aromatic hydrocarbons: A review. J. Envir. Path. Toxic. 3, 357–567.

Zhang, J., Liu, G., Wang, R., Huang, H., 2017a. Polycyclic aromatic hydrocarbons in the water-SPM-sediment system from the middle reaches of Huai River, China: Distribution, partitioning, origin tracing and ecological risk assessment. Environ. Pollut. 230, 61–71.

Zhang, K., Liang, B., Wang, J.-Z., Guan, Y.-F., Zeng, E.Y., 2012. Polycyclic aromatic hydrocarbons in upstream riverine runoff of the Pearl River Delta, China: An assessment of regional input sources. Environ. Pollut. 167, 78–84.

Zhang, R., Wang, G., Guo, S., Zamora, M.L., Ying, Q., Lin, Y., Wang, W., Hu, M., Wang, Y., 2015. Formation of urban fine particulate matter. Chem. Rev. 115, 3803–3855.

Zhang, W., Keller, A.A., Yue, D., Wang, X., 2009. Management of urban road runoff containing PAHs: Probabilistic modeling and its application in Beijing, China. J. Am. Water Resour. As. 45, 1009–1018.

Zhang, Y., Chen, J., Yang, H., Li, R., Yu, Q., 2017b. Seasonal variation and potential source regions of PM2.5-bound PAHs in the megacity Beijing, China: Impact of regional transport. Environ. Pollut. 231, 329–338.

Zhang, Y., Shen, H., Tao, S., Ma, J., 2011a. Modeling the atmospheric transport and outflow of polycyclic aromatic hydrocarbons emitted from China. Atmos. Environ. 45, 2820–2827.

Zhang, Y., Tao, S., Ma, J., Simonich, S., 2011b. Transpacific transport of benzo[a]pyrene emitted from Asia. Atmos. Chem. Phys. 11, 11993–12006.

Zhou, H., Hopke, P.K., Zhou, C., Holsen, T.M., 2019. Ambient mercury source identification at a New York State urban site: Rochester, New York. Sci. Total Environ. 650, 1327–1337.

Zou, Y., Wang, L., Christensen, E.R., 2015. Problems in the fingerprints based polycyclic aromatic hydrocarbons source apportionment analysis and a practical solution. Environ. Pollut. 205, 394–402.

Acknowledgment

Firstly, I would like to express my very great appreciation to my advisor Prof. Sung-Deuk Choi for supporting and encouraging me during my Ph.D. study. His guidance helped me in all the time of doing research and writing of this dissertation. My sincere thanks also go to the rest of my dissertation committee, including Prof. Yongwon Seo, Prof. Chang Keun Song, Prof. Jaesung Jang, and Dr. Young-Kyo Seo, who spent time for being the members of my dissertation committee and gave me their insightful comments.

I would like to extend my appreciation to the Korean Government Scholarship Program (GKS) for giving me the opportunity to study Ph.D. in Korea. I would like to offer my special thanks to all Korean teachers who are responsible for the GKS program for teaching me the Korean language, for encouraging, and helping me to adapt my best to life in South Korea.

I would like to thank Dr. Hye-Ok Kwon for her discussion when I wrote my first scientific paper. I would also like to thank all teachers in the UCRF Environmental Analysis Center for their help in instructing me to do experiment and using analysis instrument. My grateful thanks are also extended to all my lab-mates, especially Min-Kyu Park, Seong-Joon Kim, Jin-Woo Jeon, Quang, Tien, Sang-Jin Lee, and Ji-Min Son for helping me with the sampling, experiments, and discussion during my Ph.D. study.

Finally, I would like to express my deep gratitude to my family for supporting me spiritually throughout my Ph.D. and my life in general. I am extremely fortunate to be so blessed. I also thank several of my friends who have helped me throughout my career.

CURRICULUM VITAE

Tuyet Nam Thi Nguyen

School of Urban and Environmental Engineering,
Ulsan National Institute of Science and Technology (UNIST),
UNIST-gil 50, Ulsan, 44919, South Korea

Tel:+85-52-217-2875, Email: tuyetnam@unist.ac.kr

Education

2015-Current	School of Urban and Environmental Engineering, Ulsan National Institute of Science and Technology (UNIST), South Korea (PhD candidate)
2008-2010	Department of Environment, Hochiminh City University of Technology (HCMUT), Vietnam (M.S.)
2003-2007	Department of Environment, Hochiminh City University of Science (HCMUS), Vietnam (B.S.)

Research Interests

- Multimedia environmental monitoring of persistent organic pollutants
- Modelling application in atmospheric science

Language skill

English	Good
Korean	Moderate
Vietnamese	Mother tongue

Awards

- 2014 Global Korea Scholarship (GKS) for a PhD study in South Korea.
- Award for Excellent Academic Achievement. National Institute for International Education, Korean Ministry of Education. 2017-12-21.

International publications

1. Nguyen, T. N. T., Jung, K.-S., Son, J. M., Kwon, H.-O., & Choi, S.-D. (2018). Seasonal variation, phase distribution, and source identification of atmospheric polycyclic aromatic hydrocarbons at a semi-rural site in Ulsan, South Korea. Environmental Pollution, 236, 529–539. https://doi.org/10.1016/j.envpol.2018.01.080
2. Nguyen, T. N. T., Kwon, H.-O., Lee, Y.-S., Kim, L., Lee, S.-E., & Choi, S.-D. (2016). Spatial distribution and source identification of indicator polychlorinated biphenyls in soil collected from the coastal multi-industrial city of Ulsan, South Korea for three consecutive years. Chemosphere, 163, 184-191. https://doi.org/10.1016/j.chemosphere.2016.08.014
3. Nguyen, T. N. T., Lee, H.-Y., & Choi, S.-D. (2016). Contamination Profiles of Polychlorinated Biphenyls (PCBs) in the atmosphere and soil of South Korea. In Persistent Organic Chemicals in the Environment: Status and Trends in the Pacific Basin Countries I Contamination Status (Vol. 1243, pp. 193-218): American Chemical Society. https://pubs.acs.org/doi/abs/10.1021/bk-2016-1243.ch009
4. Vuong, T. Q., Kim, S.-J., Nguyen, T. N. T., Phan, Q.-T., Lee, S.-J., Ohura. T., & Choi, S.-D., Passive air sampling of halogenated polycyclic aromatic hydrocabons in the largest industrial city in Korea: Spatial distributions and source identification. Journal of Hazardous Materials, 382, 121238. https://doi.org/10.1016/j.jhazmat.2019.121238
5. Nguyen, T. N. T., Kwon, H.-O., G. Lammel, Jung, K.-S., Min, D.-M., Lee, M.-I., & Choi, S.-D. Monitoring and risk asessment of polycyclic aromatic hydrocarbons using passive air samplers and gas/particle partitioning models in a large industrial city (*Journal of Hazardous Materials, Under review*)
6. Nguyen, T. N. T., Vuong, T. Q., Lee, S.-J., H. Xiao & Choi, S.-D. Identification of sources of polycyclic aromatic hydrocabons in Ulsan, South Korea using hybrid receptor models and conditional bivariate probability function (*To be submitted*).
7. Nguyen, T. N. T., Son, J.-M., Kim, S.-J., Park, M.-K., & Choi, S.-D. Sptial distribution, temporal variation, and phase distribution of polycyclic aromatic hydrocarbons in runoff and surface water (*To be submitted*).
8. Nguyen, T. N. T., Lee. S.-J., & Choi, S.-D. Spatial distribution and seasonal variations of air-water and air-soil exchange of polycyclic aromatic hydrocarbons. (*In preparation*)
9. Vuong, T. Q., Phan, Q. T., Nguyen, T. N. T., Ohura, T., & Choi, S.-D. Seasonal variation, gas/particle partitioning, and source identification of atmospheric halogenated polycyclic aromatic hydrocarbons in Ulsan, South Korea (*Submitted, Journal of Hazardous Materials*).
10. R.J.Silva, Lee. S.-J., Nguyen, T. N. T., & Choi, S.-D. Long-range source identification of criteria air pollutants in the industrial city of Ulsan, South Korea (*In preparation*)
11. Nguyen, T. N. T., Jeon. J-W., Vuong, Q-T., & Choi, S.-D. Seasonal investigation of persistent organic pollutants using passive air sampler in a multi-industrial city of South Korea (*In preparation*).
12. Nguyen, T. N. T., & Choi, S.-D. Application of artificial neural network for a prediction of atmospheric polycyclic aromatic hydrocarbons in a multi-industrial city. (*Plan*).
13.

Presentations

1. Tuyet Nam Thi Nguyen, Hye-Ok Kwon, Yun-Se Lee, Sung-Deuk Choi. Spatial distribution and source identification of indicator polychlorinated biphenyls (PCBs) in soil of Ulsan. 2016 Symposium of the Korean Society for Environmental Analysis. 2016/05-26-27. Gyeongju.
2. Tuyet Nam Thi Nguyen, Hye-Ok Kwon, Ji-Min Son, Kuen-Sik Jung, Sung-Deuk Choi. Seasonal variations and source identification of polycyclic aromatic hedrocarbons (PAHs) in the atmosphere of Ulsan, Korea. The 17th IUAPPA World Clean Air Congress and 9th CAA Better Air Quality Conference. 2016/08/29 – 2016/09/02. Busan, Korea.
3. Tuyet Nam Thi Nguyen, Kuen-Sik Jung, Ji-Min Son, Hye-Ok Kwon, Sung-Deuk Choi. Seasonal variation and source identification of atmospheric polycyclic aromatic hydrocarbons in Ulsan. The 60th Meeting of the Korean Society for Atmospheric Environment. 2017/11/09-11. Deagu, Korea.
4. Tuyet Nam Thi Nguyen, Sang-Jin Lee, Quang Tran Vuong, Sung-Deuk Choi. Application of altitudinal potential source contribution function and concentration weighted trajectory for identifying spatial emission sources and long-range transport of PAHs. The 2nd International Conference on Bioresources, Energy, Environment, and Material Technology (BEEM 2018). 2018/06/10-13. Gangwon, Korea.
5. Tuyet Nam Thi Nguyen, Ji-Min Son, Seong-Joon Kim, Min-Kyu Park, Sung-Deuk Choi. Effect of surface runoffs on polycyclic aromatic hydrocarbons (PAHs) in watersheds of Ulsan, South Korea. 2018 Conference of the Society of Environmental Toxicology and Chemistry. 2018/09/16-19. Deagu, Korea.

Reference

Sung-Deuk Choi (Professor): PhD supervisor

School of Urban and Environmental Engineering, Ulsan National Institute of Science and Technology (UNIST), UNIST-gil 50, Ulsan, 689-805, South Korea

Tel: +82 52 217 2811; Fax: +82 52 217 2859; Email: sdchoi@unist.ac.kr

제 8286 호

상 장

학업성적 우수상

AWARD FOR
EXCELLENT ACADEMIC ACHIEVEMENT

Name	Nguyen Thi Tuyet Nam
Nationality	Vietnam
School	UNIST
Degree	Doctoral

위 사람은 대한민국 정부초청 외국인장학생으로서 우수한 학업성적으로 타 장학생들의 모범이 되었기에 이 상을 드립니다.

This award is presented to the above person in recognition of excellent academic achievement as a Korean Government Scholarship Student by the National Institute for International Education.

2017. 12. 21.

대한민국 교육부 국립국제교육원장 송 기 동

Song, Kidong
President
National Institute for International Education
Ministry of Education, The Republic of Korea

Environmental Pollution 236 (2018) 529–539

Contents lists available at ScienceDirect

Environmental Pollution

journal homepage: www.elsevier.com/locate/envpol

Seasonal variation, phase distribution, and source identification of atmospheric polycyclic aromatic hydrocarbons at a semi-rural site in Ulsan, South Korea☆

Tuyet Nam Thi Nguyen, Kuen-Sik Jung, Ji Min Son, Hye-Ok Kwon, Sung-Deuk Choi*

School of Urban and Environmental Engineering, Ulsan National Institute of Science and Technology (UNIST), Ulsan, 44919, Republic of Korea

ARTICLE INFO

Article history:
Received 18 August 2017
Received in revised form
22 January 2018
Accepted 22 January 2018

Keywords:
PAHs
Ulsan
Seasonal variation
Phase distribution
Source identification

ABSTRACT

Polycyclic aromatic hydrocarbons (PAHs) in gaseous and particulate phases (n = 188) were collected in Ulsan, South Korea, over a period of one year (June 2013–May 2014) to understand the seasonal variation and phase distribution of PAHs as well as to identify the seasonal PAH emission sources. The target compounds were the 16 US-EPA priority PAHs, with the exception of naphthalene, acenaphthylene, and acenaphthene. Winter and spring had the highest and lowest PAH concentrations, respectively. The mean of the Σ_{13} PAHs in the gaseous phase (4.11 ng/m^3) was higher than that in the particulate phase (2.55 ng/m^3). Fractions of the gaseous or 3- and 4-ring PAHs (i.e., Flu, Phe, and Ant) were high in summer, and those of the particulate or 5- and 6-ring PAHs (i.e., BkF, BaP, Ind, DahA, and BghiP) increased in winter. Gas/particle partitioning models also demonstrated the increased contributions of the particulate PAHs in spring and winter. Source identification of PAHs was undertaken using diagnostic ratios, principal component analysis, and positive matrix factorization. The results indicated that pyrogenic sources (e.g., coal combustion) were dominant in winter. Other types of pyrogenic (e.g., industrial fuel combustion) and petrogenic sources were the main PAH sources in summer and autumn. The influence of both sources, especially in summer, might be due to seasonal winds transporting PAHs from the industrial areas. Two types of pyrogenic sources, diesel and coal combustion, were identified as the main PAH sources in spring. This study clearly demonstrates a source–receptor relation of PAHs at a semi-rural site in a heavily industrialized city.

1. Introduction

Polycyclic aromatic hydrocarbons (PAHs) are compounds having at least two aromatic rings in their chemical structures. PAHs can be separated into two classes, namely low-molecular-weight (LMW) and high-molecular-weight (HMW) compounds. The former have two or three aromatic rings and exist predominantly in the vapor phase, whereas the latter have more than four aromatic rings and tend to adsorb onto airborne particles (Baek et al., 1991b). The United States Environmental Protection Agency (US-EPA) selected 16 specific species on the basis of their representative harmful effects, available information, and higher levels compared to other PAHs (Ravindra et al., 2008). Levels and the phase distribution of PAHs have been reported to differ seasonally (Albuquerque et al., 2016). In particular, winter tends to show the highest PAH concentration among the four seasons due to a decline in atmospheric vertical dispersion and an increase in domestic burning for heating. Fractions of the gaseous PAHs are higher in summer, while the particulate PAHs contribute more in winter since lower temperatures can generate condensation of PAHs on atmospheric suspended particles (Gustafson and Dickhut, 1997).

PAHs are emitted from natural sources such as forest fires and volcanic eruptions (Ravindra et al., 2008). However, the most noticeable sources are related to human activities such as combustion processes and vehicle exhaust (Choi et al., 2012b). The emission sources of PAHs can be identified through several methods, including diagnostic ratios (DRs), principal component analysis (PCA), chemical mass balance (CMB), and positive matrix factorization (PMF). The DR method determines the possible sources of PAHs by comparing the observed ratios to those from previous studies. This method assumes that the PAH isomers are

☆ This paper has been recommended for acceptance by Eddy Y. Zeng.

* Corresponding author.
E-mail address: sdchoi@unist.ac.kr (S.-D. Choi).

https://doi.org/10.1016/j.envpol.2018.01.080
0269-7491/

Chemosphere 163 (2016) 184–191

Contents lists available at ScienceDirect

Chemosphere

journal homepage: www.elsevier.com/locate/chemosphere

Spatial distribution and source identification of indicator polychlorinated biphenyls in soil collected from the coastal multi-industrial city of Ulsan, South Korea for three consecutive years

Tuyet Nam Thi Nguyen [a], Hye-Ok Kwon [a], Yun-Se Lee [a], Leesun Kim [b], Sung-Eun Lee [b], Sung-Deuk Choi [a, *]

[a] School of Urban and Environmental Engineering, Ulsan National Institute of Science and Technology (UNIST), Ulsan, 44919, Republic of Korea
[b] School of Applied Biosciences, Kyungpook National University, Daegu, 41566, Republic of Korea

HIGHLIGHTS

- Indicator PCBs in soil collected at 25 sites in Ulsan, South Korea were analyzed.
- The soils in Ulsan were slightly or moderately contaminated with indicator PCBs.
- The PCB levels at industrial and urban sites were higher than those at rural sites.
- Leakage from transformer oils appeared to be the main PCB source in major industries.
- PCB-containing paints were a major source for automobile and shipbuilding industries.

ARTICLE INFO

Article history:
Received 15 May 2016
Received in revised form
1 August 2016
Accepted 2 August 2016
Available online 16 August 2016

Handling Editor: Shane Snyder

Keywords:
PCBs
Soil
Source identification
Spatial distribution
Ulsan

ABSTRACT

The concentrations, profiles, and source-receptor relationships of seven indicator polychlorinated biphenyls (PCBs) (#28, 52, 101, 118, 138, 153, and 180) found in soil at 25 rural, urban, and industrial sites in Ulsan, South Korea were investigated. For this study, 75 soil samples were collected, 25 each in January of 2011, 2012, and 2013. Principal component analysis was used to evaluate the influence of the emission sources on the soil samples. The concentrations of total seven PCBs (Σ_7 PCBs) ranged between 0.034 ng/g and 143 ng/g (mean: 5.10 ng/g, median: 0.440 ng/g), which indicated slight or moderate contamination levels, respectively, compared to those in the other countries or other cities in Korea. The concentrations of Σ_7 PCBs at the industrial and urban sites were significantly higher than those at the rural sites, due to the direct influence of emission sources related to industrial activities rather than urban emission sources. Generally, the profiles of PCBs were dominated by penta- and hexa-chlorinated biphenyls at all the study sites, suggesting common sources of PCBs in Ulsan. PCB source identification indicated that leakage from transformer oils in the major industrial complexes and PCB-containing paints used in the automobile and shipbuilding industrial complexes were possibly the main sources of indicator PCBs in the study areas.

1. Introduction

Polychlorinated biphenyls (PCBs) are a class of persistent organic pollutants (POPs) consisting of 209 congeners (IARC, 2015) that had been synthesized and produced as industrial chemicals from 1930 to 1993 (Breivik et al., 2002). Due to their beneficial properties of thermal stability (UNEP, 1999) and resistance to both acids and alkalis (Bozlaker et al., 2008), PCBs have been used widely for industrial purposes (UNEP, 1999), such as in lubricating and hydraulic oils (Kalmaz and Kalmaz, 1979), heat transfer fluids in capacitors and transformers (Harrad et al., 1994), plastics additives (Hong et al., 2005), and plasticizers (Park et al., 2009). PCBs are unintentionally produced in chemical processes containing chlorine and hydrocarbon under high temperature (Breivik et al., 2004). Such processes include ferrous production, waste incineration, fuel combustion, and mineral production (Kim et al., 2007). After being

* Corresponding author.
E-mail address: sdchoi@unist.ac.kr (S.-D. Choi).

http://dx.doi.org/10.1016/j.chemosphere.2016.08.014
0045-6535/

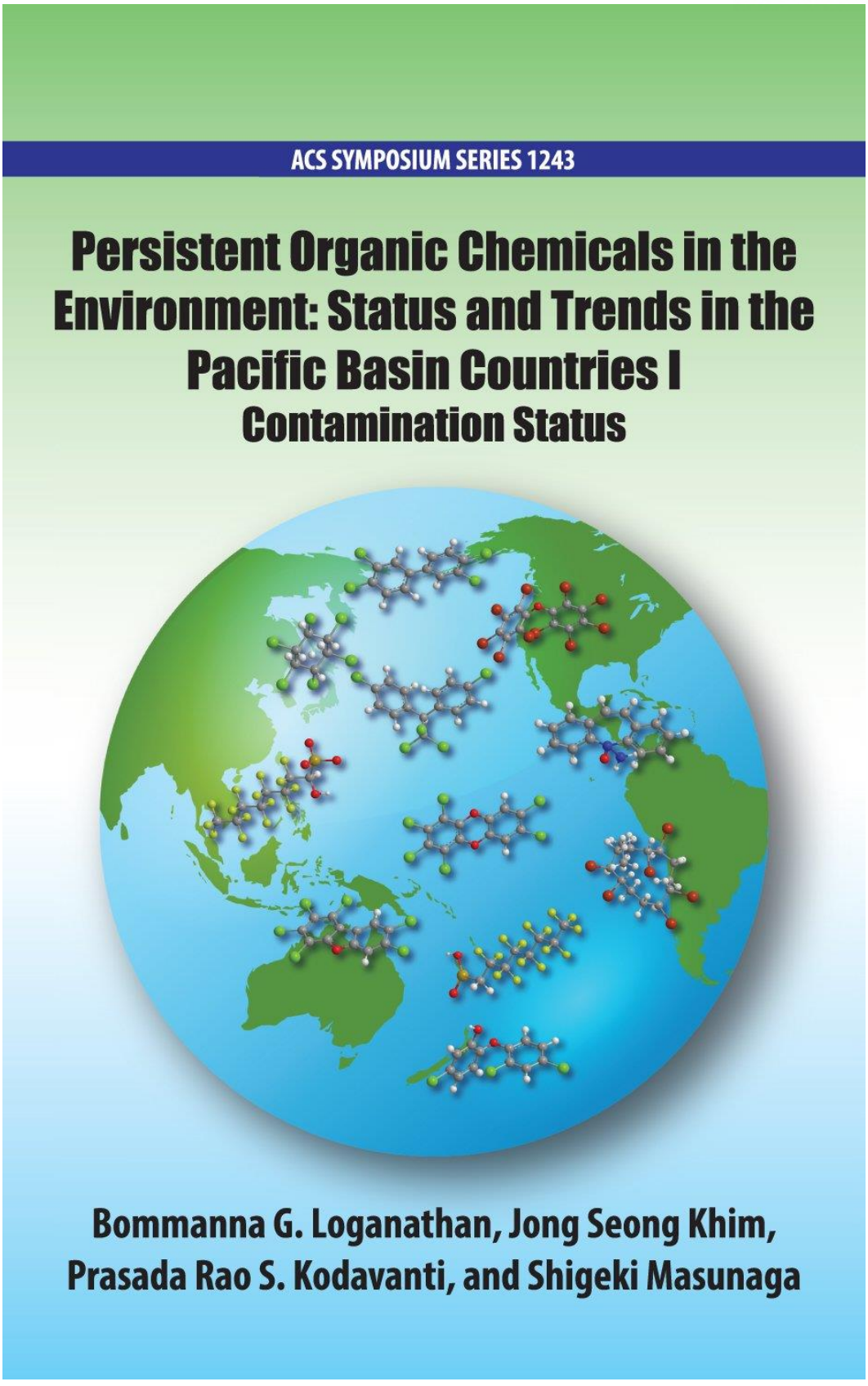

Chapter 9

Contamination Profiles of Polychlorinated Biphenyls (PCBs) in the Atmosphere and Soil of South Korea

Tuyet Nam Thi Nguyen, Ho-Young Lee, and Sung-Deuk Choi*

School of Urban and Environmental Engineering,
Ulsan National Institute of Science and Technology (UNIST),
Ulsan 44919, Republic of Korea
***E-mail: sdchoi@unist.ac.kr**

This chapter provides an overview of polychlorinated biphenyl (PCB) contamination in the atmosphere and soil of South Korea. Variations in PCB trends were evaluated via spatial distribution, temporal variation, and gas/particle partitioning. In addition, information on the history of and future plans for PCB management in Korea was examined. Levels of PCBs in the atmosphere decreased gradually, whereas those in soil samples exhibited the opposite trend, which is a steady increase over time. For the atmospheric PCBs, no significant seasonal or spatial variations in the profiles of PCBs and dioxin-like PCBs were observed. In addition, low-molecular-weight PCBs (mono- to penta-CBs) mostly appeared in the gas phase and showed high contributions in the summer. Most high-molecular-weight PCBs (hexa- to deca-CBs) existed in the particle phase and were enriched in the winter. The major emission source of the atmospheric PCBs is believed to be re-emission from PCB-containing surfaces, such as soil, water, or PCB-containing equipment. There was also no significant difference in the spatial distribution and profiles of PCBs in soil. Most of the soil samples exhibited high fractions of penta- and hexa-CBs. Moreover, the heavy PCBs at the urban and industrial sites showed higher proportions compared to those at the rural sites. Remote areas, such as a forest site, showed

Loganathan et al.; Persistent Organic Chemicals in the Environment: Status and Trends in the Pacific Basin Countries I ...
ACS Symposium Series; American Chemical Society: Washington, DC, 2016.

Journal of Hazardous Materials 382 (2020) 121238

Contents lists available at ScienceDirect

Journal of Hazardous Materials

journal homepage: www.elsevier.com/locate/jhazmat

Passive air sampling of halogenated polycyclic aromatic hydrocarbons in the largest industrial city in Korea: Spatial distributions and source identification

Quang Tran Vuong[a], Seong-Joon Kim[a], Tuyet Nam Thi Nguyen[a], Phan Quang Thang[a], Sang-Jin Lee[a], Takeshi Ohura[b], Sung-Deuk Choi[a,*]

[a] School of Urban and Environmental Engineering, Ulsan National Institute of Science and Technology (UNIST), Ulsan, 44919, Republic of Korea
[b] Faculty of Agriculture, Meijo University, Nagoya, 468-8502, Japan

GRAPHICAL ABSTRACT

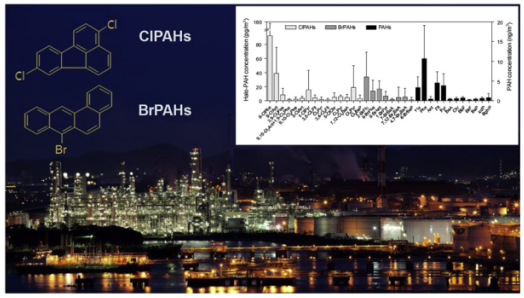

ARTICLE INFO

Editor: D. Aga

Keywords:
PUF-PAS
Halo-PAHs
ClPAHs
BrPAHs
Ulsan

ABSTRACT

Some halogenated polycyclic aromatic hydrocarbons (Halo-PAHs) are known to be more toxic than their corresponding parent PAHs, but studies on Halo-PAHs have been somewhat limited. In this study, passive air samplers were used to monitor Halo-PAH and PAH contamination at 20 sampling sites in Ulsan, one of the largest industrial cities in South Korea. The mean concentrations of Σ_{24} ClPAHs, Σ_{11} BrPAHs, and Σ_{13} PAHs were 207 pg/m^3, 84 pg/m^3, and 26 ng/m^3, respectively. Industrial areas displayed higher concentrations of both Halo-PAHs and PAHs than urban and rural areas. Strong correlations between energetically unfavorable Halo-PAHs and their corresponding parent PAHs suggest that the main formation mechanism of Halo-PAHs is not direct halogenation of PAHs. Low molecular weight Halo-PAHs with one halogen atom and their parent PAHs were dominant. The profiles of ClPAHs and BrPAHs in petrochemical, automobile, shipbuilding, and non-ferrous industrial complexes were distinguished. The toxicity equivalency quantities (TEQs) of ClPAHs, BrPAHs, and PAHs at the industrial sites also showed the highest values of 4.2, 0.5, and 18.3 pg-TEQ/m^3, respectively, reflecting the high toxicity of Halo-PAHs. To the best of our knowledge, this is the first study reporting atmospheric levels of both ClPAHs and BrPAHs using passive air samplers.

* Corresponding author.
E-mail address: sdchoi@unist.ac.kr (S.-D. Choi).

https://doi.org/10.1016/j.jhazmat.2019.121238
Received 23 February 2019; Received in revised form 25 August 2019; Accepted 14 September 2019
Available online 17 September 2019